NASA Contractor Report 158908

ESTIMATES OF OCEANIC SURFACE WIND SPEED AND DIRECTION USING ORTHOGONAL BEAM SCATTEROMETER MEASUREMENTS AND COMPARISON OF RECENT SEA SCATTERING THEORIES

R. K. Moore, A. K. Fung, G. J. Dome, and I. J. Birrer

UNIVERSITY OF KANSAS CENTER FOR RESEARCH, INC.
2291 Irving Hill Road, Campus West
Lawrence, KS 66044

NASA Contract NAS1-10048

June 1978

National Aeronautics and Space Administration

Langley Research Center
Hampton, Virginia 23665

TABLE OF CONTENTS

LIST OF ILLUSTRATIONS

LIST OF TABLES

1.0 SUMMARY

The radar backscatter from the sea depends upon both the magnitude and direction of the wind vector. This dependence can be explained by both theoretical and empirical models. These results are extremely important since in the near future NASA proposes to launch the SeaSat-A oceanographic satellite. One of the goals of this satellite is to demonstrate the feasibility of global wind speed and direction measurements over the ocean. Such wind vector information will provide meteorologists with essential input into wave and weather forecast models.

Several regression models are proposed to explain the wind direction dependence of the 1975 JONSWAP (Joint North Sea Wave Project) scatterometer data, in which continuous directional observations were made by flying in a circle. The models consider the radar backscatter as a harmonic function of wind direction. The constant term accounts for the major effect of wind speed and the sinusoidal terms for the effects of direction. The fundamental accounts for the difference in upwind and downwind returns, while the second harmonic explains the upwind-crosswind difference. Possible higher order effects would appear as coefficients of the higher harmonics. The first model considers only terms involving the fundamental and second harmonic. The second and third models are more general, since third and fourth harmonics are included, respectively.

The results, for angles of incidence of 40° and 65°, indicate that third order effects are negligible. Also, for all cases, the first model, which used only cosine terms up through the second harmonic, appears to explain the angular variation adequately. The coefficients of this model are related to the wind speed by a power-law expression. The relationship is extremely valuable, since it simplifies the process needed to determine a wind direction from two orthogonal scatterometer measurements. Thus, the results are of value to future satellite observations of the ocean.

An inversion technique is also proposed which will eliminate the effects of wind speed and direction. This approach assumes that two orthogonal scattering measurements are available. Also, if swell or the large-scale waves do not line up with the wind waves, it is assumed that the necessary information is available to correct for these effects. The technique performs adequately under these constraints, and also, when possible higher order wave effects are present.

A comparison between two different types of sea scatter theories, one type represented by the work of Wright and the other by that of Chan and Fung, was made with recent scatterometer measurements. Wright's theoretical model differs from that of Chan and Fung in two major aspects: (1) Wright uses Phillips' model for the sea spectrum, while Chan and Fung use Mitsuyasu and Honda's spectrum as proposed by Pierson; (2) Wright uses the modified slick-sea slope distribution of Cox and Munk defined with respect to the horizon, while Chan and Fung use Cox and Munk's slick-sea slope distribution defined with respect to the plane perpendicular to the look direction.

Satisfactory agreement between theory and experimental data were obtained when Chan and Fung's model was used to explain the wind and azimuthal variation of the radar backscatter. Wright's theory does not include anistropic characteristics, and hence, can be only used to show wind speed and incidence angle dependence. Since Phillip's sea spectrum is independent of wind speed, Wright's model does not show significant wind dependence, and thus, leads to poorer agreements with experimental data.

2.0 AN EMPIRICAL MODEL FOR OCEAN RADAR BACKSCATTER AND ITS APPLICATION IN INVERSION ROUTINE TO ELIMINATE WIND SPEED AND DIRECTION EFFECTS

A. Modelling the Wind Speed Dependence of Sea Return

The ocean surface can be viewed simplistically as consisting of waves of two scales: (i) gravity waves which have wavelengths much longer than those of the radar, and (ii) capillary waves which have wavelengths on the order of or smaller than the radar wavelength. At microwave frequencies and for incidence angles in the range $80° \geq \theta \geq 25°$, the radar return, especially the vertically polarized case, can be adequately explained in terms of the first order Bragg scattering theory. The selected ocean wavelength predicted by this theory is related to the radar wavelength by

$$\Lambda \sin \theta = \frac{\lambda}{2} \tag{2-1}$$

where Λ = ocean wavelength

λ = radar wavelength

Thus, a strong dependence of the radar return upon the sea spectrum in the capillary region is expected. Pierson (1975), Mitsuyasu and Honda (1974), and others have shown that the sea spectrum in the capillary region grows with increasing wind speed. For this reason, a strong correlation between radar sea return and the wind speed over the sea surface is anticipated.

Work by many experimenters, most recently Young and Moore (1976), and Jones, Schroeder, and Mitchell (1977) suggest that the wind speed can be determined from the radar backscatter by using an empirical relation of the form:

$$\sigma^\circ = AU^Y \tag{2-2a}$$

or

$$\sigma^\circ_{dB} = A_{dB} + Y(10 \log U) \tag{2-2b}$$

where A = levelling constant

U = wind speed

γ = wind speed power coefficient.

The effect of wind direction on sea returns has not been as extensively explored as the magnitude dependence. The majority of research in this area has been conducted under the NASA AAFE (Advanced Aircraft Flight Experiment) program. Attempts at modelling this effect, however, have never been truly satisfactory, since a relationship between the coefficients of the models and wind speed has not been shown previously (Afarani (1975)).

Several regression models were applied to the 1975 JONSWAP (Joint North Sea Wave Project)[1] circle-flight data in an attempt to determine the wind direction and speed dependence of the radar returns. The proposed models assume the backscatter to be a harmonic function of wind direction. The constant term accounts for the major effects of the wind speed magnitude and the sinusoidal terms account for the effects of wind direction. The fundamental accounts for the difference in the upwind and downwind returns, while the second harmonic explains the upwind-cross-wind difference. Possible higher order effects which may occur are accounted for in some of the models by the higher order harmonics. To include these possibilities the following regression models were proposed.

$$\text{Model 1}: \quad \sigma^{o}(U,\theta,\phi) = \sum_{n=0}^{2} A_n(U,\theta) \cos\left[n(\phi-\phi_u)\right] \qquad (2\text{-}3a)$$

$$\text{Model 2}: \quad \sigma^{o}(U,\theta,\phi) = \sum_{n=0}^{3} A_n(U,\theta) \cos\left[n(\phi-\phi_u)\right] \qquad (2\text{-}3b)$$

$$\text{Model 3}: \quad \sigma^{o}(U,\theta,\phi) = \sum_{n=0}^{4} A_n(U,\theta) \cos\left[n(\phi-\phi_u)\right] \qquad (2\text{-}3c)$$

where $A_n(U,\theta)$ = coefficient to be determined through regression

ϕ = measurement direction from North, in degrees

ϕ_u = upwind direction, in degrees

U = wind speed, m/s

θ = incidence angle (relative to vertical)

[1] (Jones, Schroeder, Mitchell, 1978)

The multiple correlation coefficient, R^2, was chosen to provide a numerical evaluation of the regression analysis. R^2 is a measure of the "proportion of total variation about the mean explained by the regression;" a perfect fit has a value of one (Draper and Smith, 1966).

By fitting Model 3 to the measured data, values for the A_n's are obtained as shown in Table 1. These A_n's are for a given incidence angle, θ, and a given flight (or wind speed). Reasonable improvements in the R^2 value due to use of third and/or fourth harmonics would imply that higher order effects are significant. As Table 1 shows, this is not the case. Even flight 16, which has unequal crosswind values, appears to be adequately explained by Model 1, as shown in Figure 1.

Since the second-harmonic model adequately explains the wind direction effects on backscatter, an attempt was made to determine a relationship between the three regression coefficients of this model and wind speed. The scattering coefficient is known to have a power-law dependence on the wind speed. A power-law relation of the following form is assumed for the A_n's,

$$A_n(U,\theta) = \rho_n(\theta)\, U^{\gamma_n(\theta)} \qquad (2\text{-}4)$$

where $\rho_n(\theta)$ = levelling coefficient

$\gamma_n(\theta)$ = wind speed power coefficient

This expression is fitted to the A_n's shown in Table 1 at a given incidence angle. Figure 2 is an illustration of this case when $\theta = 40^\circ$. It is clear from Figure 2 that the assumed expression for A_n does provide satisfactory fits, with the possible exception of A_1(VV). Table 2 shows the coefficients in (4) obtained through regression analysis for $\theta = 40^\circ$ (Figure 2). This relationship is also shown using both AAFE and JONSWAP results in Appendix B.

B. <u>WINDVEC - A Simple Inversion Technique to Eliminate Wind Speed and Direction Effects from SeaSat Orthogonal Radar Backscatter Measurements</u>

In the near future (1978), NASA intends to launch the SeaSat-A oceanographic satellite, carrying as one of its instruments the SeaSat Active Scatterometer System (SASS). The SASS will use four antennas

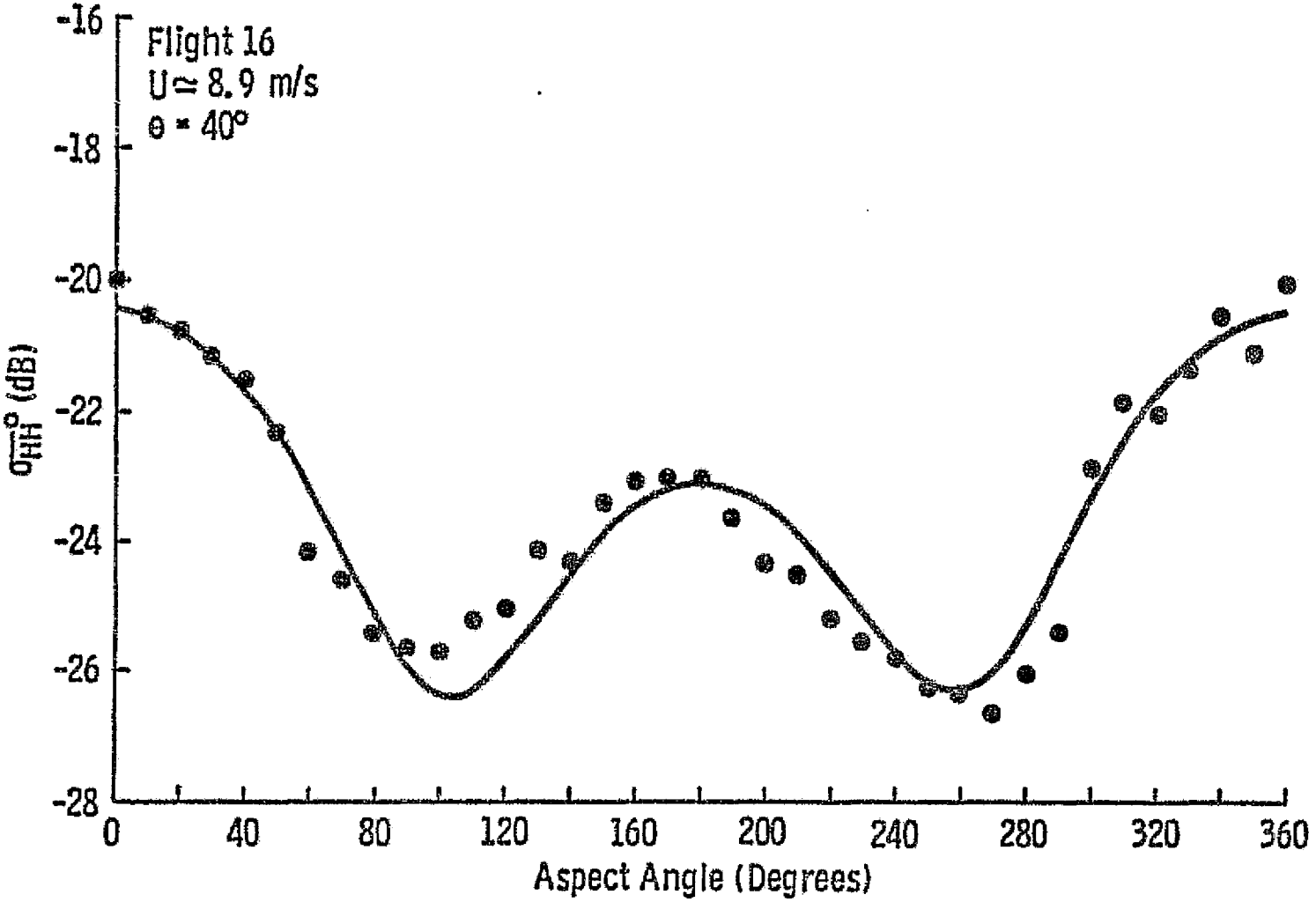

Figure 1a: Regression and observed values of σ^{o}_{HH} plotted versus the azimuth angle, U ≃ 8.9 m/s.

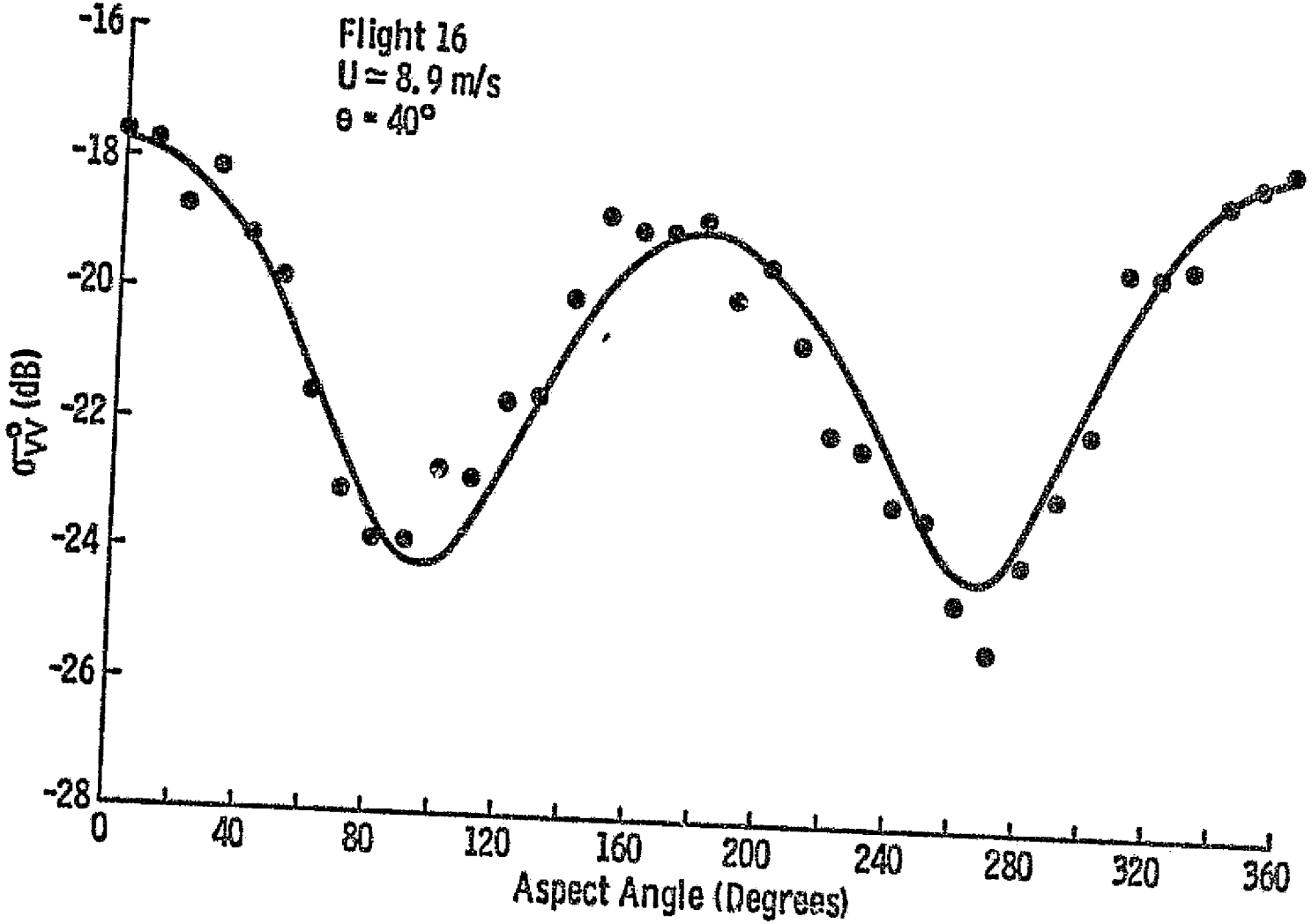

Figure 1b: Regression and observed values of σ^0_{VV} plotted versus the azimuth angle, U = 8.9 m/s.

JONSWAP Regression Results ($\theta = 40^0$).
(Individual Flights)

(a). HH Polarization

Date	Flight	Wind Speed	A_0 $(\times 10^{-3})$	A_1 $(\times 10^{-3})$	A_2 $(\times 10^{-3})$	A_3 $(\times 10^{-3})$	A_4 $(\times 10^{-3})$	R_2^2	R_3^2	R_4^2
8/29/75	13	4.5	1.91	0.58	0.85	***	***	0.91	***	***
9/02/75	14	5.5	2.01	1.05	0.83	0.10	***	0.98	0.98	***
9/08/75	16	8.8	4.74	2.02	2.20	***	***	0.95	***	***
9/09/75	17	12.8	15.41	5.07	7.80	0.63	***	0.97	0.97	***
9/09/75	18	11.3	11.13	3.71	4.93	***	***	0.97	***	***
9/10/75	19	7.5	5.96	2.02	2.68	0.54	***	0.95	0.98	***

(b). VV Polarization

Date	Flight	Wind Speed	A_0 $(\times 10^{-3})$	A_1 $(\times 10^{-3})$	A_2 $(\times 10^{-3})$	A_3 $(\times 10^{-3})$	A_4 $(\times 10^{-3})$	R_2^2	R_3^2	R_4^2
8/29/75	13	4.5	2.95	***	1.62	***	***	0.92	***	***
9/02/75	14	5.5	4.00	1.07	1.90	***	***	0.94	***	***
9/08/75	16	8.8	9.32	1.95	5.43	***	***	0.92	***	***
9/09/75	17	12.8	27.31	3.73	15.54	1.50	***	0.97	0.98	***
9/09/75	18	11.3	21.63	4.12	12.86	0.90	-0.69	0.98	0.98	0.98
9/10/75	19	7.5	11.60	0.70	6.55	0.97	***	0.97	0.98	***

*** These terms of the regression were not statistically significant.

JONSWAP Regression Results ($\theta = 65^{\circ}$)

(a). HH Polarization

Date	Flight	Wind Speed	A_0 $(\times 10^{-3})$	A_1 $(\times 10^{-3})$	A_2 $(\times 10^{-3})$	A_3 $(\times 10^{-3})$	A_4 $(\times 10^{-3})$	R_2^2	R_3^2	R_4^2
9/02/75	14	5.5	0.17	0.068	0.032	0.011	***	0.84	0.86	***
9/08/75	16	8.9	0.29	0.18	0.16	0.032	***	0.93	0.94	***
9/09/75	17	12.3	1.26	0.83	0.55	***	***	0.96	***	***
9/09/75	18	10.5	0.97	0.69	0.47	***	***	0.92	***	***

(b). VV Polarization

Date	Flight	Wind Speed	A_0 $(\times 10^{-3})$	A_1 $(\times 10^{-3})$	A_2 $(\times 10^{-3})$	A_3 $(\times 10^{-3})$	A_4 $(\times 10^{-3})$	R_2^2	R_3^2	R_4^2
9/02/75	14	5.5	0.85	0.098	0.44	***	***	0.95	***	***
9/08/75	16	8.9	2.83	0.89	2.22	0.28	***	0.93	0.95	***
9/09/75	17	12.3	7.14	1.70	4.33	***	-0.58	0.92	0.94	***
9/09/75	18	10.5	5.36	2.75	3.82	***	***	0.83	***	***
9/10/75	19	7.5	2.86	0.40	2.22	0.30	-0.22	0.96	0.98	0.99

* Flight 13 contained no 65° data. Also, the horizontal polarization data for flight 19 was deleted due to small number observations.

*** These terms of the regression were not statistically significant.

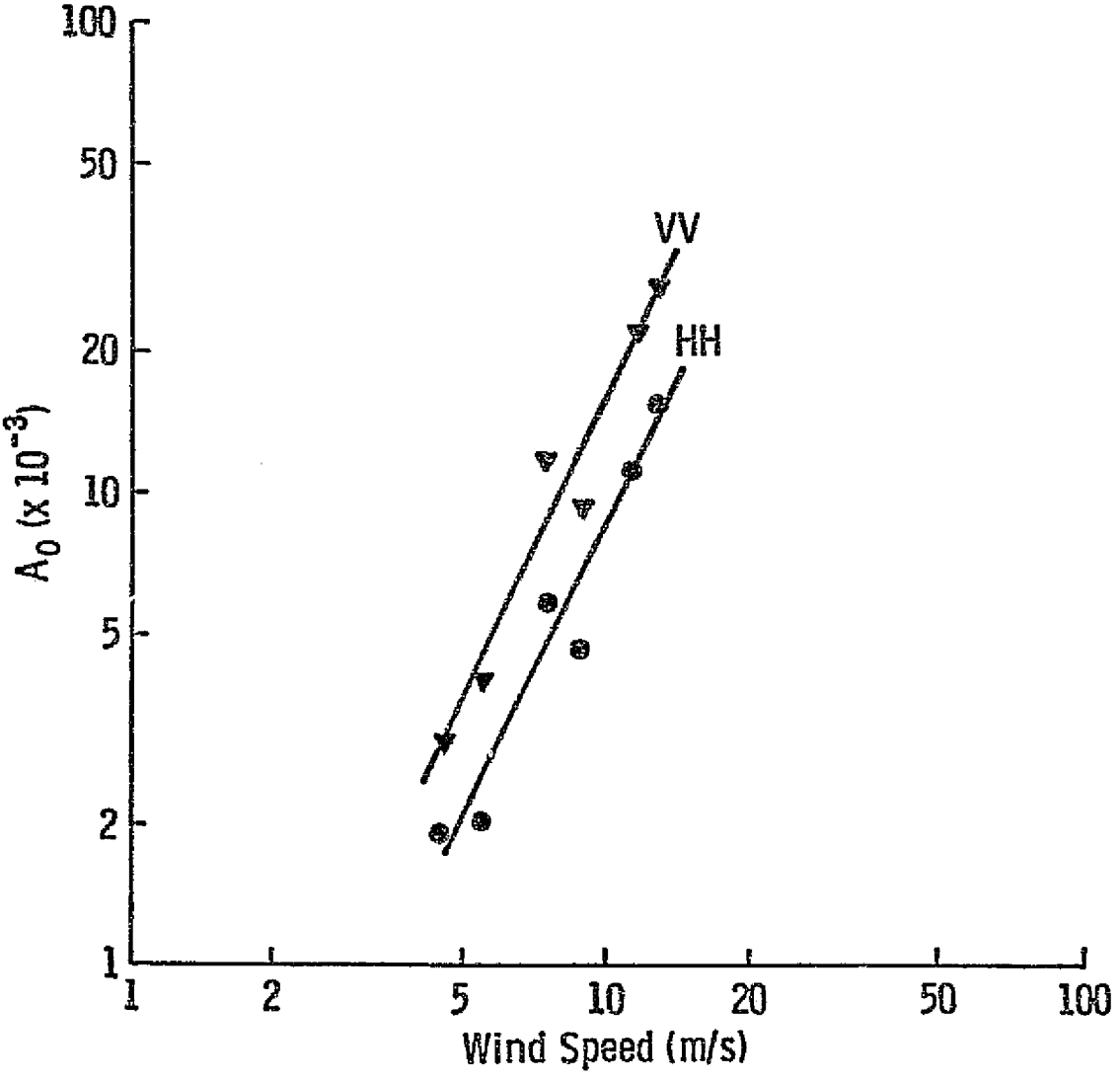

2a: Regression fit to A_o coefficient of the 2nd harmonic model.

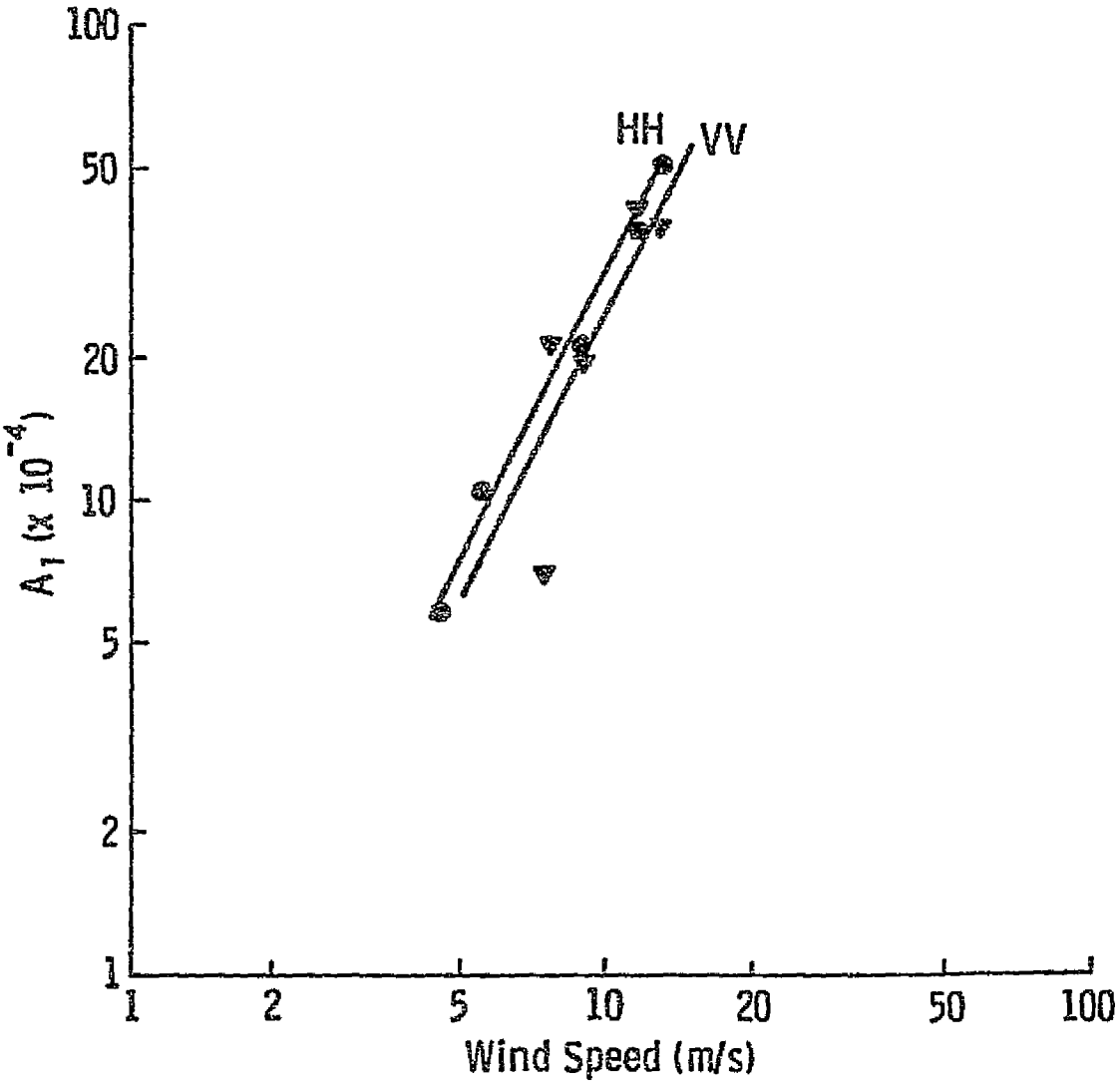

Figure 2b: Regression fit to A_1 coefficient of the 2nd harmonic model.

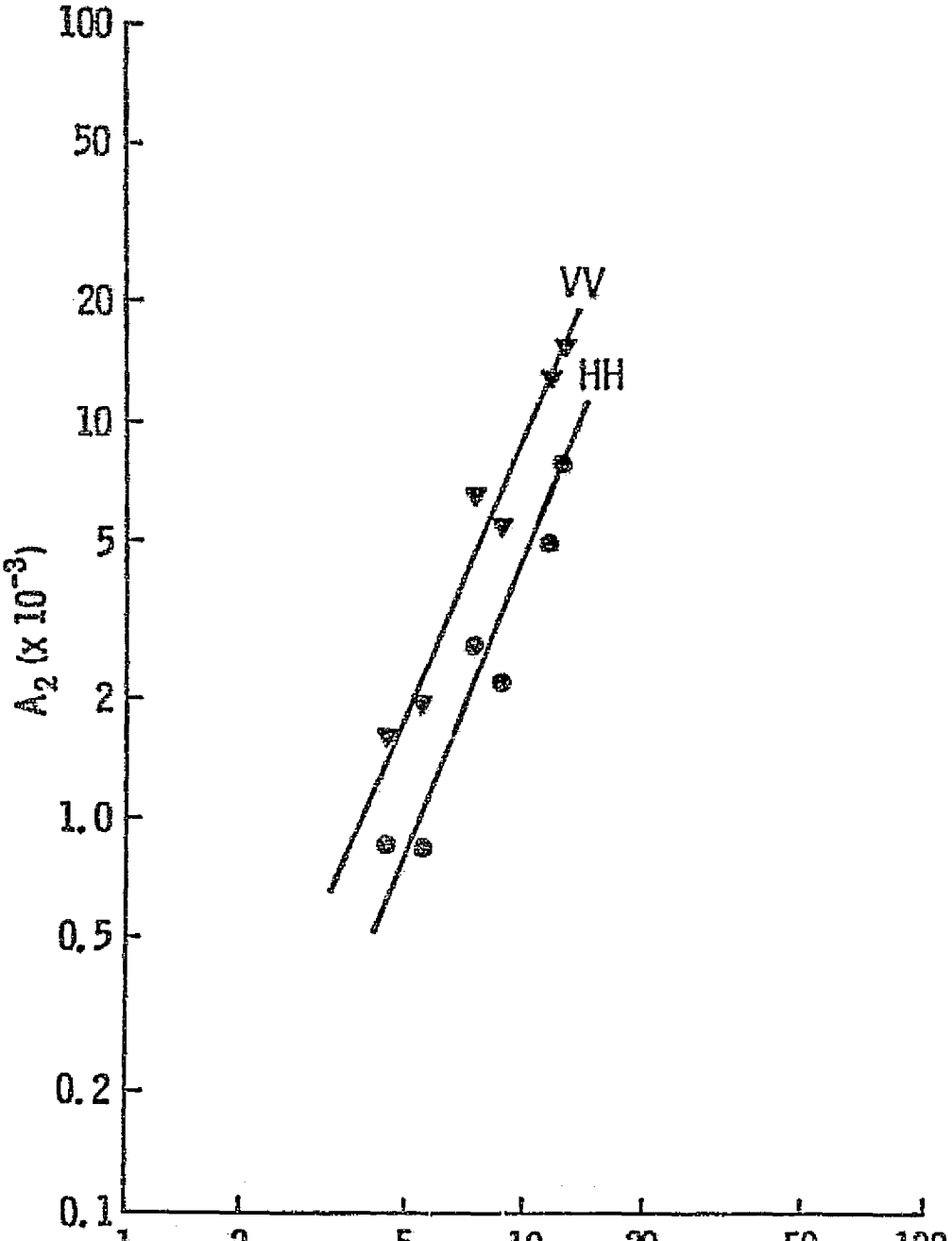

Figure 2c: Regression fit to A_2 coefficient of the 2nd harmonic model.

Table 2: POWER LAW RELATIONSHIP OF REGRESSION COEFFICIENTS OF 2nd HARMONIC MODEL AT $\theta = 40^{o}$.

Coefficient	Horizontal Polarization			Vertical Polarization		
	ρ_N ($\times 10^{-5}$)	V_n	R^2	ρ_N ($\times 10^{-5}$)	V_n	R^2
A_o	7.53	2.05	0.94	11.75	2.13	0.96
A_1	3.46	1.94	0.96	2.68	1.95	0.73
A_2	2.55	2.16	0.93	5.02	2.26	0.95

squinted 45° off the satellite subtrack to achieve "a star-like illumination on the earth's surface," Grantham, et al.(1975). An operational frequency of 14.6 GHz was chosen to provide maximum wind sensitivity and minimal atmospheric absorption. Both vertical and horizontal like - polarization measurements will be made over an incidence angle range of [25°, 55°]. Doppler filtering will be used to divide this 1000 km. swath into either 25 km. or 50 km. cells as specified by the SeaSat User Working Group (UWG).

The User Working Group has also specified that the SASS should be capable of measuring wind velocity within an accuracy of ±2m/s ($U \leq 20$m/s) or ±10% ($U \geq 20$m/s) for wind speed, and an accuracy for wind direction of ±20°. This creates the need for an inversion technique, which will use the orthogonal measurements, to infer these quantities. This problem can be solved in two steps: (1) wind speed, and (2) wind direction.

1. Wind Speed

The wind speed can be estimated within the user's requirements by using the average for the same point from orthogonal viewing angles. This average is approximately equal to the radar cross section when the aspect angle is 45°, i.e.

$$\sigma^\circ(\phi = 45^\circ) \approx \sigma^\circ_{AV} = \frac{\sigma^\circ_1(\phi_1) + \sigma^\circ_2(\phi_1 + 90^\circ)}{2} \qquad (2\text{-}5)$$

From Model 1, it can be shown that (5) becomes exact for $\phi_1 = -45$ and it provides the worst estimate when $\phi_1 = 135°$. This is true for any incidence angle for which Model 1 is valid. It should also be noted that (5) provides poorer estimates when the upwind-downwind ratio becomes larger.

As an illustration, the relationship between $\sigma^\circ(\phi = 45°)$ and wind speed is shown in Figure 3 for $\theta = 40°$. Again a power-law dependence of the form

$$\sigma^\circ(\phi = 45^\circ) = a_1(\theta) U^{\gamma_1(\theta)} \qquad (2\text{-}6)$$

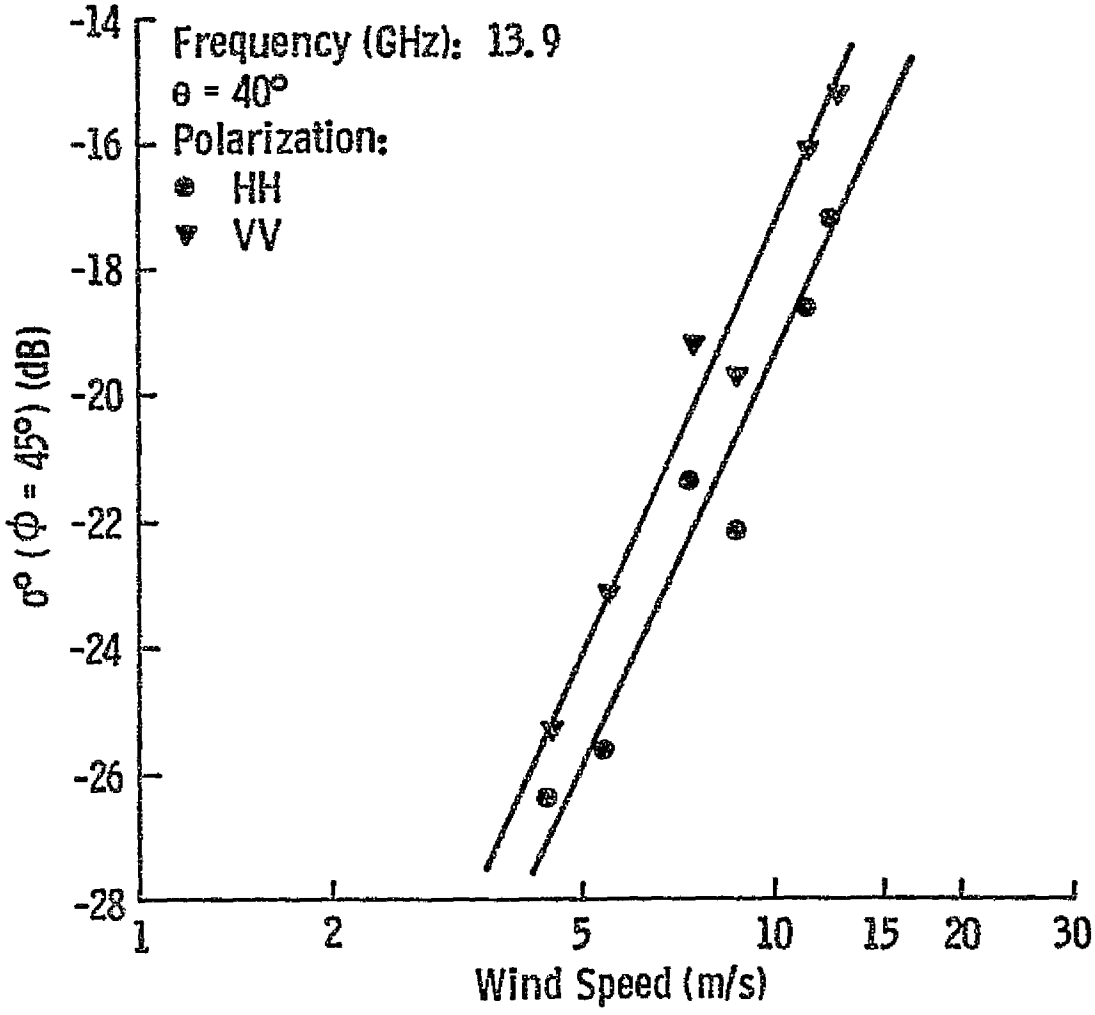

Figure 3: Wind speed power-law dependence of the radar cross section at $\phi = 45^{\circ}$.

provides satisfactory fits to the data. Consequently, the wind speed can be estimated knowing the average of the two scatterometer measurements, i.e.

$$\hat{U} = \left[a\ \sigma^{o}_{AV}\right]^{\gamma} \tag{2-7}$$

where $a = 1/a_1$: $a(HH) = 85.1$, $a(VV) = 60.0$

$\gamma = 1/\gamma_1$: $\gamma(HH) = 0.47$, $\gamma(VV) = 0.45$

As a test, wind speed errors were obtained from scattering coefficients calculated using the wind direction models. As seen from the results in Figure 4, the wind speed error can be expressed by

$$U_{err} = C_o + C_1 \cos(\phi_1 + 45^o).$$

A wind speed correction of this form would offer considerable improvement if the data set had no fading or other random fluctuations. However, the SASS measurements will include fading and instrument bias.

At present, no wind speed correction is employed. When this technique is applied to orthogonal pairs of JONSWAP measurements the results are still within the UWG's guideline of ±2 m/s ($u \leq 20$ m/s) or ±10% ($u \geq 20$ m/s). As an illustration, the wind speed errors for flight 17 are shown in Figure 5. Appendix C shows the wind speed error for the remaining JONSWAP flights.

2. Wind Direction

In the previous section, it was shown that the wind direction effects on σ^o can be modelled by expression (3a). The regression coefficients of (3a) have a wind speed dependence given by Equation (4). In Section A, a method was discussed for determining an estimate of the wind speed, $\hat{U}$. Using this estimate of wind speed, the scattering measurement can be modelled by

$$\sigma^o = \hat{A}_2 \cos 2\phi_w + \hat{A}_1 \cos\phi_w + \hat{A}_o \tag{2-8}$$

where $\hat{A}_N$ are estimates obtained from (4) using the $\hat{U}$ from (7). Consequently, the wind direction, ϕ_w, can be found from

$$\phi_w = \cos^{-1}\left\{\frac{-\hat{A}_1 \pm \sqrt{\hat{A}_1^2 - 8\hat{A}_2(\hat{A}_o - \hat{A}_2 - \sigma^o)}}{4\hat{A}_2}\right\} \tag{2-9}$$

Figure 4a: Predicted wind speed errors vs U for HH-polarization

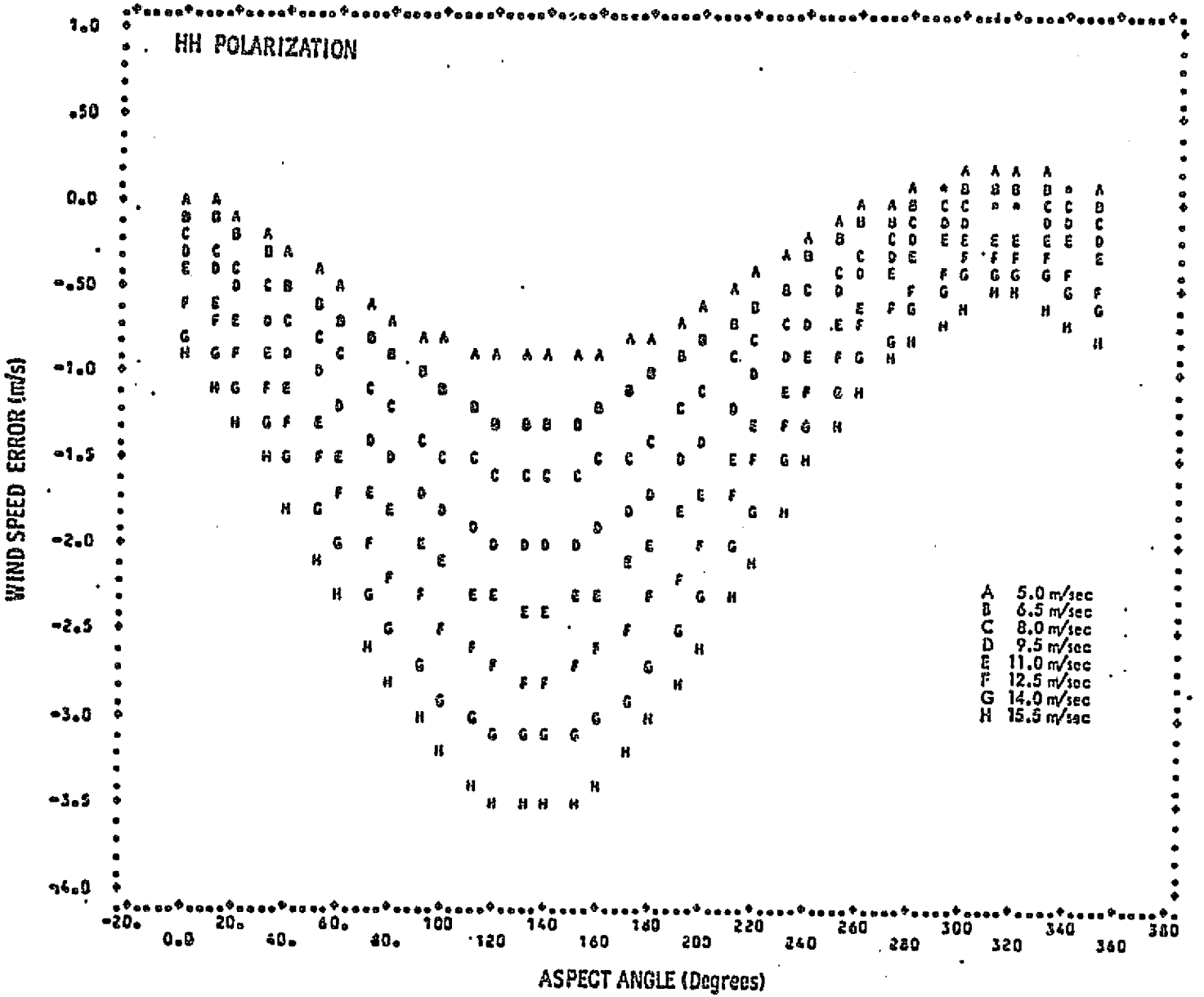

Figure 4b: Predicted wind speed errors vs U for VV-polarization

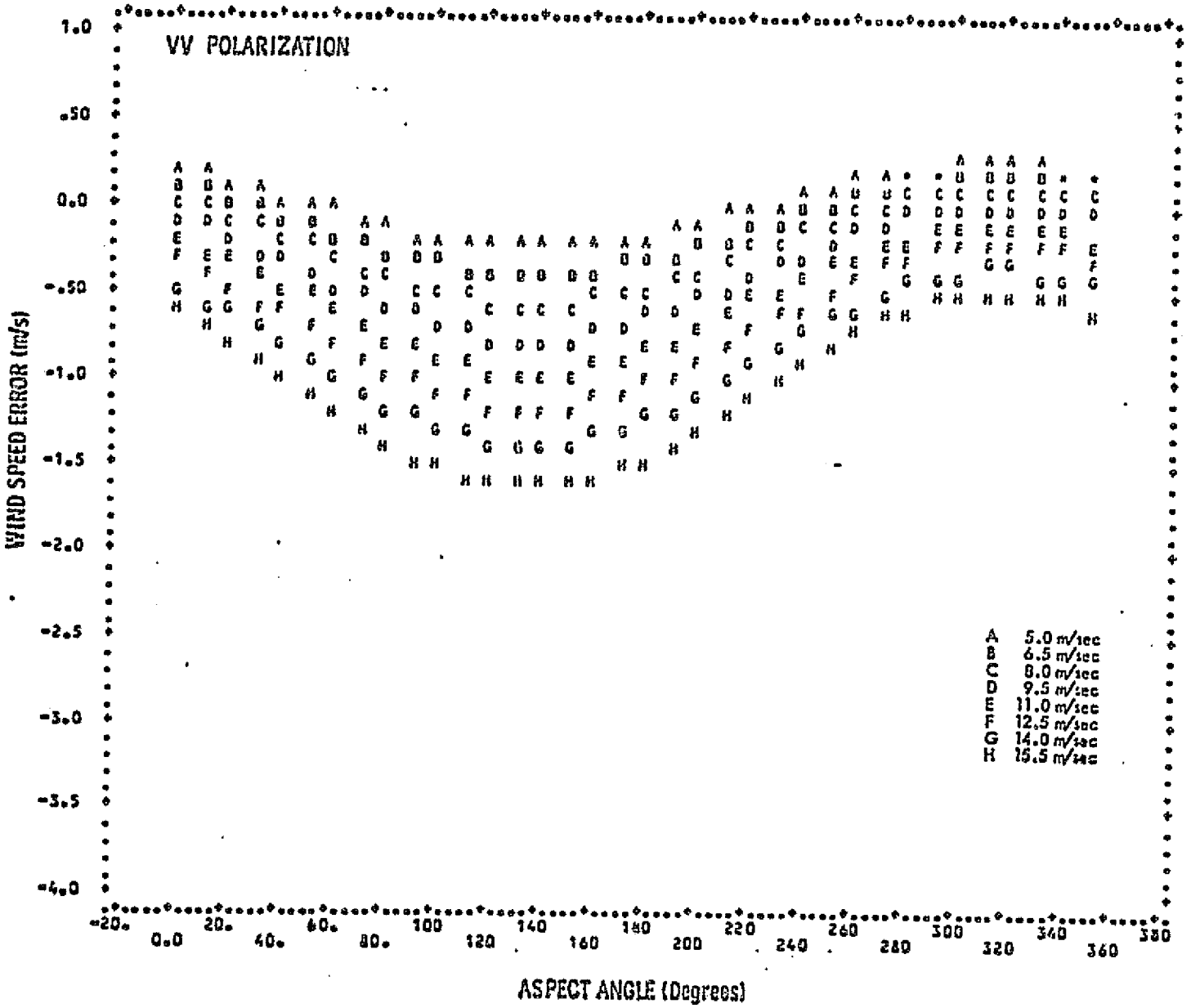

Figure 5a: Wind speed errors vs U for Flight 17, HH.

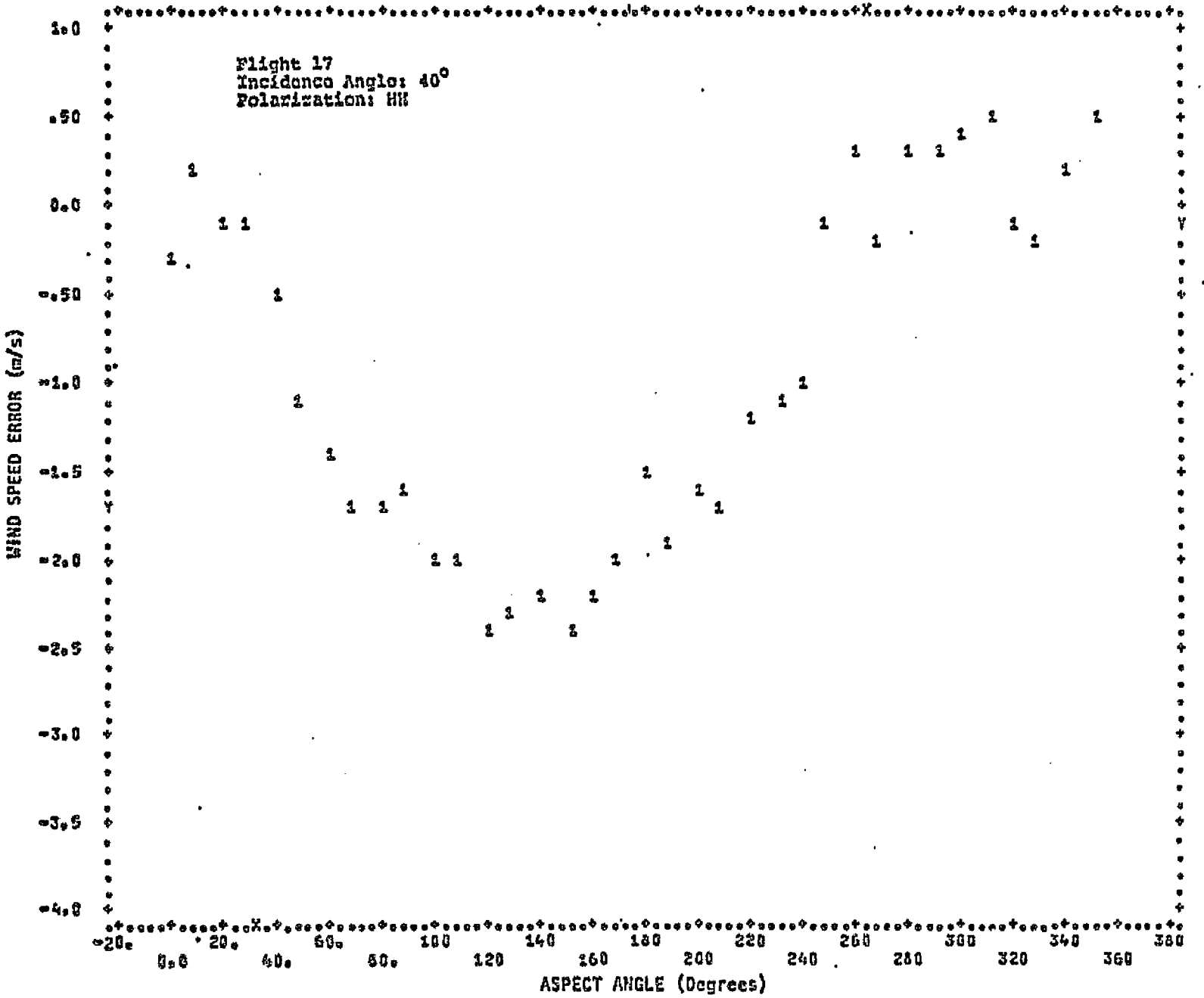

Figure 5b: Wind speed errors vs U for flight 17, VV.

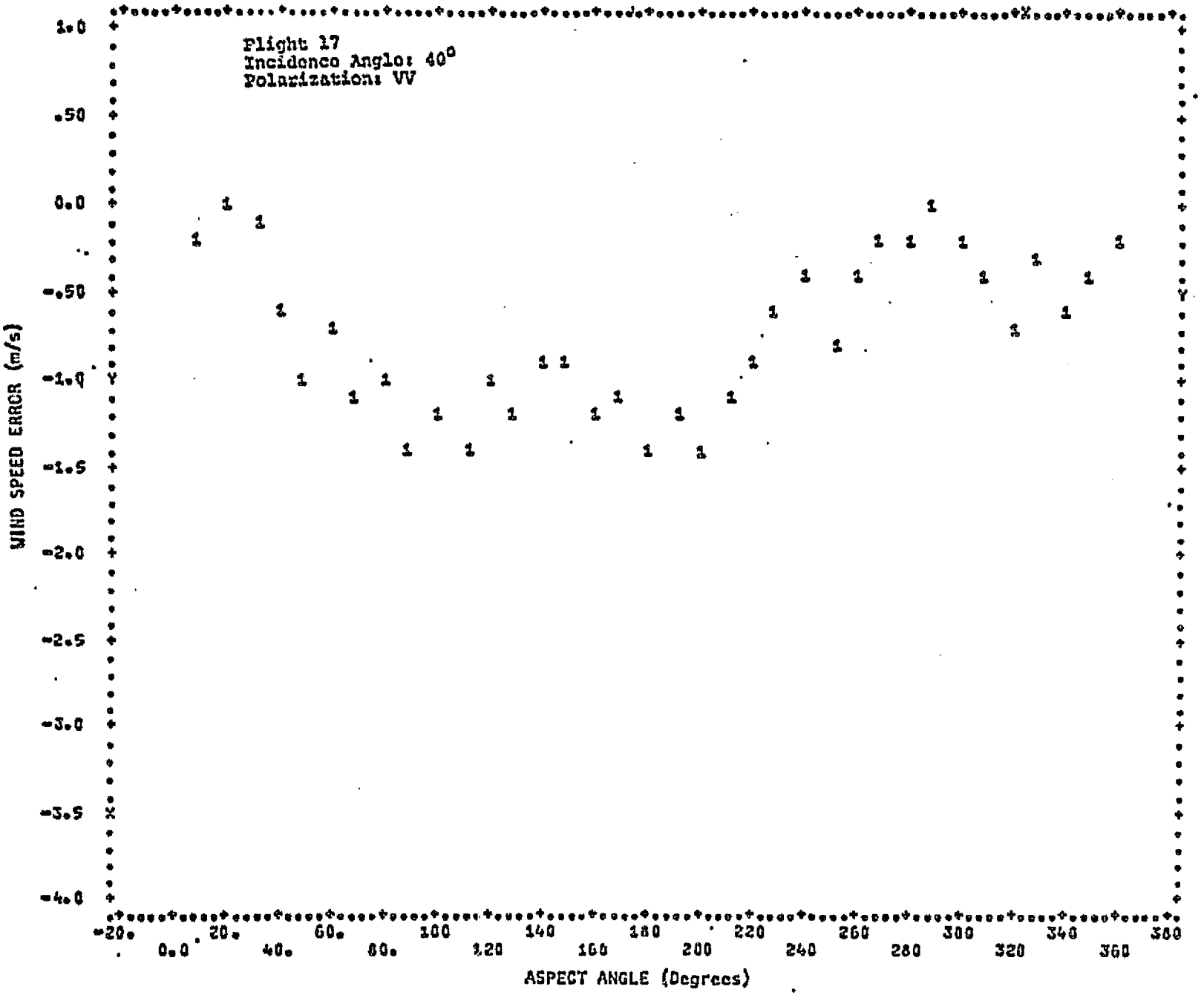

Equation (9) holds for all incidence angles for which Model 1 is valid.

This inversion yields two estimated wind directions for each scatterometer measurement, one in the first quadrant and one in the second. These are mirrored to obtain estimates in the third and fourth quadrants, respectively. No information is known from the measurements themselves to determine the wind quadrant, but in an operational satellite system, such as SeaSat, this can be obtained from V-IR or conventional meteorological data.

Examples of the wind direction errors obtained when applying this technique to JONSWAP flight 17 are shown in Figure 6, where A and B are the fore and aft beam results, respectively. Considerable improvement can be obtained by averaging the results of both fore and aft measurements after they have been corrected to North. Results for flight 17 using this correction are shown in Figure 7. The wind direction errors produced by this method for vertical polarization are considerably lower than those for horizontal polarization, as seen by Table 3. One explanation for this observation is that the upwind-downwind scattering coefficient ratio increases with the wind speed much faster for the horizontally polarized case. Also, the scattering coefficient for the horizontal polarization can be much smaller than that for the vertical polarization and it drops off rapidly at large incidence angles. These later properties make it much more difficult to obtain reliable measurements.

C. Conclusion

The wind direction properties of radar backscatter were modelled by cosine fourier series through the fourth harmonic in wind direction from upwind. A comparison with JONSWAP data indicated that the effects of the third and fourth harmonic are neglible.

A simple inversion technique, which uses two orthogonal scattering measurements, is also shown which eliminates the effect of wind speed and direction. The procedure used is as follows:

(1) Estimate wind speed from average σ^o from 2 antennas

(2) Estimate coefficients of directional equation by using σ^o estimate from (1) and previously determined wind-speed dependence of coefficients.

Figure 6a: Wind direction errors vs ϕ using only 1 beam, HH.

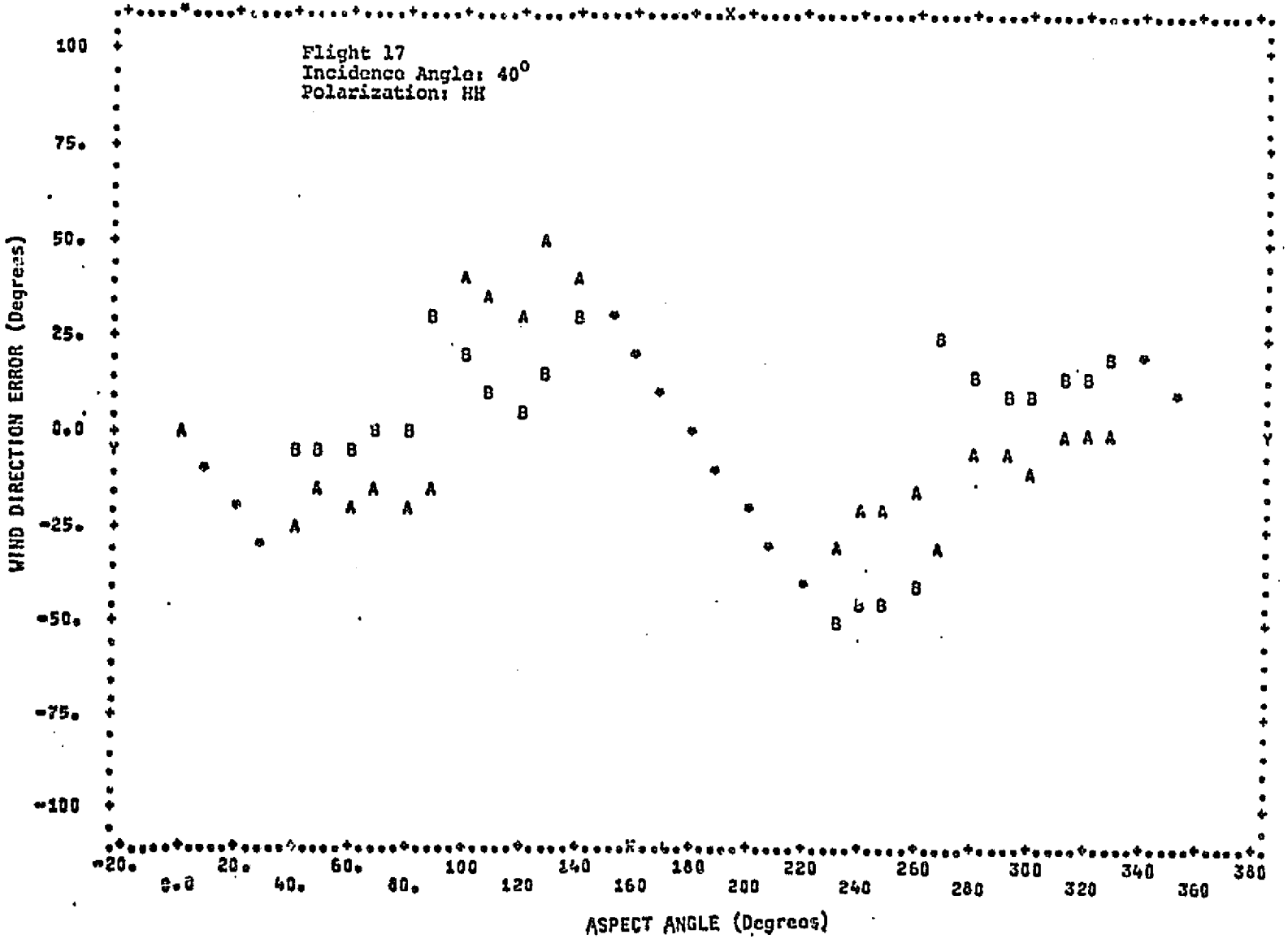

Figure 6b: Wind direction errors vs ϕ using only 1 beam, VV.

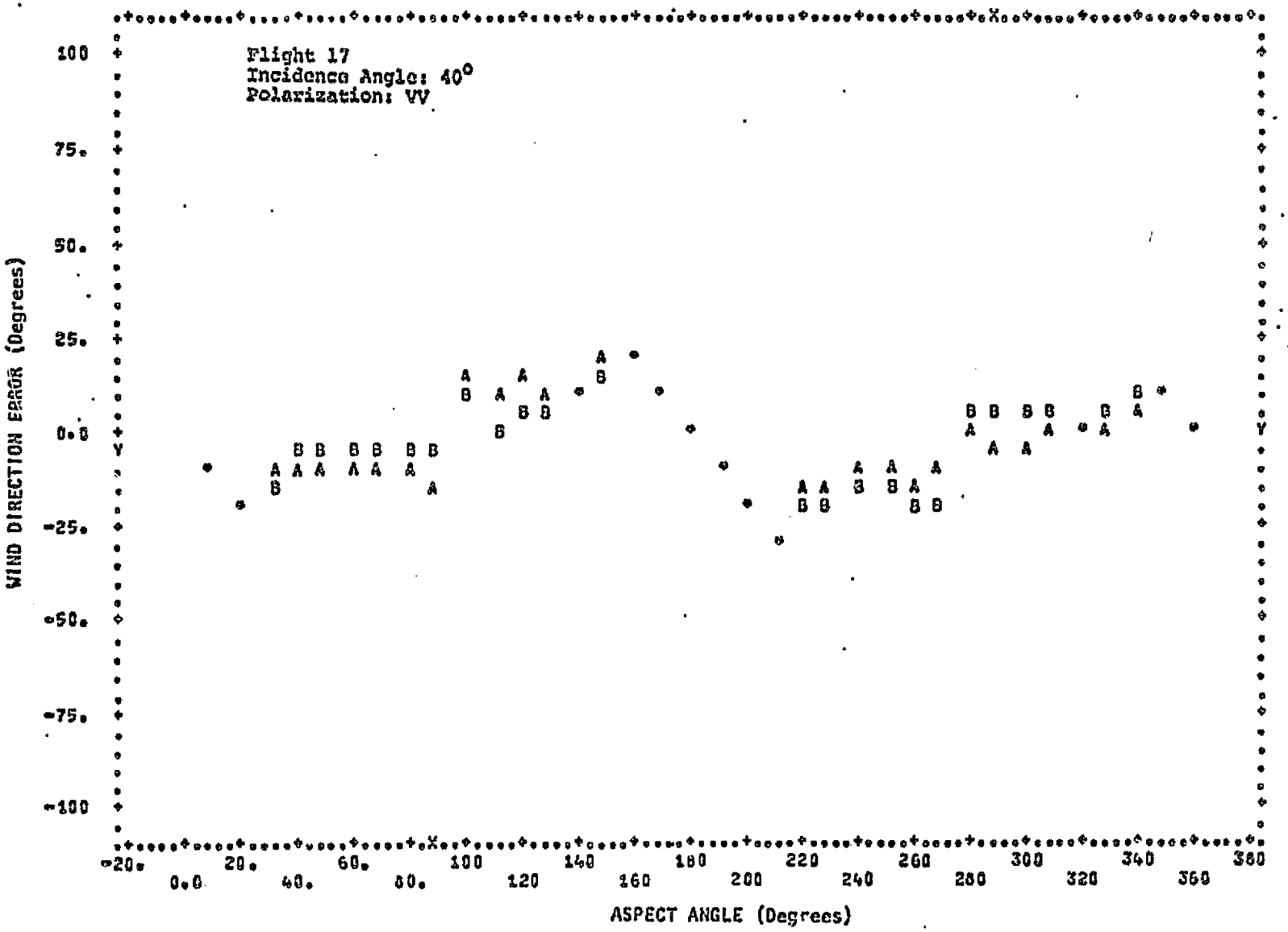

Figure 7a: Wind direction errors vs ϕ using corrected averaged results of fore and aft beams, HH.

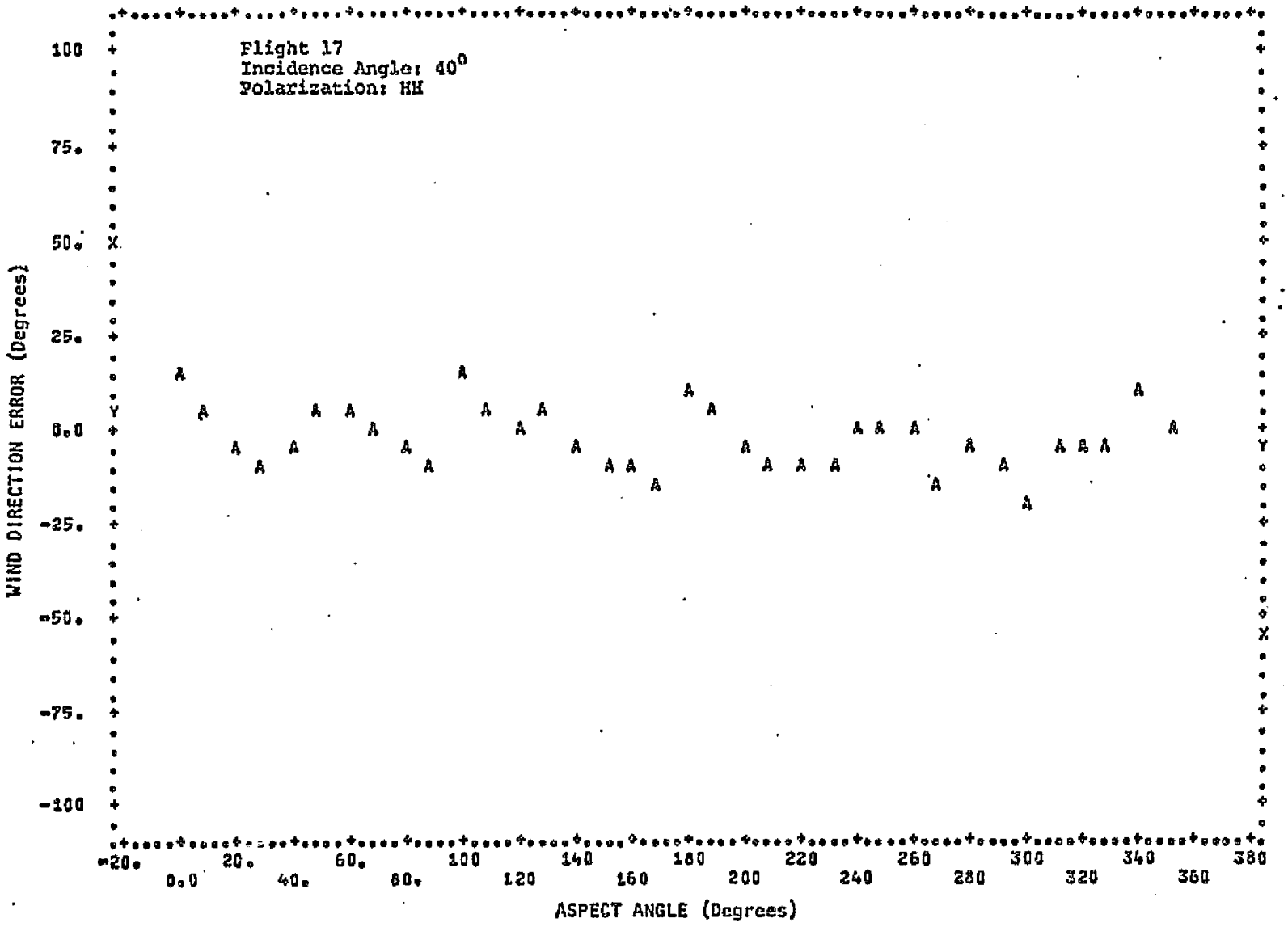

Figure 7b: Wind direction errors vs ϕ using corrected averaged results of fore and aft beams, VV.

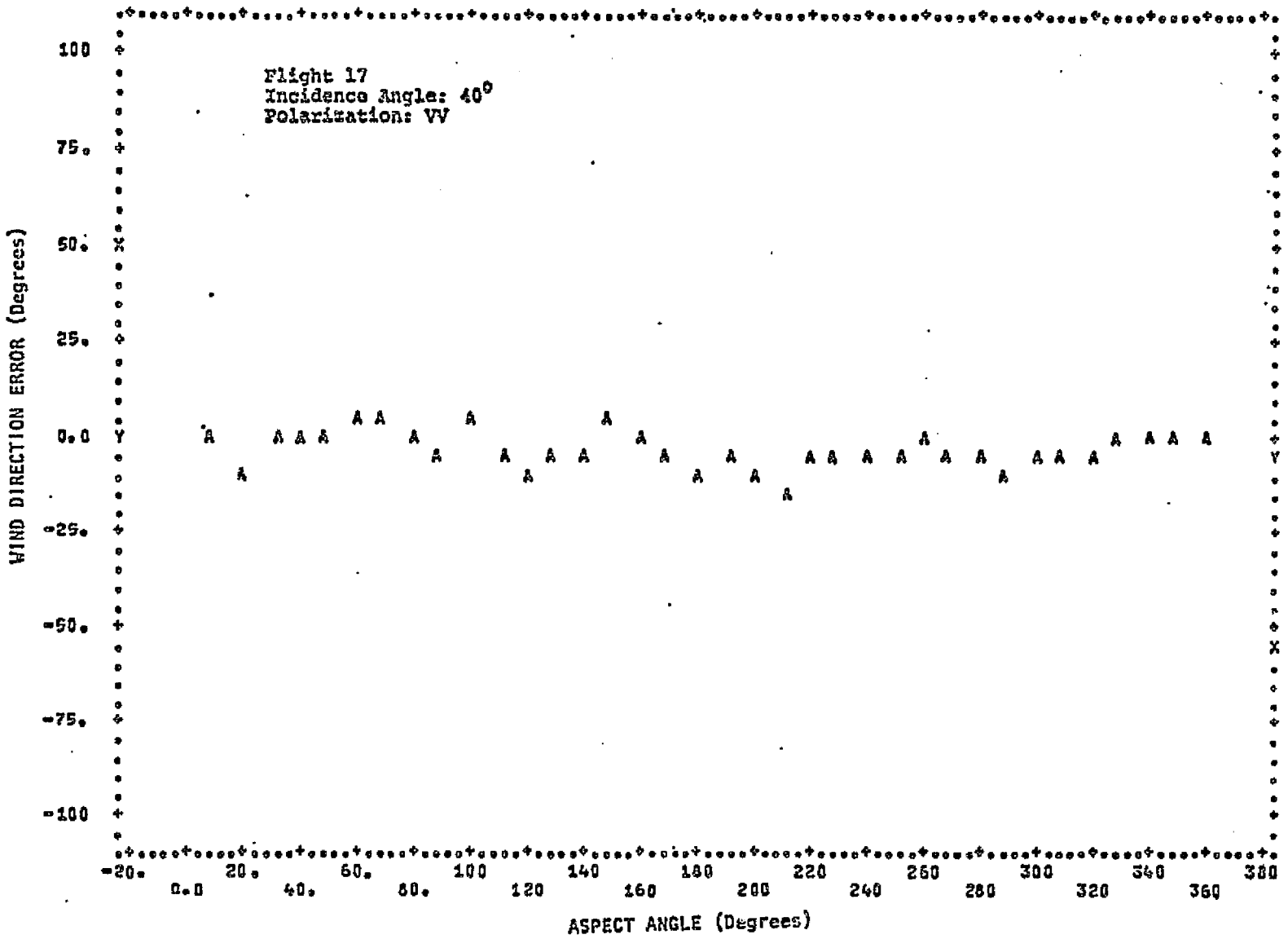

Table 3: WIND DIRECTION ESTIMATE ERRORS (IN DEGREES)

FLIGHT	HORIZONTAL POLARIZATION		VERTICAL POLARIZATION	
	MEAN ERROR	STD. DEV.	MEAN ERROR	STD. DEV.
13	-3.87	11.21	-4.19	9.42
14	1.49	12.78	2.87	5.45
16	3.19	10.77	3.81	6.85
17	-2.21	8.45	-3.34	4.57
18	-0.81	8.90	-1.23	5.42
19	-1.55	11.95	-0.75	7.43

(3) Estimate direction using coefficients from (2) and σ^o measured with antenna 1.

(4) Estimate direction using coefficients from (2) and σ^o measured with antenna 2.

(5) Average estimates of direction from (3) and (4) to produce new estimate of direction.

(6) Determine quadrant by comparing the 4 estimates of (5) with data from other sources such as:
    (A) concurrent satellite photos
    (B) meteorological analysis and forecasts based on observations at other times and places.

The results show that vertical-polarization is more effective in determining both wind speed and direction than horizontal-polarization.

3.0 COMPARISON OF SOME SCATTERING THEORIES WITH RECENT SCATTEROMETER MEASUREMENTS

A. Introduction

In recent years there has been general agreement that the scattering properties of the sea surface can be explained reasonably well in terms of a two-scale roughness model. It is understood in the two-scale model that the small waves are assumed to satisfy the small perturbation assumptions and that the large scale waves are to satisfy the Krichhoff approximation. This means that only certain high and low frequency portions of the entire sea spectrum are included as significant contributors to sea scatter. The basic approach is to use the first order result of the small perturbation method to compute the scattering coefficient due to small scale waves and to account for the tilting effect of the large scale waves by averaging this scattering coefficient over the slope distribution of the large scale waves. The tilting process not only produces an averaging effect but also causes depolarization of the incident electromagnetic field in the local reference frame leading to additional higher order terms (Fung, 1976). However, these higher order terms are unimportant when dealing with small sea slopes. As a result most authors ignore these higher order terms. It is known that the first order perturbation approach invariably produces a larger scattering coefficient for the vertical polarization than that for the horizontal polarization near grazing incidence. This fact remains unchanged after averaging. Since some recent near-grazing observations (Long, 1974) indicate that there are cases where the converse is true, special care must be exercised when applying such a theory to explain data at incident angles greater than 80°. As Wright (1968) pointed out, this type of theory is valid only in the mid-angular range approximately 30° to 80°.

Sea scatter theories using the two-scale model (Wright, 1968, Chan and Fung, 1977, Bass, et al., 1968, Wu and Fung, 1972, Long, 1974, Valenzuela, 1967) may be further categorized into two types: (a) those which use Phillips' (1966) sea spectrum together with a slope distribution of the

large scale waves defined with respect to the horizontal plane, and (b) those which use a growing sea spectrum (Pierson, 1975, Mutuyasu and Honda, 1974, Sutherland, 1967) and a slope distribution of the large scale waves defined with respect to the plane normal to the look direction. In the next section we shall briefly describe these two types of theory following Wright for type (a) and Chan and Fung for type (b). The predictions of these theories are compared with experimental observations in Section C and conclusions are given in Section D.

B. The Two-Types of Two-Scale Models

Wright's Sea Model. Many authors (Wright, 1968, Chan and Fung, 1977 and Valenzuela, 1967) have shown that for a slightly rough surface which satisfies the small perturbation assumption, the backscattering coefficient is given by

$$\sigma_{pp}(\theta,\phi) = 8k^4\sigma^2|\alpha_{pp}|^2 W(\theta,\phi) \qquad (3\text{-}1)$$

where for horizontal polarization, p = h and

$$\alpha_{hh} = \cos^2\theta R_h$$

R_h is the Fresnel reflection coefficient for horizontal polarization defined in terms of the electric field. For vertical polarization, p = v and

$$\alpha_{vv} = R_v\cos^2\theta + (k'^2 - k^2)T_v^2\sin^2\theta/(2k'^2)$$

where R_v and T_v are the Fresnel reflection and transmission coefficients defined in terms of the magnetic field for vertical polarization. In α_{pp}, k is the wave number in air; k' is the wave number in sea water and θ is the angle of incidence. $W(\theta,\phi)$ is the normalized anisotropic sea spectrum and σ^2 is the variance of the small scale sea waves. To include the tilting effect of the large scale waves, $|\alpha_{pp}|^2$ should first be modified by including higher order correction terms due to tilting and then (3-1) is averaged with respect to the slope distribution functions of the large

scale waves recognizing that θ in (3-1) is to be replaced by the local incidence angle, θ', which is a function of the local slopes. Wright indicated that satisfactory approximation could be achieved by assuming the spectrum to be independent of the tilt angles except as they affect the local incidence angle. Letting α be the tilt angle in the plane of incidence and β be the tilt angle in the orthogonal direction, he obtained the backscattering coefficient as

$$\sigma^\circ_{pp}(\theta) = 8k^4\sigma^2 \iint |G_{pp}(\theta, Z_x, Z_y)|^2 W(k\sin\theta') P(Z_x, Z_y) dZ_x dZ_y \qquad (3\text{-}2)$$

where
$$G_{vv} \cong \alpha_{vv}(\theta')$$
$$G_{hh} \cong -\alpha_{hh}(\theta') + \frac{\tan^2 Z_y}{\sin^2\theta'}\alpha_{vv}(\theta')$$
$$\theta' \cong \theta + Z_x$$
$$P(Z_x, Z_y) = (2\pi s^2)^{-1} \exp\left[-\frac{Z_x^2 + Z_y^2}{2s^2}\right]$$
$$s^2 = 0.004 + 0.81 \times 10^{-3} U$$
$$\sigma^2 W(2k\sin\theta') = 0.585 \times 10^{-2} (2k\sin\theta')^{-4}$$

and U is the windspeed in m/sec measured 12.5 m above sea level. Note that higher order correction terms due to tilting are considered negligible for vertical polarization so that $G_{vv} \cong \alpha_{vv}(\theta')$ while for horizontal polarization a correction term is added to $\alpha_{hh}(\theta')$ to form G_{hh}. The slope distribution, $P(Z_x, Z_y)$, is a simplified form reported by Cox and Munk (1954). From the definition of the sea spectrum it is clear that it is independent of wind speed. Thus, wind dependence in $\sigma^\circ_{pp}(\theta)$ comes only through the slope distribution, $P(Z_x, Z_y)$.

Chan and Fung's Model. The model reported by Chan and Fung (1977) for the backscattering coefficient is as follows:

$$\sigma^\circ_{pp}(\theta) = 8k^4\sigma^2 \int_{-\infty}^{\infty}\int_{-\infty}^{\infty} |\alpha_{pp}|^2 W(\theta', \phi) P_\theta(Zx', Zy') dZx dZy \qquad (3\text{-}3)$$

which is essentially the same as (3-2) except for the definitions of $P(Zx', Zy')$ and $W(\theta', \phi)$ and the fact that higher order corrections to α_{pp} are ignored. In Chan and Fung (1977) it was shown that the probability of occurrence of a given slope varies with the direction of observation. For this reason

the probability distribution function $P(Zx',Zy')$ reported by Cox and Munk is projected along the look direction first before it is used in the averaging process, i.e.

$$P_\theta(Zx',Zy') = (1 + Z\tan\theta)P(Zx',Zy') \tag{3-4}$$

In (3-4), $P(Xx', Zy')$ is the slope distribution of the large scale waves as viewed at an incidence angle θ and is defined in the prime coordinates (Figure 8) whose x'-axis is parallel to the wind direction. It is assumed that the plane of incidence is the XZ plane and that the angle between the x-axis and the x'-axis is ϕ so that an upwind observation occurs when $\phi = 0$. In view of Figure 1, the slopes in the primed and the unprimed coordinates are related as follows:

$$Zx' = Zx\cos\phi + Zy\sin\phi$$
$$Zy' = Zy\cos\phi - Zx\sin\phi$$

The form of the slope distribution of a sea surface, $P(Zx',Zy')$, was reported by Cox and Munk (1954) to be

$$P(Zx',Zy') = \frac{F(Zx',Zy')}{2\pi\sigma_u\sigma_c}\exp\left[-\frac{Zx'^2}{2\sigma_u^2} - \frac{Zy'^2}{2\sigma_c^2}\right]$$

where

$$F(Zx',Zy') = 1 - \frac{C_{21}}{2}\left(\frac{Zy'^2}{\sigma_c^2} - 1\right)\frac{Zx'}{\sigma_u} - \frac{C_{03}}{6}\left(\frac{Zx'^3}{\sigma_u^3} - \frac{3Zx'}{\sigma_u}\right)$$
$$+ \frac{C_{40}}{24}\left(\frac{Zy'^4}{\sigma_c^4} - 6\frac{Zy'^2}{\sigma_c^2} + 3\right) + \frac{C_{22}}{4}\left(\frac{Zy'^2}{\sigma_c^2} - 1\right)\left(\frac{Zx'^2}{\sigma_c^2} - 1\right)$$
$$+ \frac{C_{04}}{24}\left(\frac{Zx'^4}{\sigma_u^4} - 6\frac{Zx'^2}{\sigma_u^2} + 3\right)$$

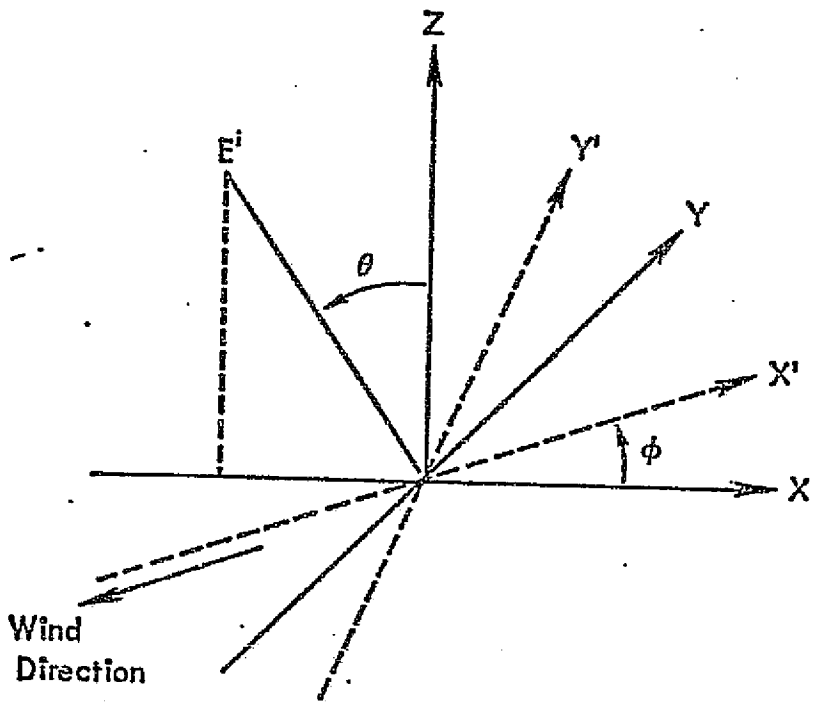

Figure 8: Geometry of the problem.

$$C_{40} = 0.4 \qquad C_{22} = 0.12 \qquad C_{04} = 0.23$$

$$C_{21} = 0.001 - 0.0086U$$

$$C_{03} = 0.04 - 0.033U$$

$$\sigma_u^2 = \sigma_s^2/(1 + R_o)$$

$$\sigma_c^2 = R_o\sigma_u^2$$

$$R_o = \{0.003 + 1.92 \times 10^{-3}U)/3.16 \times 10^{-3}U$$

$$\sigma_s^2 = \int_0^{0.359} K^2 s(K)dK$$

In the expressions above U is the wind speed in meters per second at an altitude of 12.5 m above the sea horizon. The definition of s(K) is given in accordance with Pierson (1975) as

$$S(K) = S_i(K), \qquad K_{i-1} < K < K_i$$

$$S_1(K) = \frac{a}{K^3} \exp\left[-\frac{0.74g^2}{K^2U(U_*)^4}\right], \qquad 0 < K < K_1 = \frac{K_2U_{*m}^2}{U_*^2}$$

$$S_2(K) = aK_1^{-1/2}K^{-5/2}, \qquad K_1 < K < K_2 = 0.359$$

$$S_3(K) = S_4(K_3)\ (K/K_3)^q, \qquad K_2 < K < K_3 = 0.942$$

$$S_4(K) = 0.875(2\pi)^{\rho_1 - 1}\frac{g + 3gK^2/13.1769}{(gK + gK^3/13.1769)^{(\rho_1 + 1)/2}} \qquad K_3 < K < K_4$$

$$S_5(K) = 1.473 \times 10^{-4}U_*^3K_m^6K^{-9} \qquad K_4 < K < \infty$$

K_4 can be found numerically by setting $S_4(K_4)$ equal to $S_5(K_4)$.

U_* = friction velocity, $U_* > U_{*m}$

$K_m = (13.1769)^{1/2}$

$q = \log_{10}[S_2(K_2)/S_4(K_3)]/\log_{10}(K_2/K_3)$

$\rho_1 = 5.0 - \log_{10}U_*$

$z_o = 0.684/U_* + 4.28 \times 10^{-5}U_*^2 - 4.43 \times 10^{-2}$

$U(U_*) = (U_*/0.4)\ \ln\ (z/z_o)$ cm/sec

$a = 4.05 \times 10^{-3}$

$g = 980$ cm/sec^2

$U_{*m} = 12$ cm/sec

The important characteristics to be noted in this spectral model are: (i) the spectrum grows with the wind; (ii) in the capillary region defined approximately by $S_4(K)$ the larger the K number the faster is the growth (i.e. faster growth of the sea spectrum occurs at larger incident angles and higher frequencies); and (iii) this model is valid to about 38 knots (Pierson and Stacy, 1973). In accordance with Mitsuyasu and Honda, their model can be valid to velocity as high as 33m/sec at 10 meters above the sea horizon. Thus, the theory may be valid to higher wind speed than the 38 knots when operating frequency is such that only their portion of the sea spectrum is the significant contributor.

The relationship between S(K) and $W(\theta',\phi)$ can be shown to be (Chan and Fung, 1977)

$$\sigma^2 W(K,\phi) = \frac{S(K)}{2\pi K} \left[1 + 2\,\frac{1-R}{1+R}\cos 2\phi\right] \tag{3-5}$$

where $K = 2k\sin\theta'$ and R is the ratio of the crosswind slope variance to the upwind slope variance. Note that R_o is the same as R except that it is for the large scale waves only. It is believed that R should be somewhat less than R_o. However, since the exact expression is not known, the theory is illustrated using Cox and Munk's clean sea model for R. Upon substituting (3-4), (3-5) into (3-3) we obtain

$$\sigma^o_{pp}(\theta,\phi) = \int_{-\infty}^{\infty}\int_{-\cot\theta}^{\infty} \frac{2}{\pi} k^3 |\alpha_{pp}|^2 \left[1 + \frac{2(1-R)}{1+R}\cos 2\right] \frac{S(2k\sin\theta')}{\sin\theta'} \cdot (1 + Z_x\tan\theta)\, P\,(Zx', Zy')\, dZ_x dZ_y \tag{3-6}$$

Equation (3-2) and (3-6) represent the two different types of sea scatter theory considered in this paper. Note that the lower limit for Zx in (3-6) is -cotθ instead of minus infinity. This is necessary in order to avoid looking at the back side of a facet. As a result, the probability density function should be renormalized with respect to this range of limit which varies with the incident angle.

C. Comparison with Sea Scatter Measurements

1. Comparison of $\sigma^o(\theta,\phi)$ versus Azimuth

The $\sigma^o(\theta,\phi)$ versus ϕ data reported by Jones and Schroeder (1977) are all at 30^o incidence angle. Comparisons between Chan and Fung's theory and these data are shown in Figure 9a and 9b for the vertically and horizontally polarized cases respectively. Wright's theory is not shown since it does not include azimuth dependence. In making these comparisons, the absolute levels of σ^o_{vv} and σ^o_{hh} at different wind speeds are disregarded. It is seen that satisfactory agreement is obtained for the variations of σ^o versus ϕ for wind speeds at 6.5 m/sec and 15 m/sec and for both polarizations. As will be shown in $\sigma^o(\theta,\phi)$ versus wind speed comparisons in Figure 10, it is rather meaningless in most cases to compare the absolute levels of $\sigma^o(\theta,\phi)$ at a single incident angle, polarization, and wind speed. This comes about because of the unavoidable scatter which is always associated with limited amount of data.

2. Comparison of $\sigma^o(\theta,\phi)$ Versus Wind Speed

Figure 10a, b, and c, show the comparisons between σ^o data reported by Jones and Schroeder (1977) and $\phi^o_{hh,vv}(\theta,\phi)$ computed using (3-2) and (3-6) versus wind speed at 19.5 m above the sea horizon for downwind and crosswind cases respectively at incidence angles 30^o, 40^o, and 50^o. In these comparisons the computed absolute levels

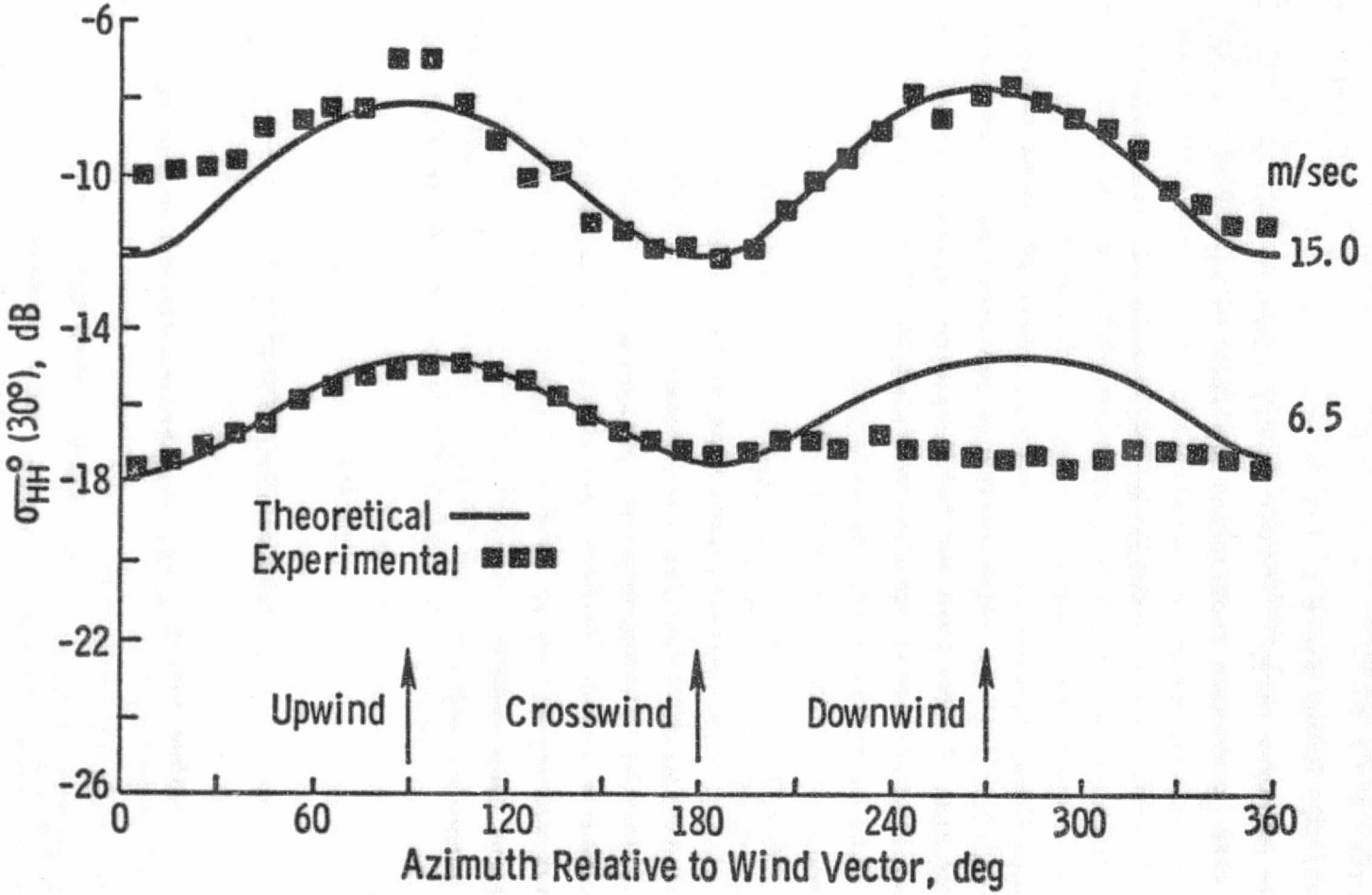

Figure 9a: Theoretical and observed values of σ° plotted versus the azimuth angle.

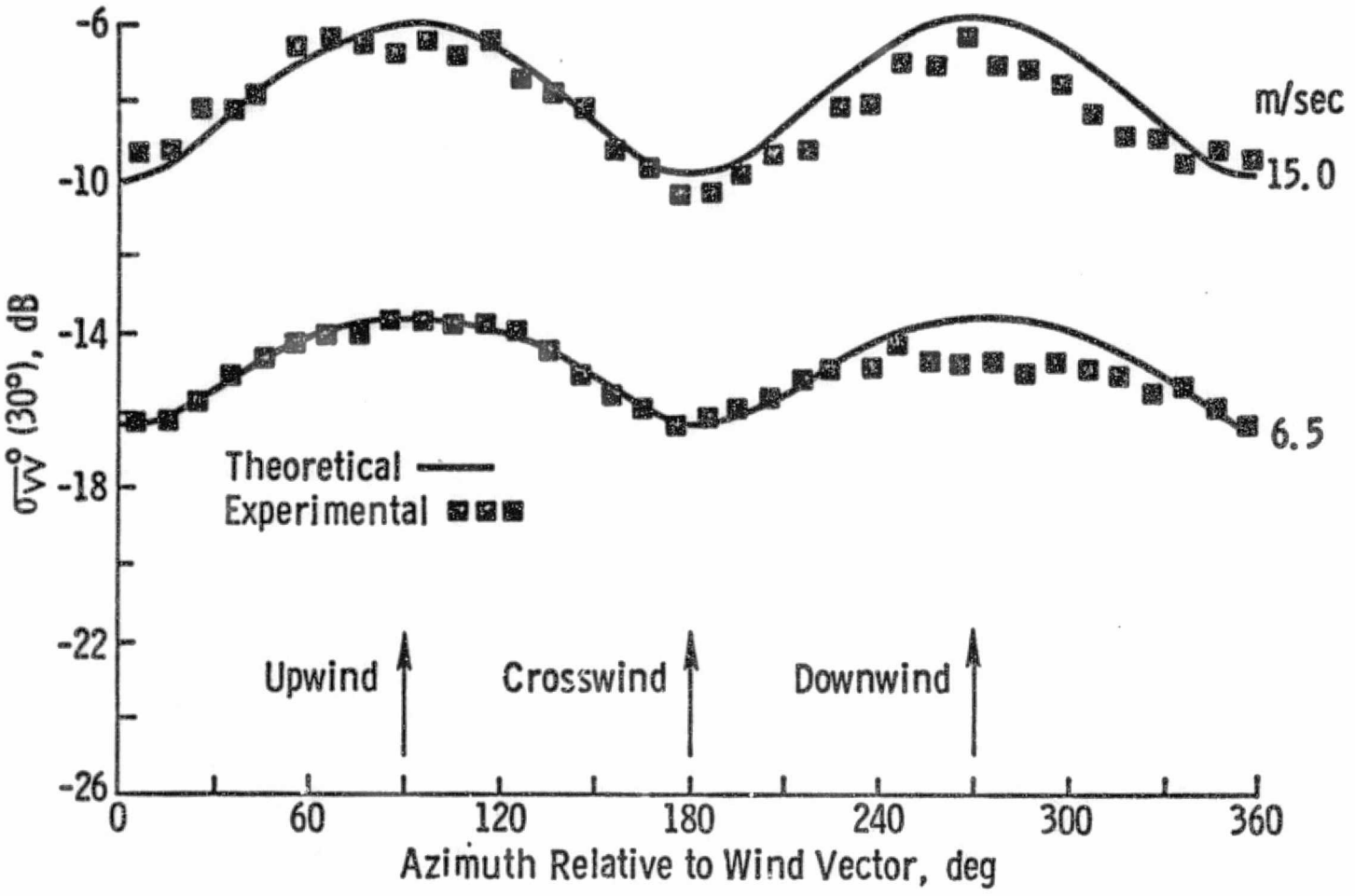

Figure 9b: Theoretical and observed values of σ^{o} plotted versus the azimuth angle.

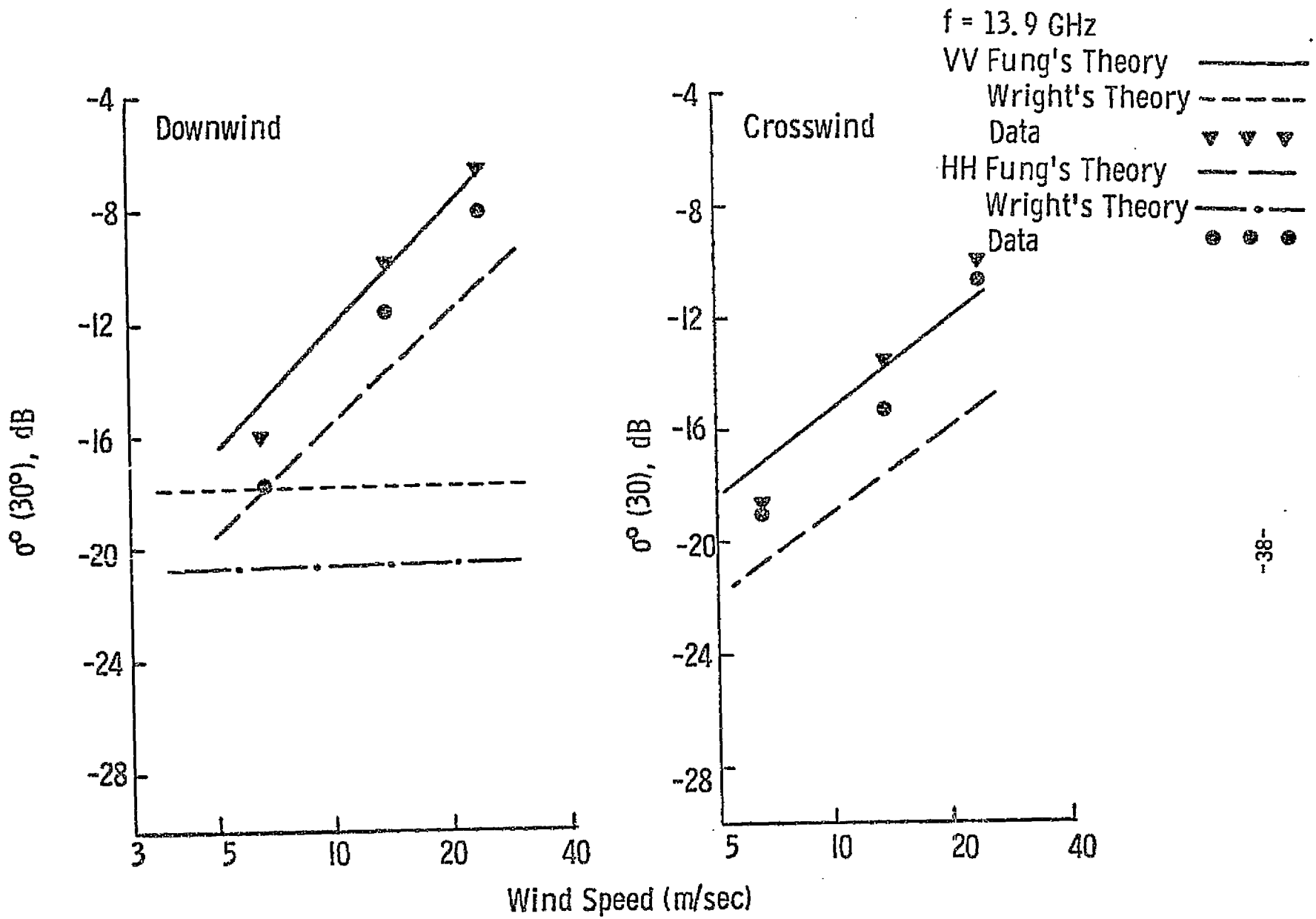

Figure 10a: Theoretical and observed values of σ° plotted versus wind speed.

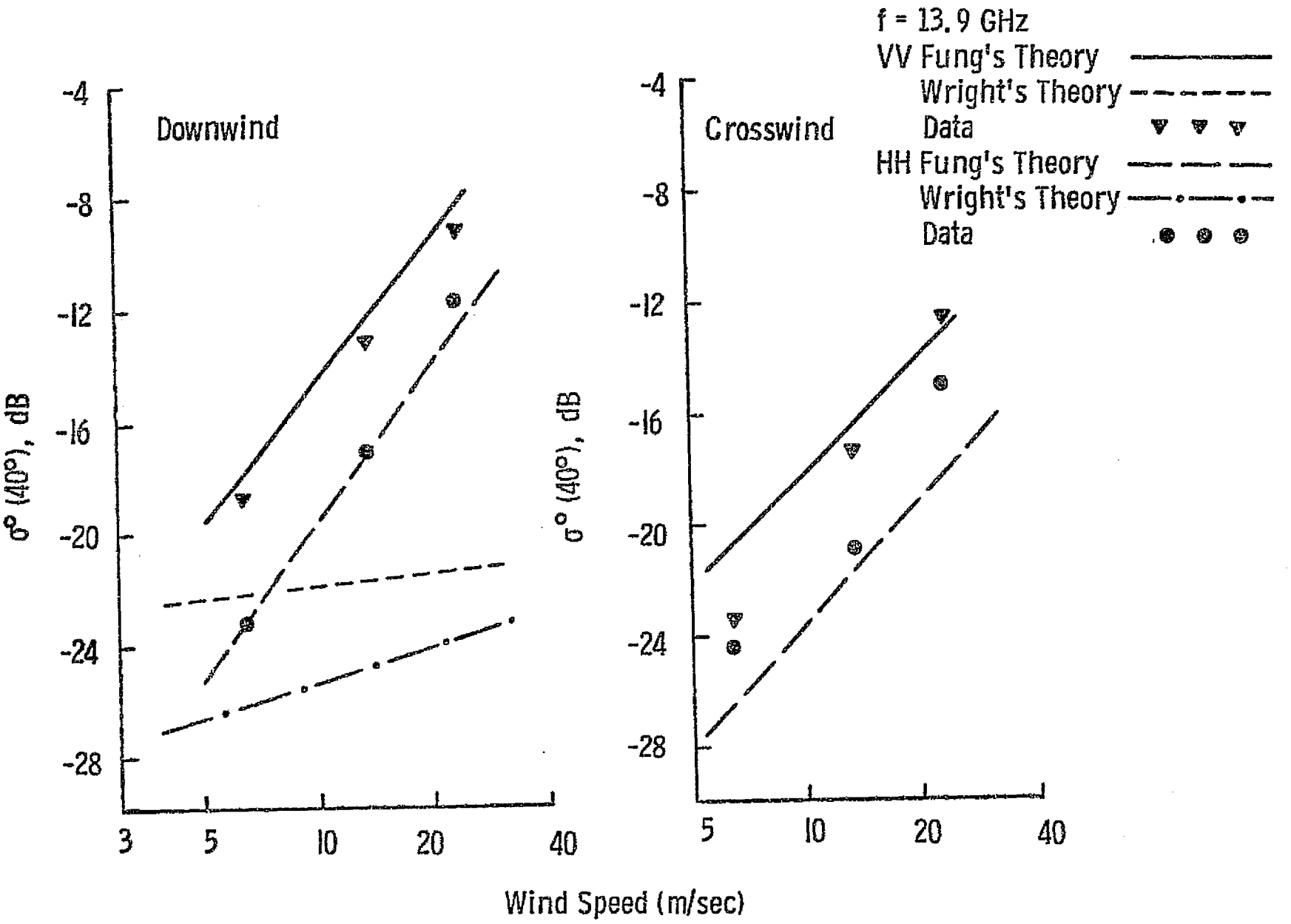

Figure 10b: Theoretical and AAFE values of σ^{o} plotted vs the wind speed, $\theta = 40^{o}$.

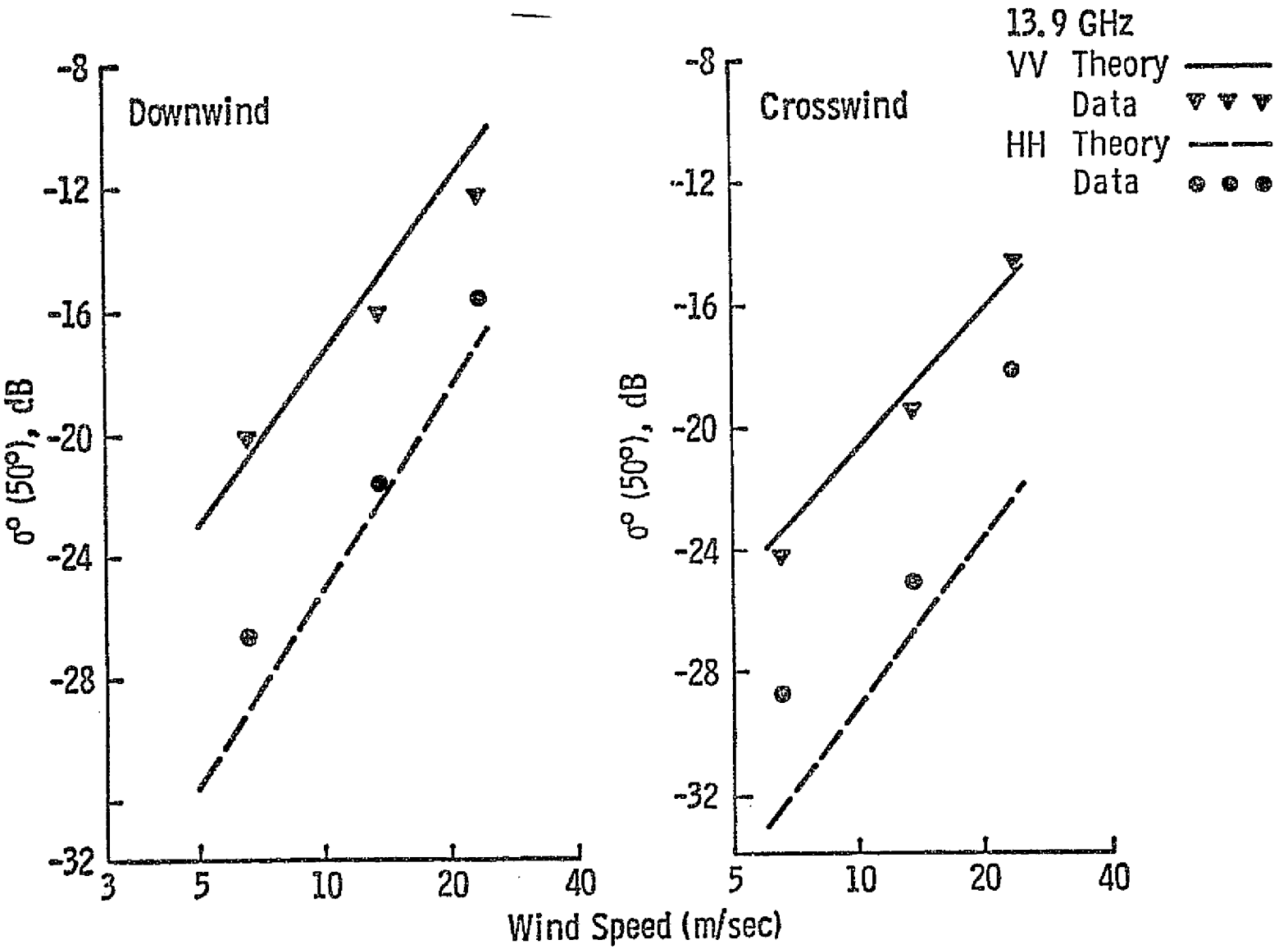

Figure 10c: Theoretical and AAFE values of σ^{o} plotted vs the wind speed, $\theta = 50^{o}$.

of $\sigma^o_{hh,vv}(\theta,\phi)$ are retained. The range of wind speeds considered is approximately between 6.2 m/sec and 15 m/sec. It is noted that the reason why $\sigma^o_{vv}(\theta,\phi)$ is much higher in level than $\sigma^o_{hh}(\theta,\phi)$ is the inherent characteristics of the first order perturbation theory. While the AAFE data are limited, they seem to agree with the predicted theoretical level separation. Also, uncorrected data, Figures 11a and b, taken from Skylab SL-2 and SL-3 at 43^o and 50^o do show a clear level separation of the predicted order of magnitude. Note that data selected from Skylab are those taken during Hurricane Ava and Tropical Storm Christine, where a continuous measurement of σ^o versus wind speed, was available. Despite clear differences at particular incident angles and wind speeds, a general agreement in absolute levels in wind speed trends and in incident angle variations is observed.

Also included in Figures 10a and 10b are the theoretical predictions from Wright's theory. It is seen that σ^o exhibits much less dependence on wind speed. This appears to be due primarily to the use of Phillips' sea spectrum model which is independent of the wind speed. Recent studies on the hydrodynamic effects of the long and the short wave interactions may serve as another explanation for the observed increase in σ^o. However, since non-linear interaction is of higher order, it does not seem likely that a full explanation can be made in terms of this effect alone. In view of the fact that the measured σ^o values do increase significantly with the wind, it appears that the two-scale scatter theory cannot provide correct predictions unless the sea spectrum is allowed to increase with the wind speed.

D. Conclusions

When an appropriate sea spectrum and sea-surface slope distribution for the large scale waves are incorporated, the two-scale scatter model appears to provide satisfactory explanations of the variation of the scattering coefficients versus polarization, azimuth, and wind speed.

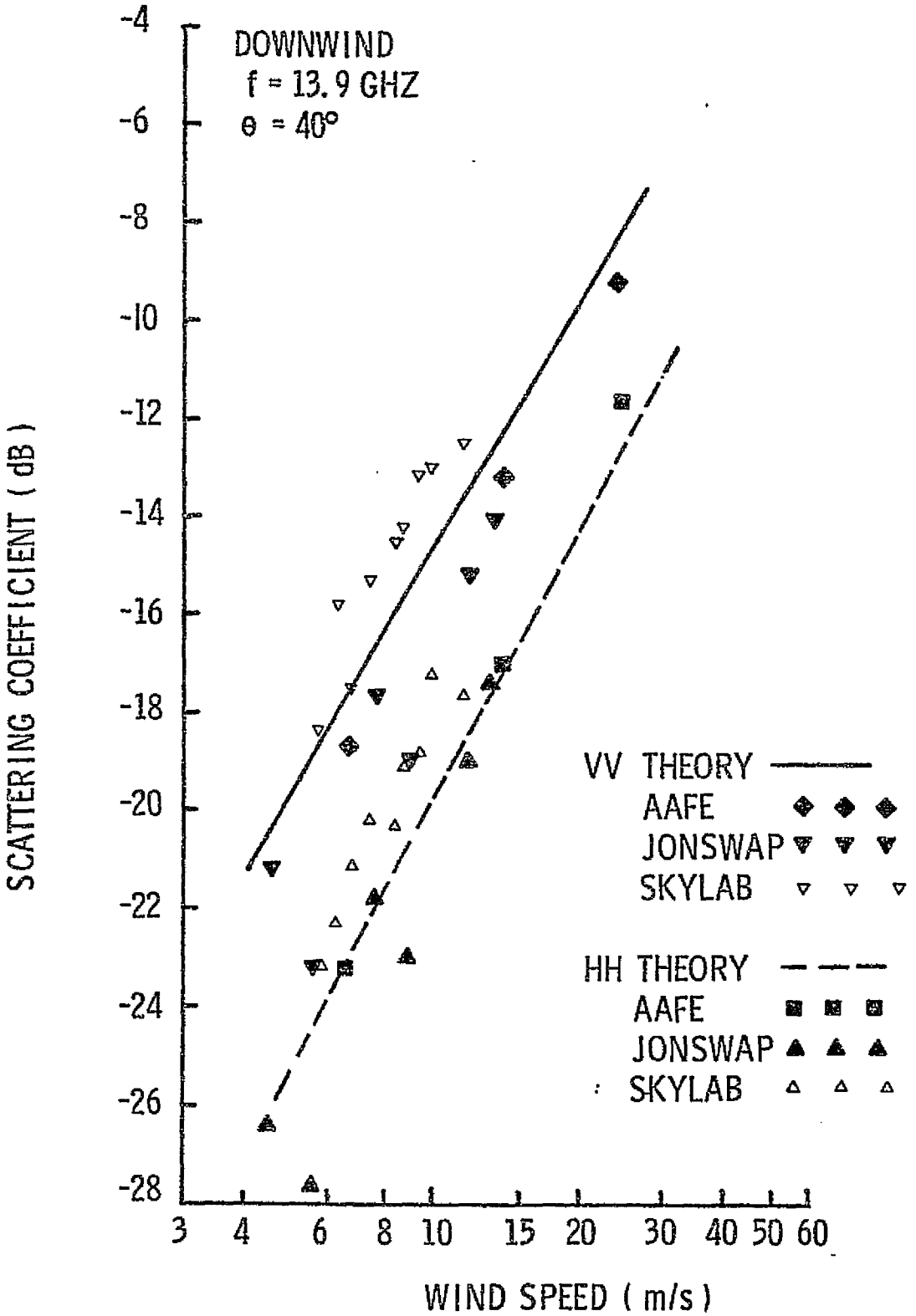

Figure IIa: Theoretical and combined experimented values of σ^o plotted vs wind speed, $\theta = 40^o$.

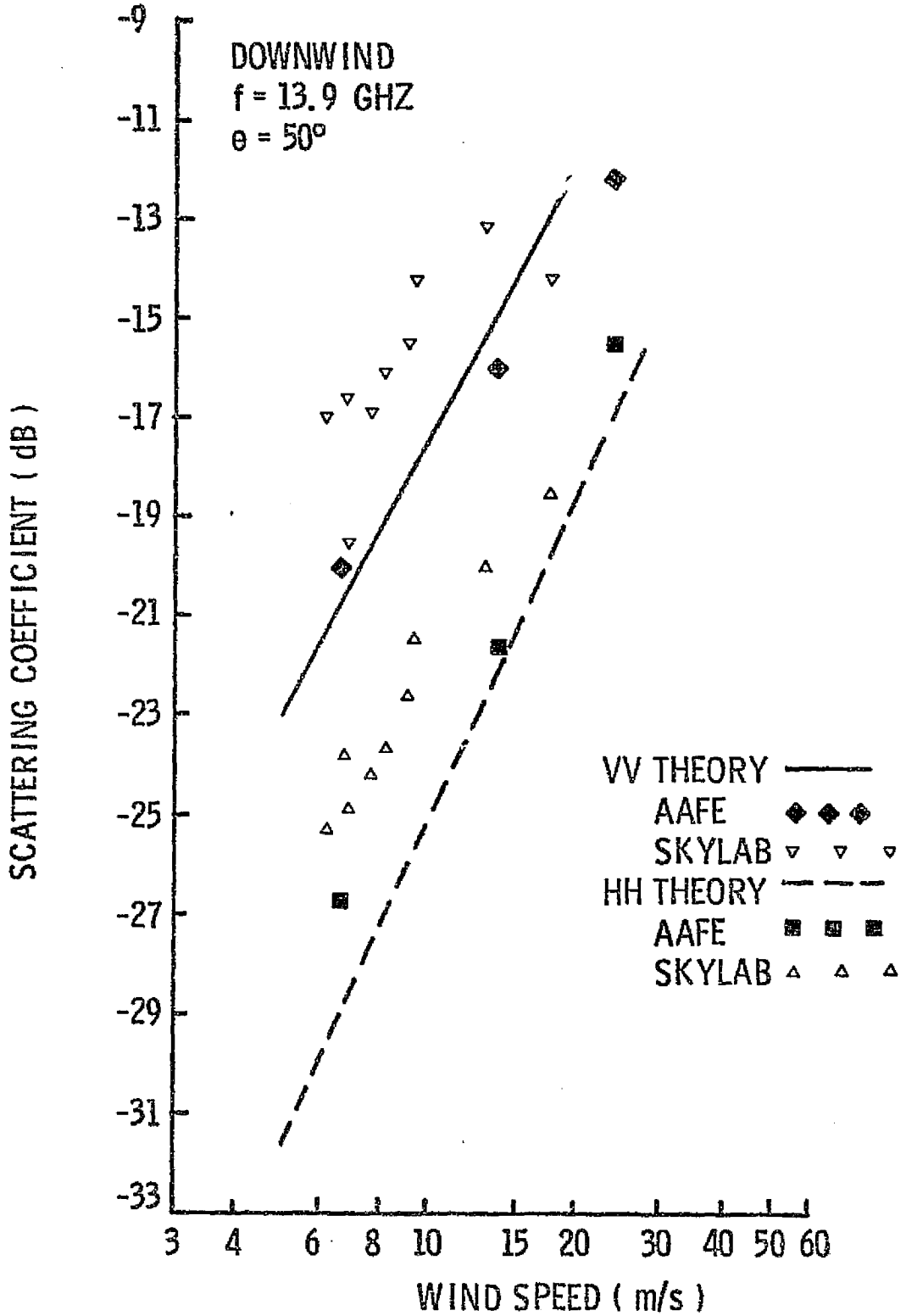

Figure 11b: Theoretical and combined experimented values of σ^o plotted vs wind speed, $\theta = 50^o$.

4.0 CONCLUSIONS AND RECOMMENDATIONS

The 1975 JONSWAP circle flight data appears to be adequately modelled by

$$\sigma^{\circ}(U,\theta,\phi_w) = A_o(U,\theta) + A_1(U,\theta)\cos(\phi_w) + A_2(U,\theta)\cos(2\phi_w) \quad (2\text{-}3a)$$

The coefficients of this model, determined through regression analysis were shown to be related to wind speed by

$$A_n(U,\theta) = \rho_n(\theta)\, U^{\gamma_n(\theta)} \quad (2\text{-}4)$$

However, previous circle flight data sets exhibit an assymetry not accomodated by this model, Afarani (1975). Explanations for these observations include both experimental problems and the possibility that they are caused by the effect of underlying wave or swell trains traveling in a direction different from the wind direction. The difficulty of making such measurements from an aircraft cannot be overestimated. Not only must the aircraft maintain a constant altitude during the circle, but either the wind conditions must be the same at all points in the five-mile diameter circle or some kind of correction must be made for differences that can only be inferred because wind measurements are made at a point near but not in the circle. Consequently, measurements from a tower seem in order since the wind can be measured on the tower and no observation point is far enough away to be in a different wind field.

The feasibility of the WINDVEC inversion algorithm to determine the wind speed and direction from the orthogonal scattering measurements was demonstrated. In this algorithm, an estimate of the wind speed is obtained from the average of the radar cross section by the power-law relationship.

$$\hat{U} = a(\theta)\sigma_{AV}^{\circ\,\gamma(\theta)} \quad (2\text{-}7)$$

Using this estimated wind speed values for the A_n coefficients in (2-3a) can be obtaind. Clearly, the only remaining unknown in this expression is the wind direction, which can be solved for by

$$\phi_w = \cos^{-1}\left\{\frac{-\hat{A}_1 \pm \sqrt{\hat{A}_1^2 - 8\hat{A}_2(\hat{A}_o - \hat{A}_2 - \sigma^o)}}{4\hat{A}_2}\right\} \qquad (2\text{-}9)$$

This yields two estimates for the wind direction, one in the first quadrant and the other in the second. These values are mirrored to obtain values in the third and fourth quadrant, respectively. The estimates of wind direction from the fore and aft beam are corrected to North and then averaged to improve the wind direction estimate. Vertical polarization estimates of both wind speed and direction are considerably better than those for horizontal polarization.

Satisfactory application of this inversion to SASS (SeaSat Active Scatterometer System) will require a larger data bank with a wider range of incidence angles. At present sufficient good data exists only for $\theta = 40^o$. Consequently, before SeaSat launch there is a need for more experimentation, either tower or aircraft, so that optimum advantage can be obtained from its data.

Also, comparison between different scattering theories and scatterometer measurements have shown different results. First, better agreement is obtained when the slope distribution reported by Cox and Munk is projected along the look direction before it is used in the averaging process. Second, use of a sea spectrum which grows with wind speed also yields more satisfactory results.

REFERENCES

1. Afarani, M., "Directional Properties of Ocean Radar Backscatter - A Harmonic Regression Analysis of AAFE Circle Experiments," RSL Technical Report 186-15, Center for Research, The University of Kansas, 1975.

2. Bass, F. G., I. M. Fuks, A. I. Kalmykov, I. E. Ostrovsky, and A. D. Rosenberg, "Very High Frequency Radiowave Scattering by a Disturbed Sea Surface," IEEE Trans. on Antennas and Propagation, v. AP-16, no. 5, September, 1968, pp. 560-568.

3. Chan, H. L., and A. K. Fung, "A Theory of Sea Scatter at Large Incident Angles," to be published, J. Geophys. Res., 1977.

4. Cox, C. and W. Munk, "Measurement of the Roughness of the Sea Surface from Photographs of the Sun Glitter," J. Opt. Soc. Am., v. 44, no. 11, November, 1954, pp. 838-850.

5. Daley, J. C., W. T. Davis, and N. R. Mills, "Radar Return in High Sea States," NRL Report 7142, September, 1970.

6. Draper, N. R., and H. Smith, Applied Regression Analysis, John Wiley and Sons, Inc., 1966.

7. Fung, A. K., "Scattering of EM Waves from a Tilted Perturbed Plane," RSL Technical Report 2960-3, Center for Research, The University of Kansas, July, 1976.

8. Jones, W. L., L. C. Schroeder, and J. L. Mitchell, "Aircraft Measurements of the Microwave Scattering Signature of the Ocean," IEEE Trans. on Antennas and Propagation, v. AP-25, no. 1, January, 1977, pp. 52-61.

9. Jones, W. L., L. C. Schroeder, and J. L. Mitchell,"Aircraft Measurements of the Anisotropic Microwave Scattering Signature Over the Ocean for the 1975 JONSWAP and 1976 East Coast Mission," NASA TMX 78646, 1978.

10. Long, M. C., "On a Two-Scatterer Theory of Sea Echo," IEEE Trans. on Antennas and Propagation, v. AP-22, no. 5, September, 1974, pp. 667-672.

11. Mitsuyasu, H. and T. Honda, "The High Frequency Spectrum of Wind-Generated Waves," J. Oceanographical Soc. of Japan, v. 30, no 4, August, 1974, pp. 185-198.

12. Phillips, O. M., The Dynamics of the Upper Ocean, London: Cambridge University Press, 1966.

13. Pierson, W. J., "The Theory and Application of Ocean Wave Measuring Systems At and Below the Sea Surface, on the Land, from Aircraft and Spacecraft," Contractor Report, Goddard Space Flight Center, (NAS 5-22041), 1975.

14. Pierson, W. J. and R. A. Stacy, "The Elevation, Slope and Curvature Spectrum of a Wind Roughened Sea," NASA Contractor Report CR-2247, 1973.

15. Sutherland, A. J., "Spectral Measurements and Growth Rates of Wind-Generated Water Waves," Technical Report 84, Department of Civil Engineering, Stanford University California, August, 1967.

16. Valenzuela, G. R., "Depolarization of EM Waves by Slightly Rough Surfaces," IEEE Trans. on Antennas and Propagation, v. AP-15, no. 4, July, 1967, pp. 552-557.

17. Wright, J. W., "A New Model for Sea Clutter," IEEE Trans. on Antennas and Propagation, v. AP-16, no. 2, March, 1968, pp. 217-223.

18. Wu, S. T. and A. K. Fung, "A Noncoherent Model for Microwave Emissions and Backscattering from the Sea Surface," J. Geophysical Res., v. 77, no. 30, October, 1972, pp. 5917-5929.

19. Young, J. D. and R. K. Moore, "Active Microwave Measurements from Space of Sea-Surface Winds," to be published, IEEE Trans on Ocean Engineering, 1977.

APPENDIX A

Examples of Regression Analysis of Circle Flight Data

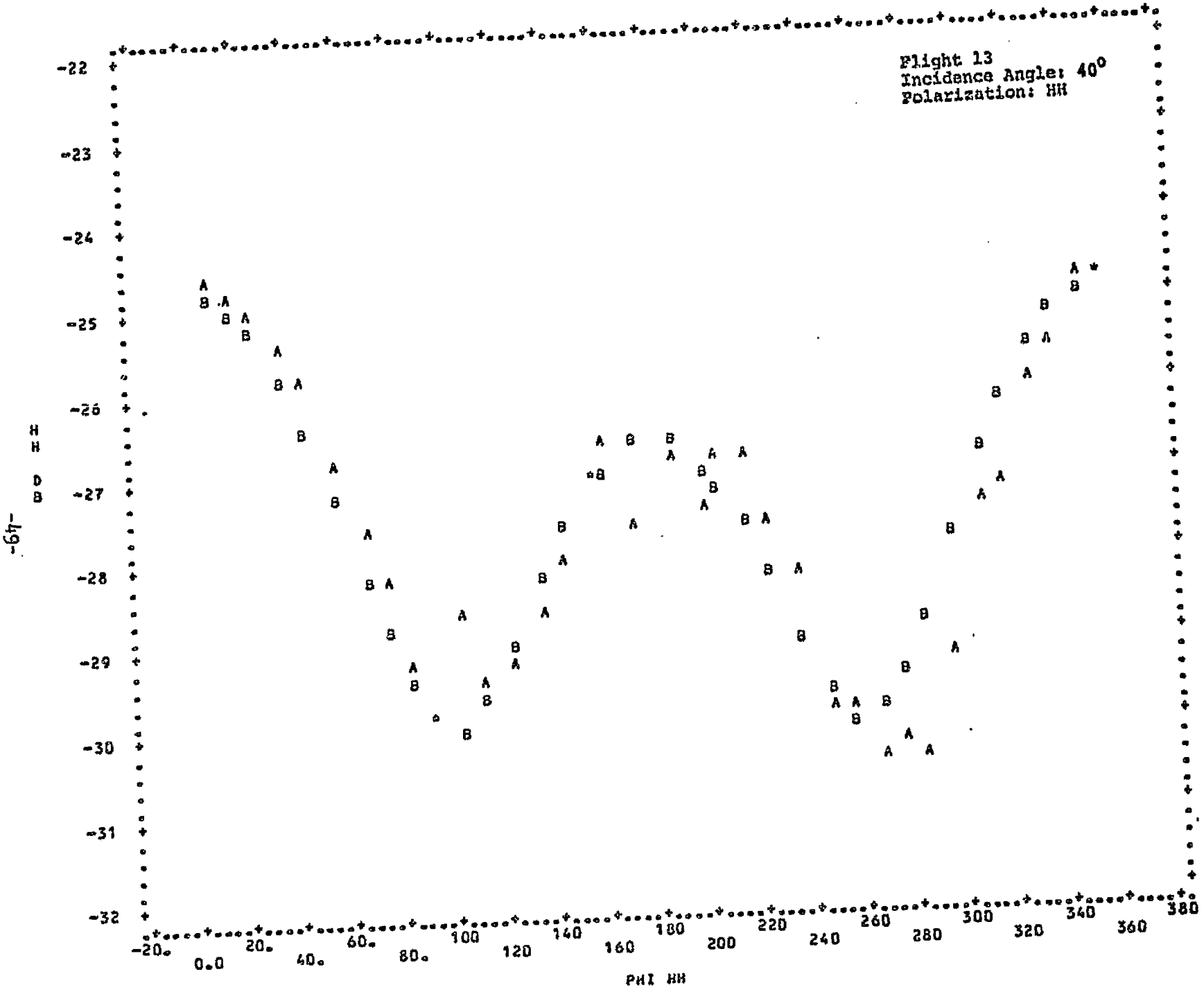
Flight 13
Incidence Angle: 40°
Polarization: HH
-22
-23
-24
-25
-26
-27
-28
-29
-30
-31
-32
HH
DB
-20.
0.0
20.
40.
60.
80.
100
120
140
160
180
200
220
240
260
280
300
320
340
360
380
PHI HH

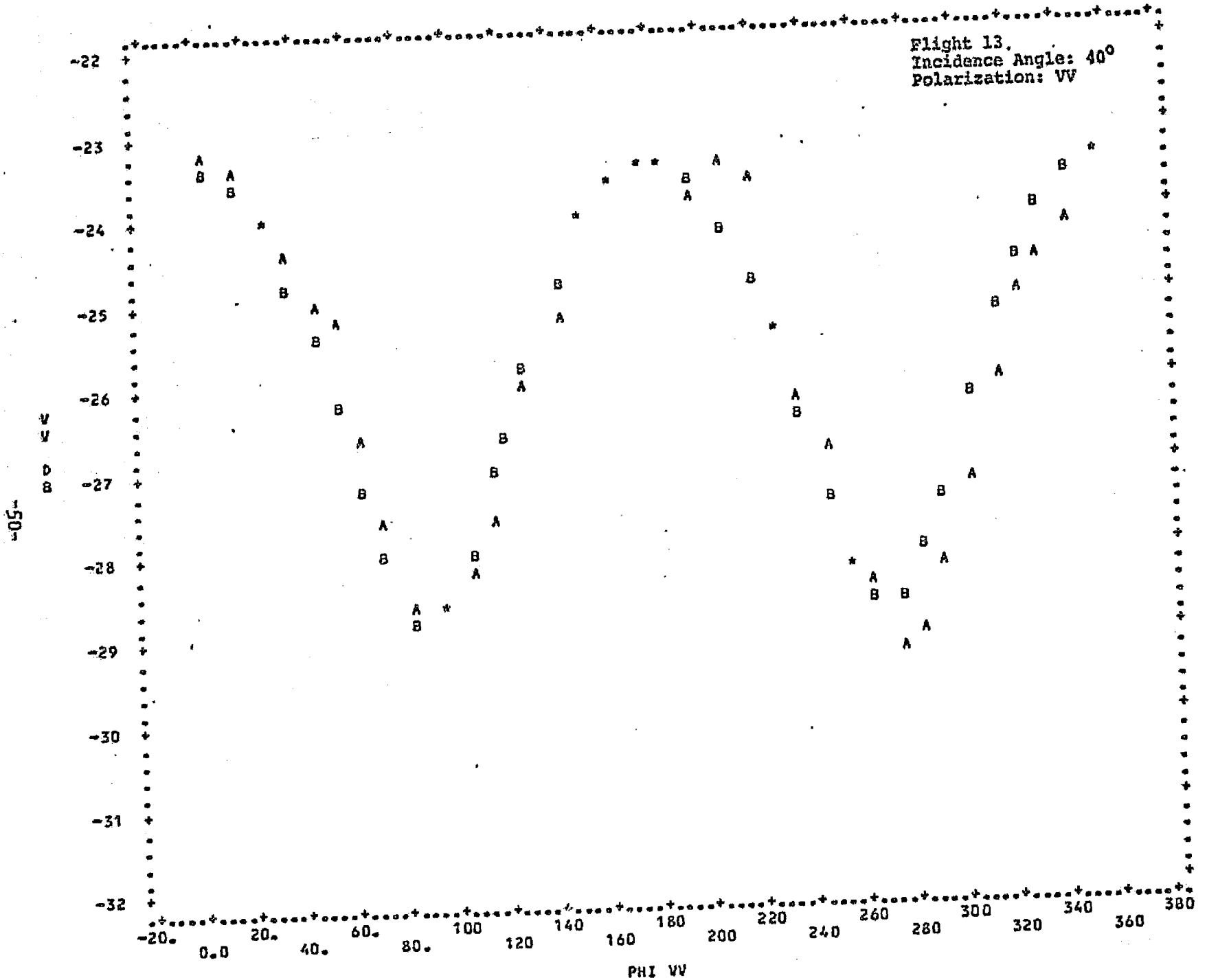
Flight 13.
Incidence Angle: 40°
Polarization: VV
-22
-23
-24
-25
-26
-27
-28
-29
-30
-31
-32
V
V
D
B
-50-
-20.
0.0
20.
40.
60.
80.
100
120
140
160
180
200
220
240
260
280
300
320
340
360
380
PHI VV

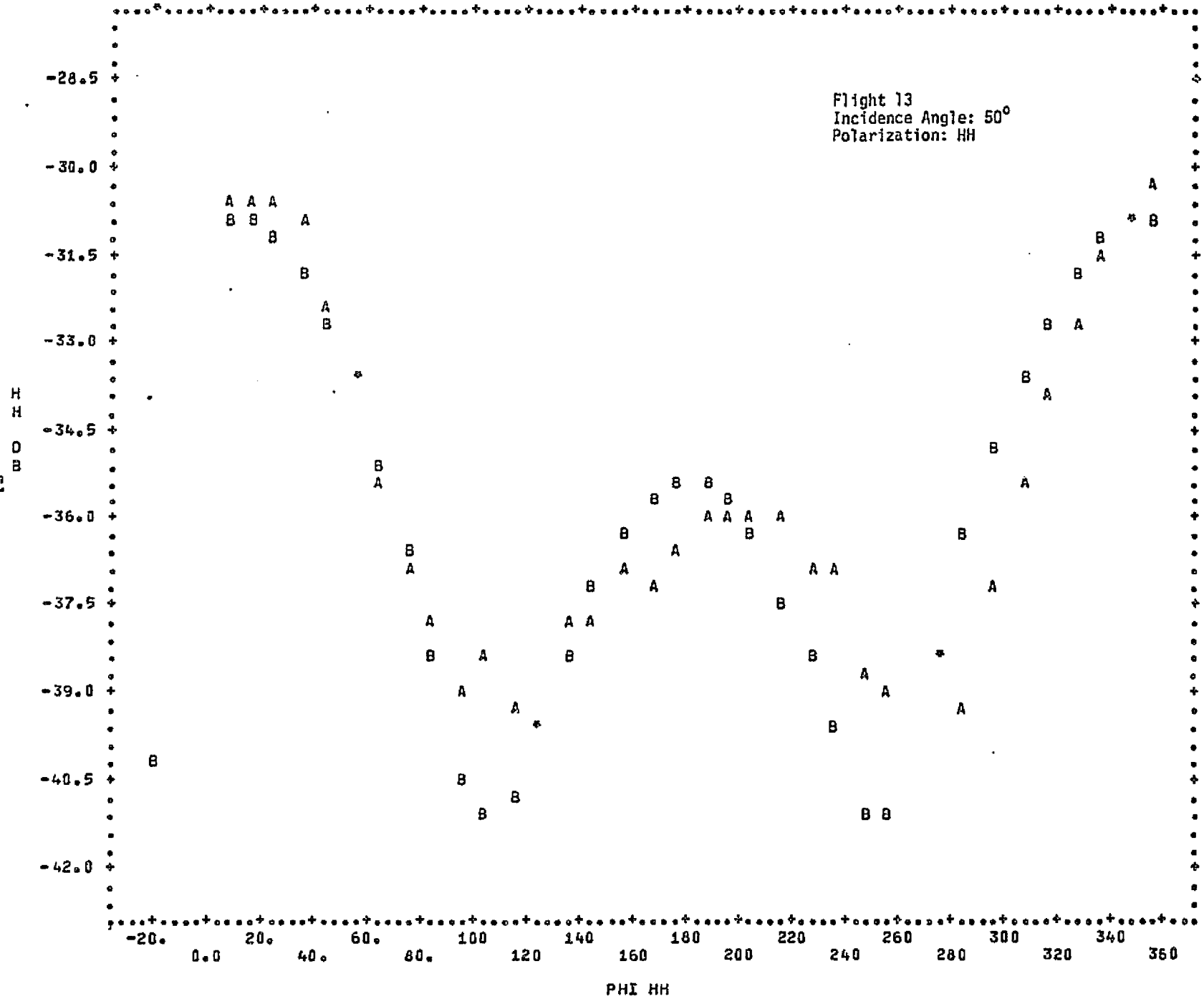
Flight 13
Incidence Angle: 50°
Polarization: HH
-28.5
-30.0
-31.5
-33.0
-34.5
-36.0
-37.5
-39.0
-40.5
-42.0
HH DB
-20.
0.0
20.
40.
60.
80.
100
120
140
160
180
200
220
240
260
280
300
320
340
360
PHI HH

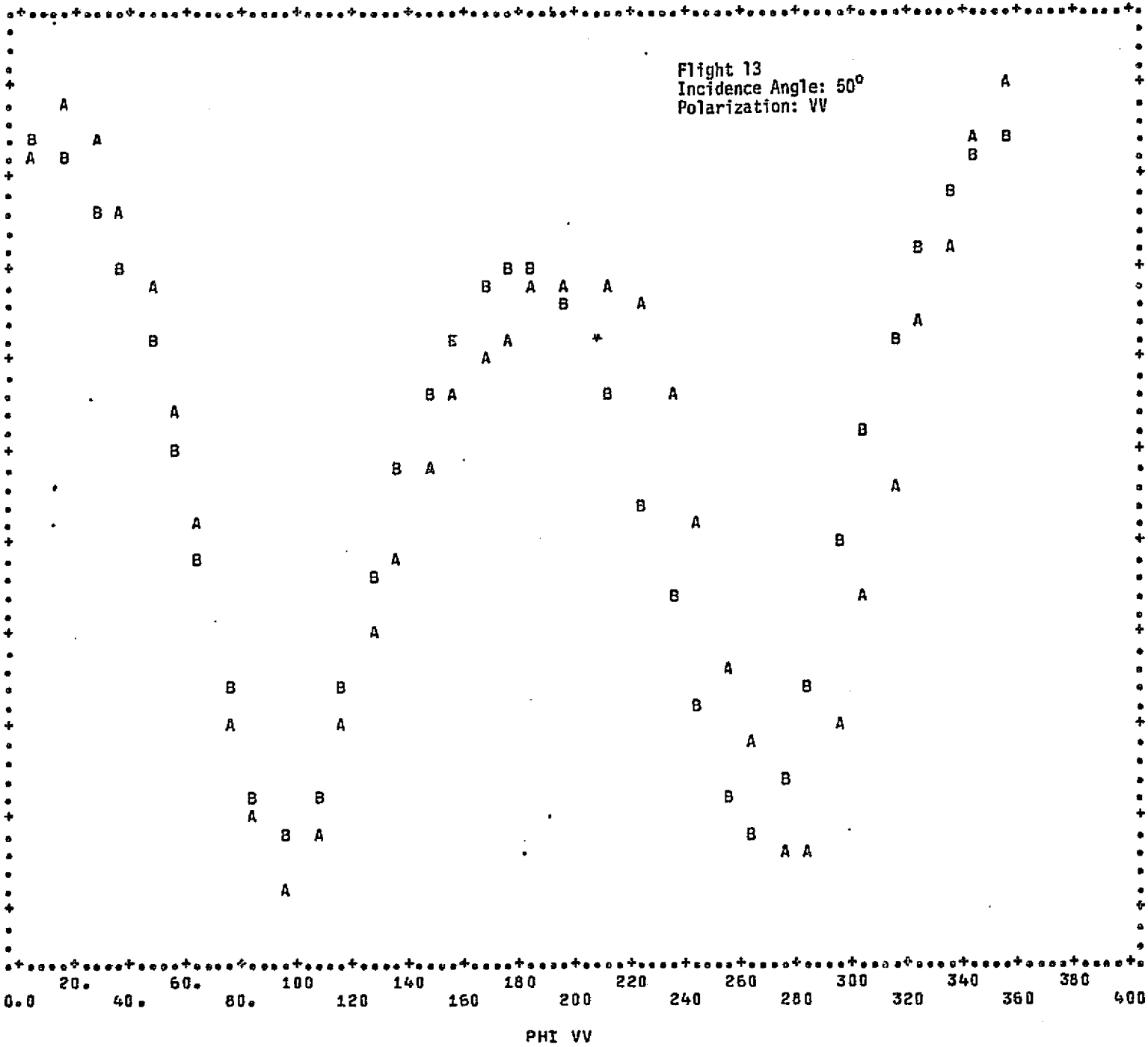
Flight 13
Incidence Angle: 50°
Polarization: VV
-26.1
-27.0
-27.9
-28.8
-29.7
-30.6
-31.5
-32.4
-33.3
-34.2
VV DB
0.0
20.
40.
60.
80.
100
120
140
160
180
200
220
240
260
280
300
320
340
360
380
400
PHI VV

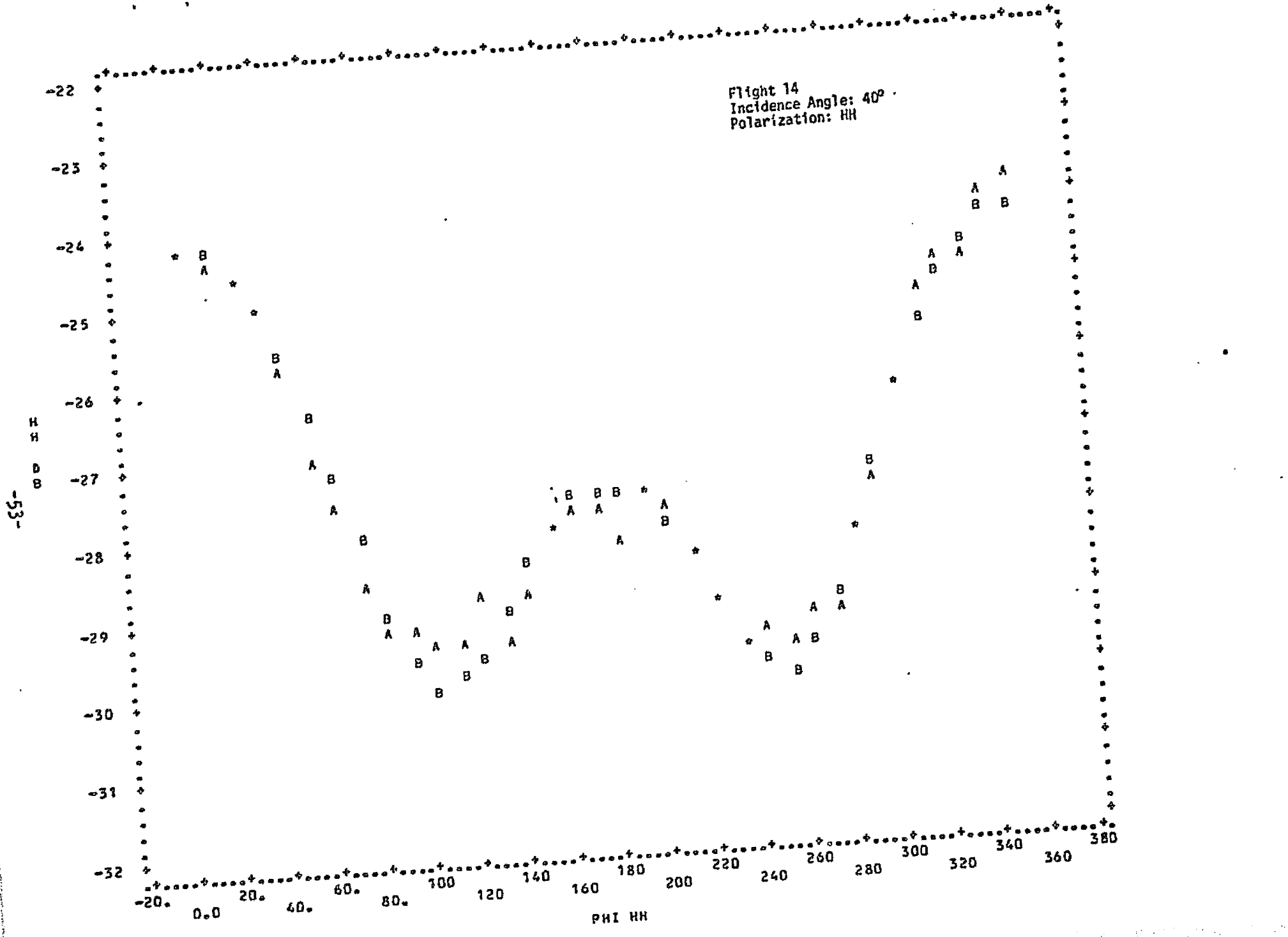
Flight 14
Incidence Angle: 40°
Polarization: HH
-22
-23
-24
-25
-26
-27
-28
-29
-30
-31
-32
-20.
0.0
20.
40.
60.
80.
100
120
140
160
180
200
220
240
260
280
300
320
340
360
380
PHI HH
HH
-53-

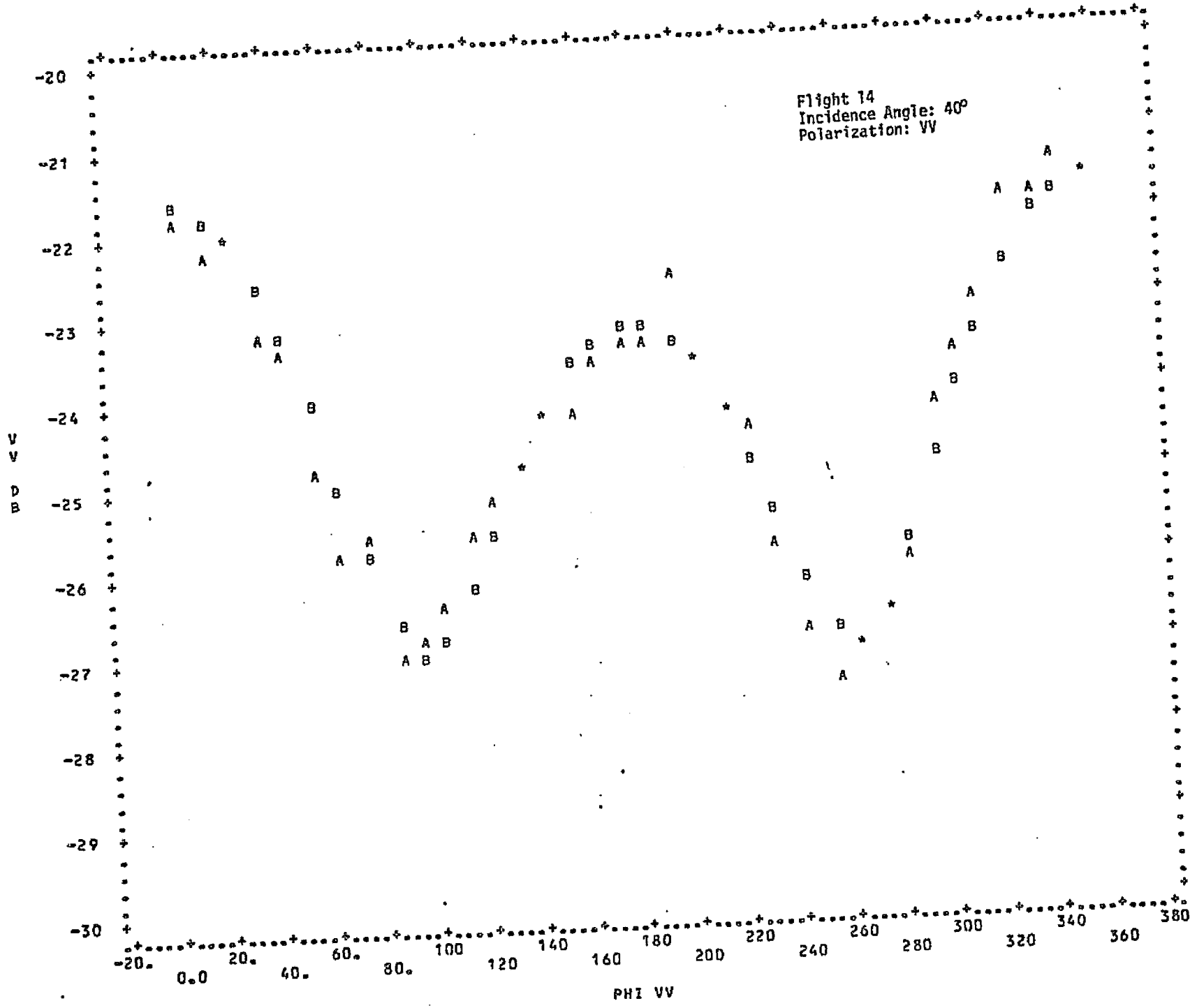
Flight 14
Incidence Angle: 40°
Polarization: VV
-20
-21
-22
-23
-24
-25
-26
-27
-28
-29
-30
V
V
D
B
-20.
0.0
20.
40.
60.
80.
100
120
140
160
180
200
220
240
260
280
300
320
340
360
380
PHI VV

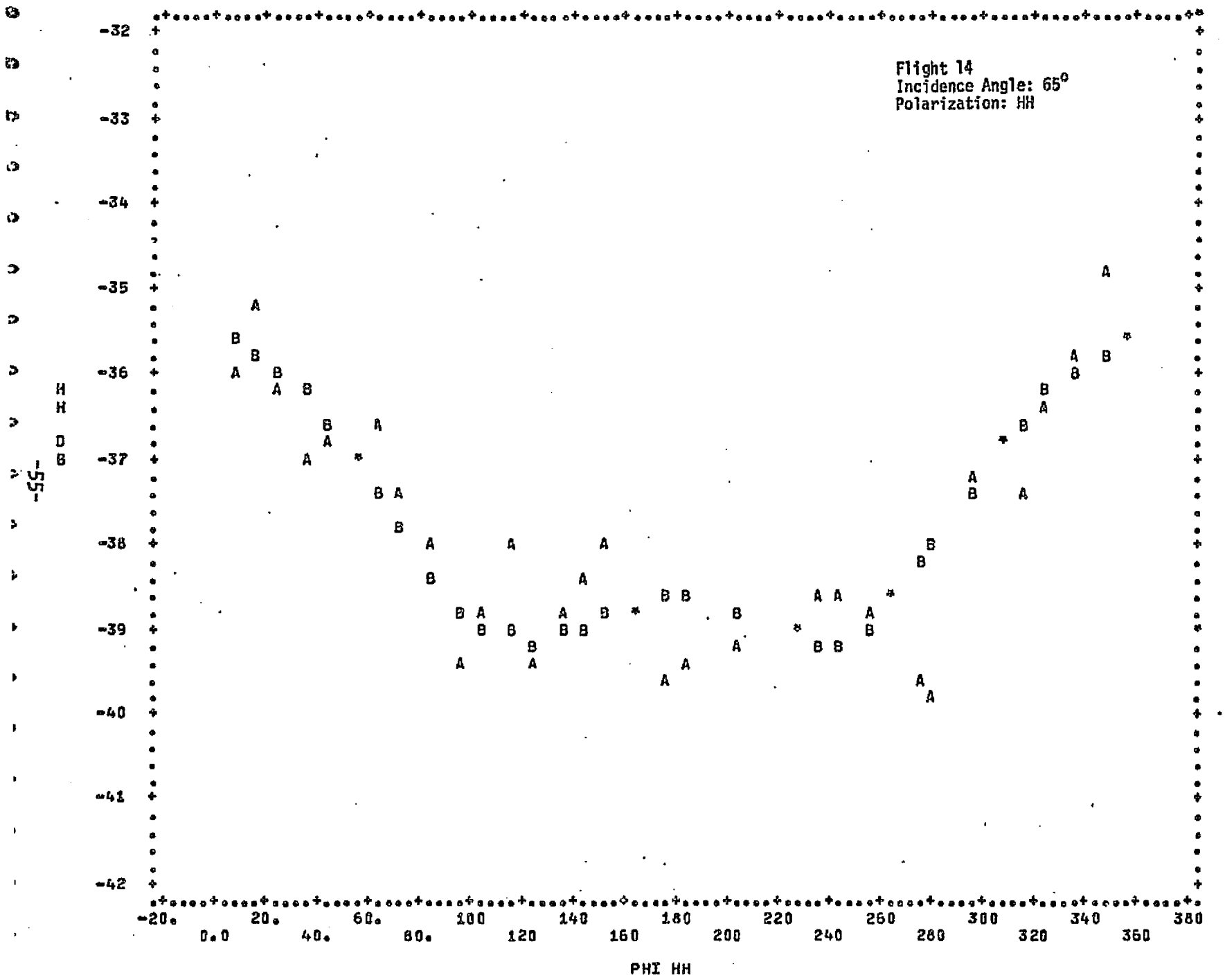
Flight 14
Incidence Angle: 65°
Polarization: HH
-32
-33
-34
-35
-36
-37
-38
-39
-40
-41
-42
-20.
0.0
20.
40.
60.
80.
100
120
140
160
180
200
220
240
260
280
300
320
340
360
PHI HH

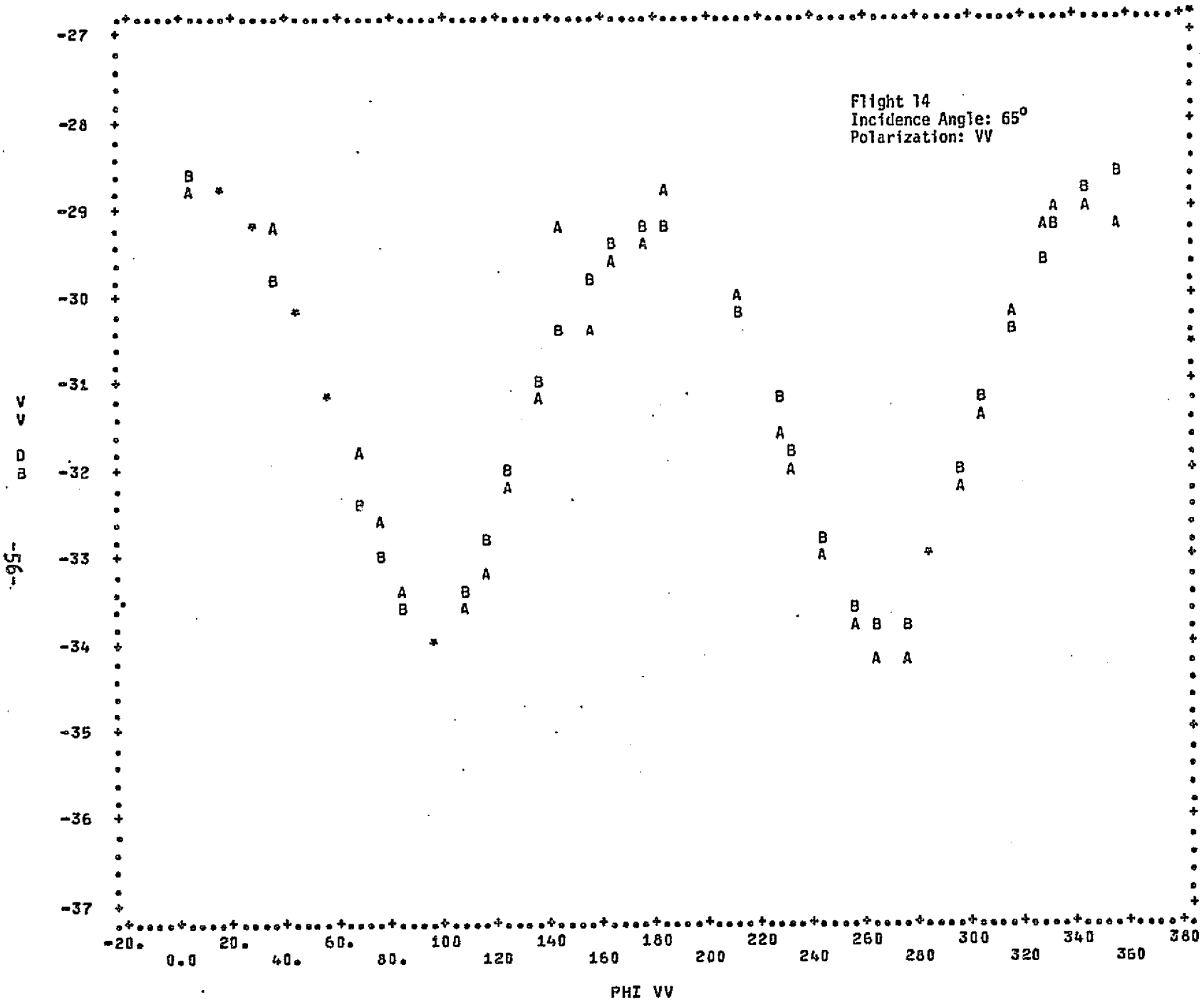
Flight 14
Incidence Angle: 65°
Polarization: VV
-27
-28
-29
-30
-31
-32
-33
-34
-35
-36
-37
VV DB
-20.
0.0
20.
40.
60.
80.
100
120
140
160
180
200
220
240
260
280
300
320
340
360
PHI VV

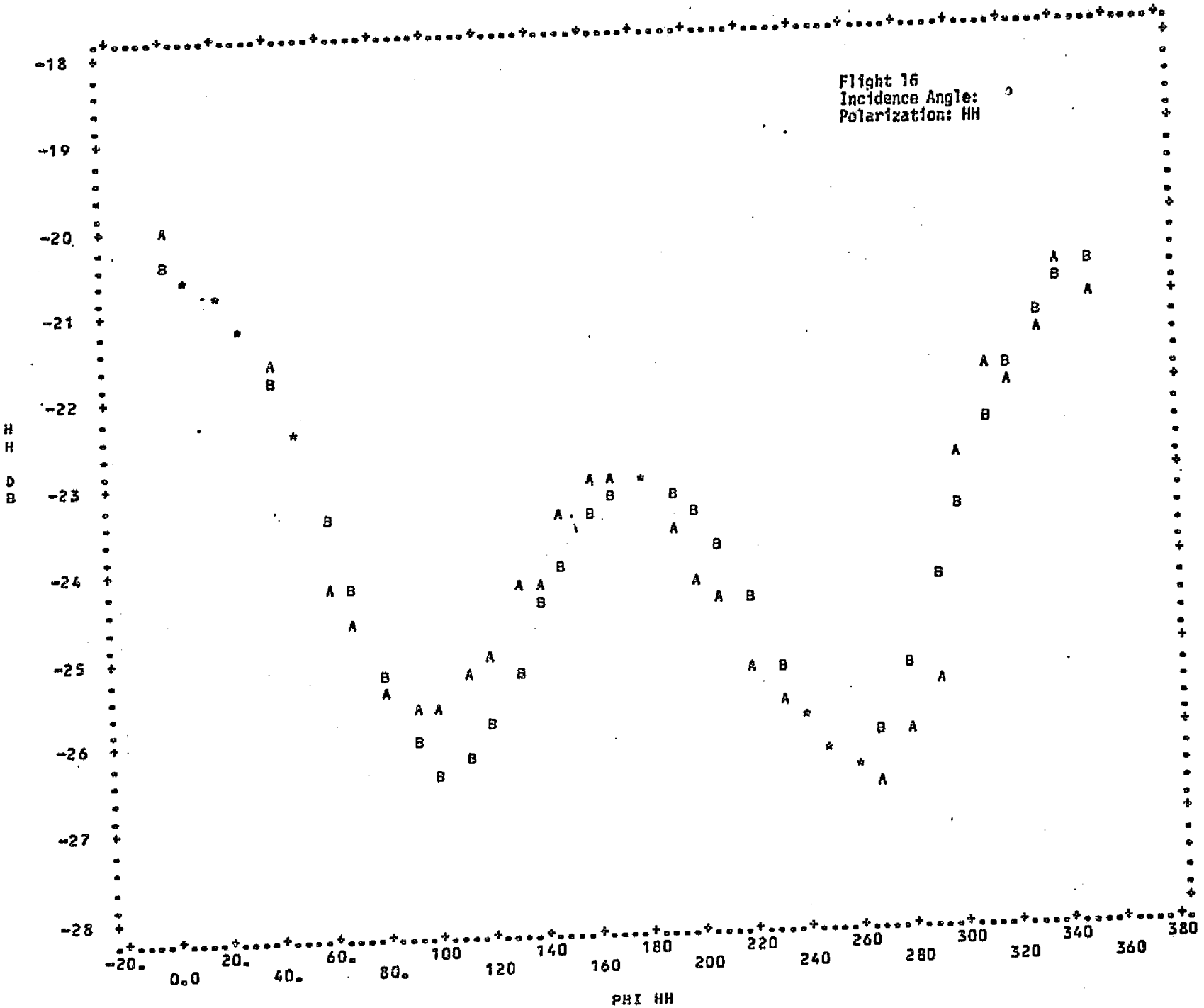
Flight 16
Incidence Angle:
Polarization: HH
-18
-19
-20
-21
-22
-23
-24
-25
-26
-27
-28
H
H
D
B
-20.
0.0
20.
40.
60.
80.
100
120
140
160
180
200
220
240
260
280
300
320
340
360
380
PHI HH

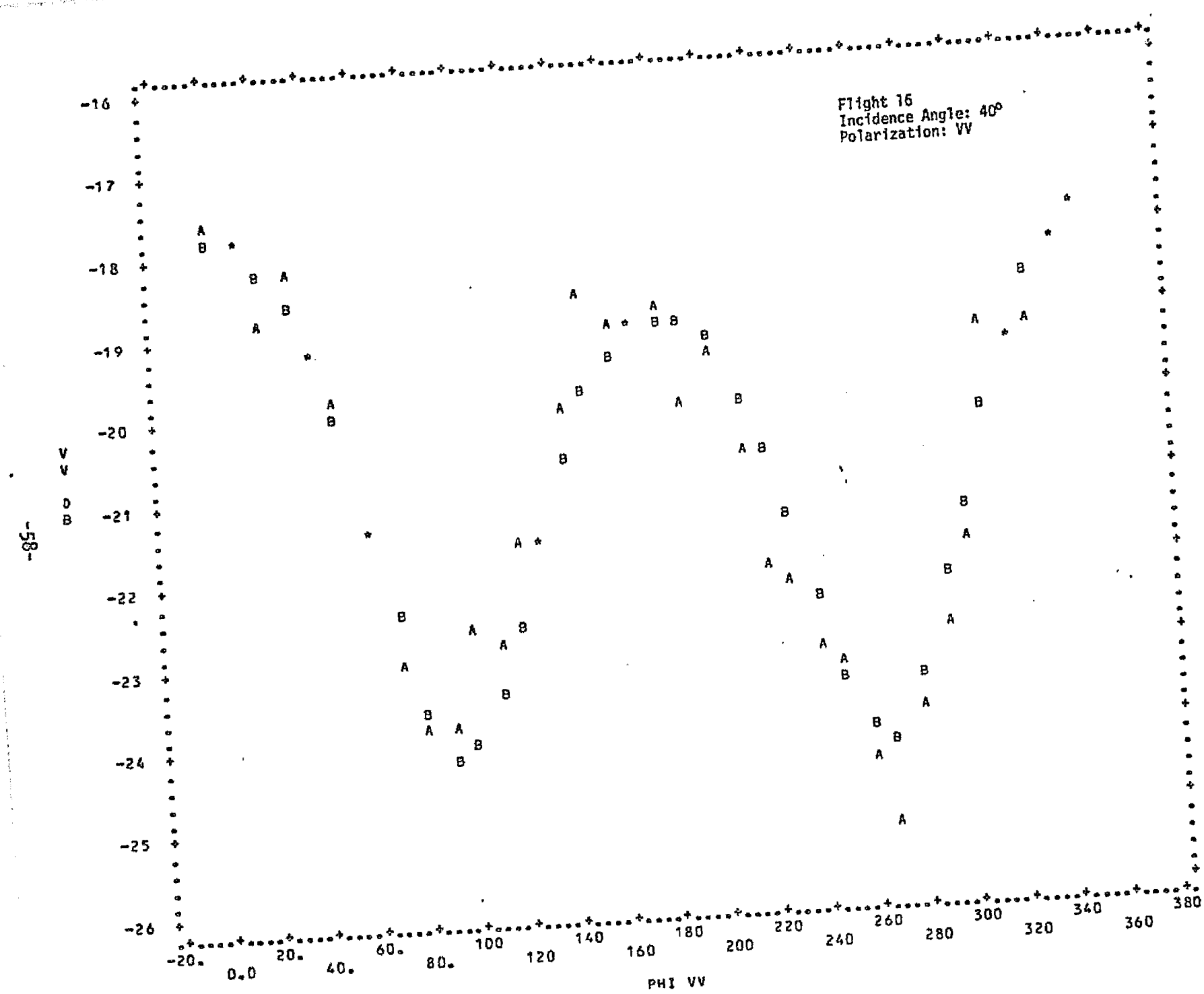
Flight 16
Incidence Angle: 40°
Polarization: VV
-16
-17
-18
-19
-20
-21
-22
-23
-24
-25
-26
VV DB
-20.
0.0
20.
40.
60.
80.
100
120
140
160
180
200
220
240
260
280
300
320
340
360
380
PHI VV

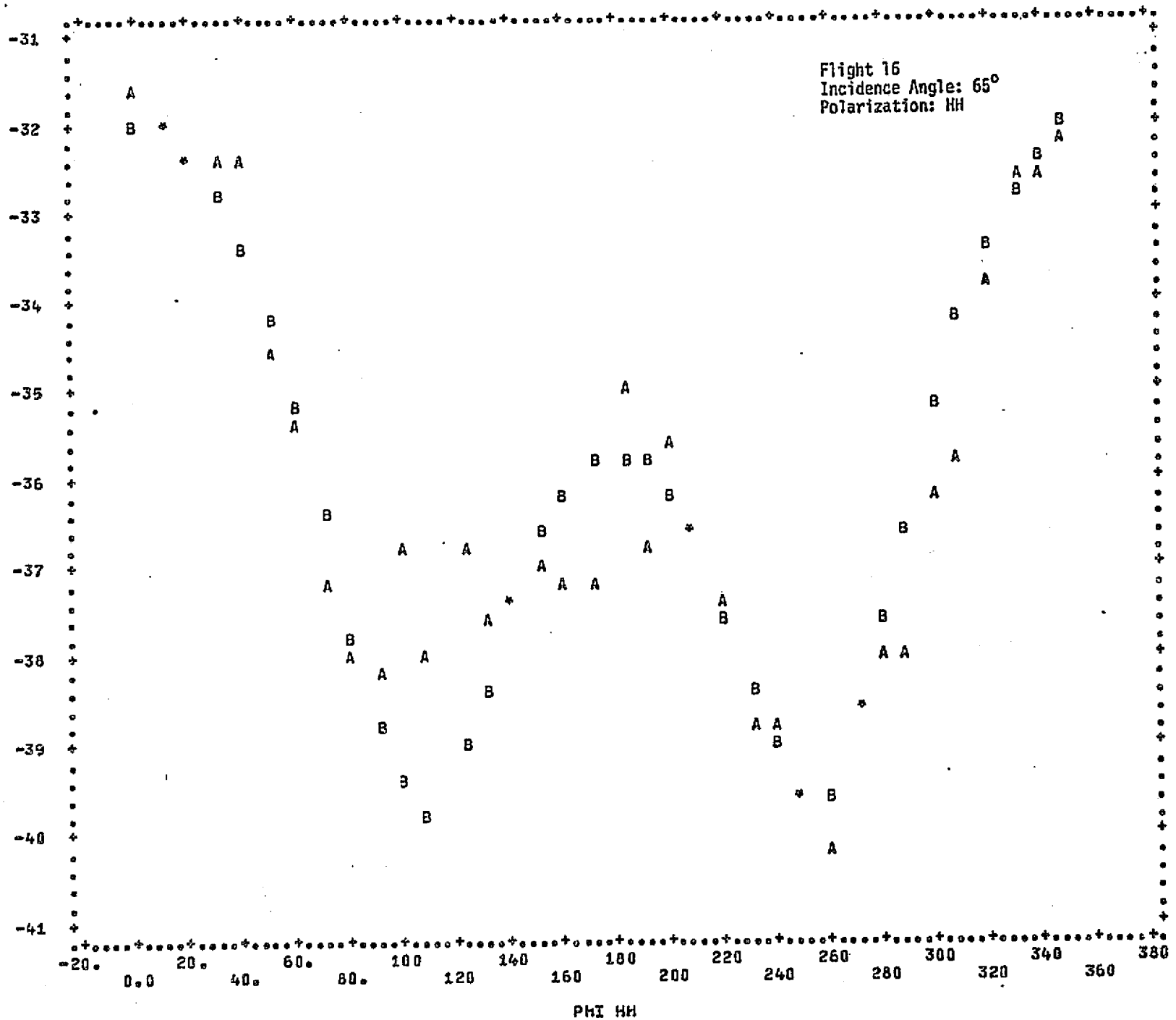
Flight 16
Incidence Angle: 65°
Polarization: HH
-31
-32
-33
-34
-35
-36
-37
-38
-39
-40
-41
H
H
D
B
-20.
0.0
20.
40.
60.
80.
100
120
140
160
180
200
220
240
260
280
300
320
340
360
PHI HH

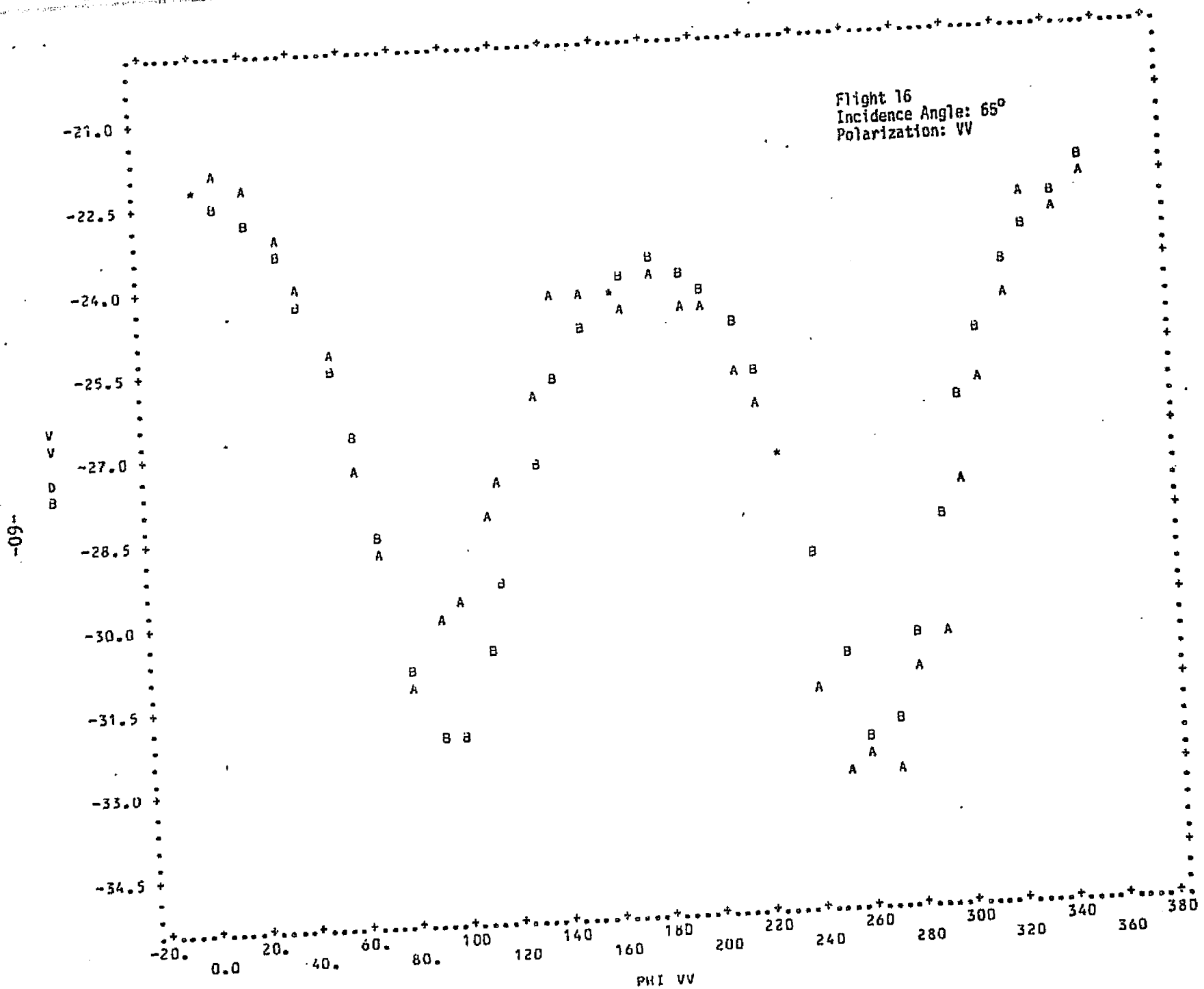
Flight 16
Incidence Angle: 65°
Polarization: VV
-21.0
-22.5
-24.0
-25.5
-27.0
-28.5
-30.0
-31.5
-33.0
-34.5
VV DB
-60-
-20.
0.0
20.
40.
60.
80.
100
120
140
160
180
200
220
240
260
280
300
320
340
360
380
PHI VV

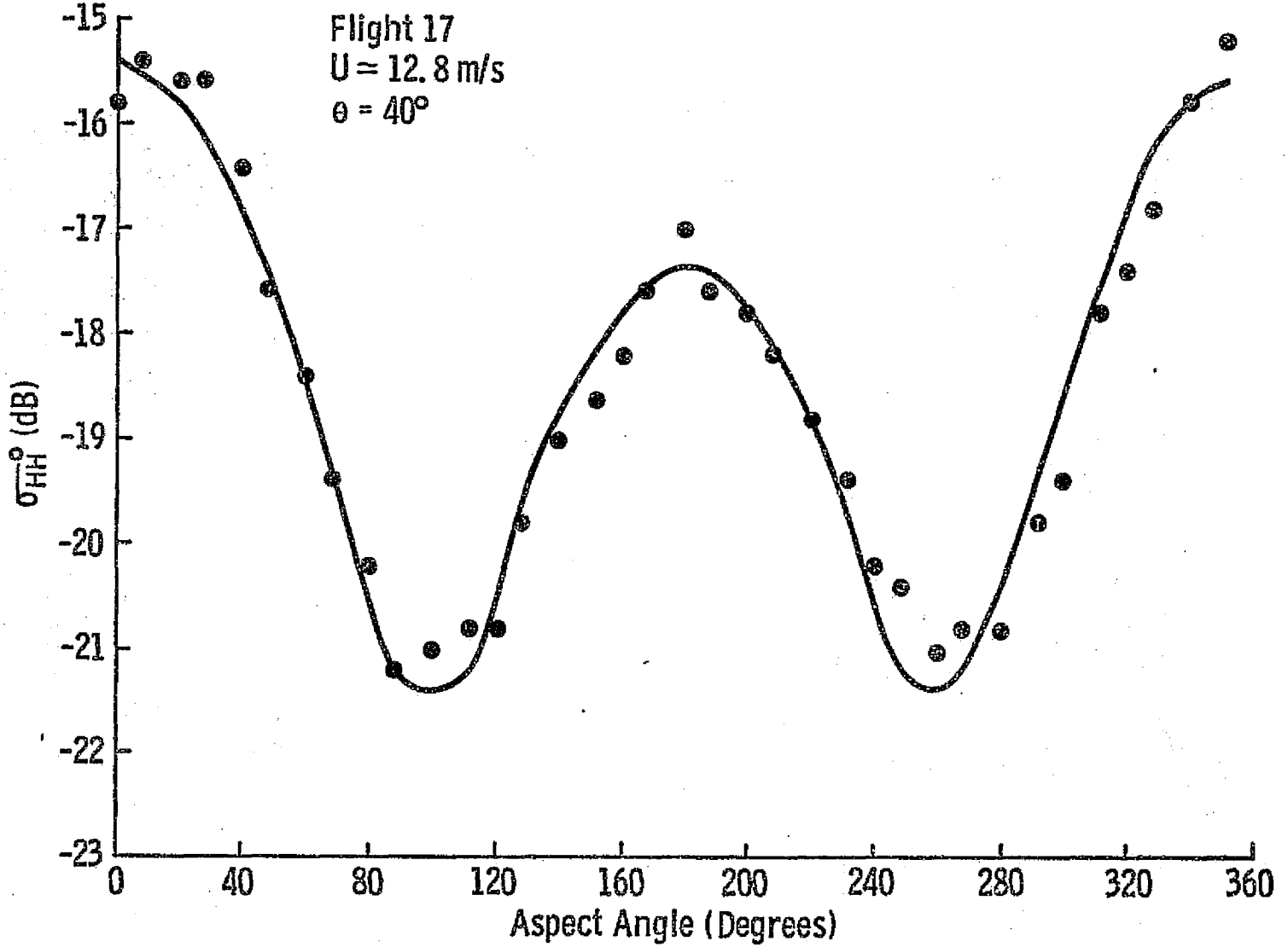
Flight 17
U = 12.8 m/s
θ = 40°
-15
-16
-17
-18
-19
-20
-21
-22
-23
$\overline{\sigma^{\circ}_{HH}}$ (dB)
0
40
80
120
160
200
240
280
320
360
Aspect Angle (Degrees)

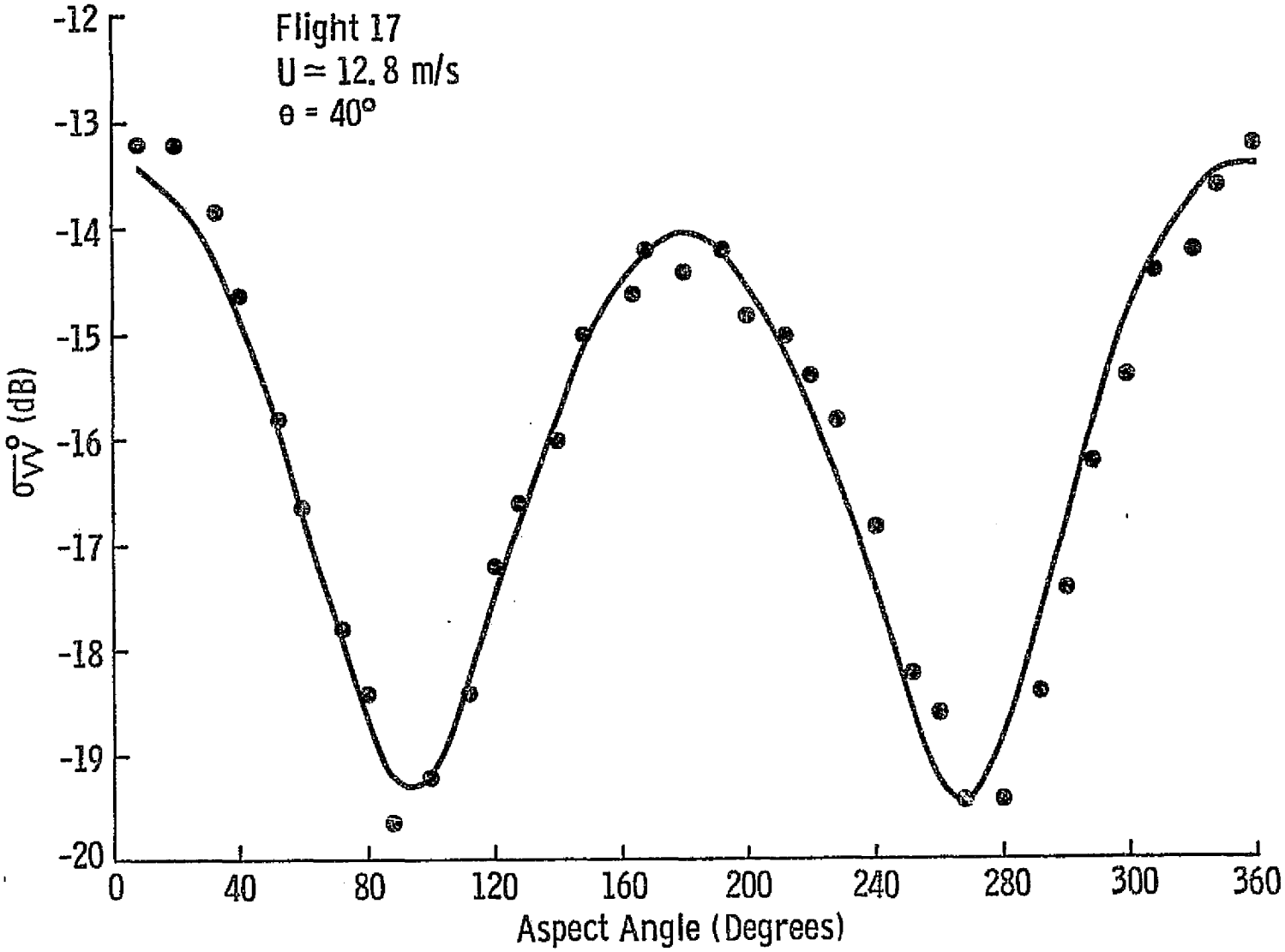
Flight 17
U ≃ 12.8 m/s
θ = 40°
-12
-13
-14
-15
-16
-17
-18
-19
-20
σ_{VV}^{o} (dB)
0
40
80
120
160
200
240
280
300
360
Aspect Angle (Degrees)

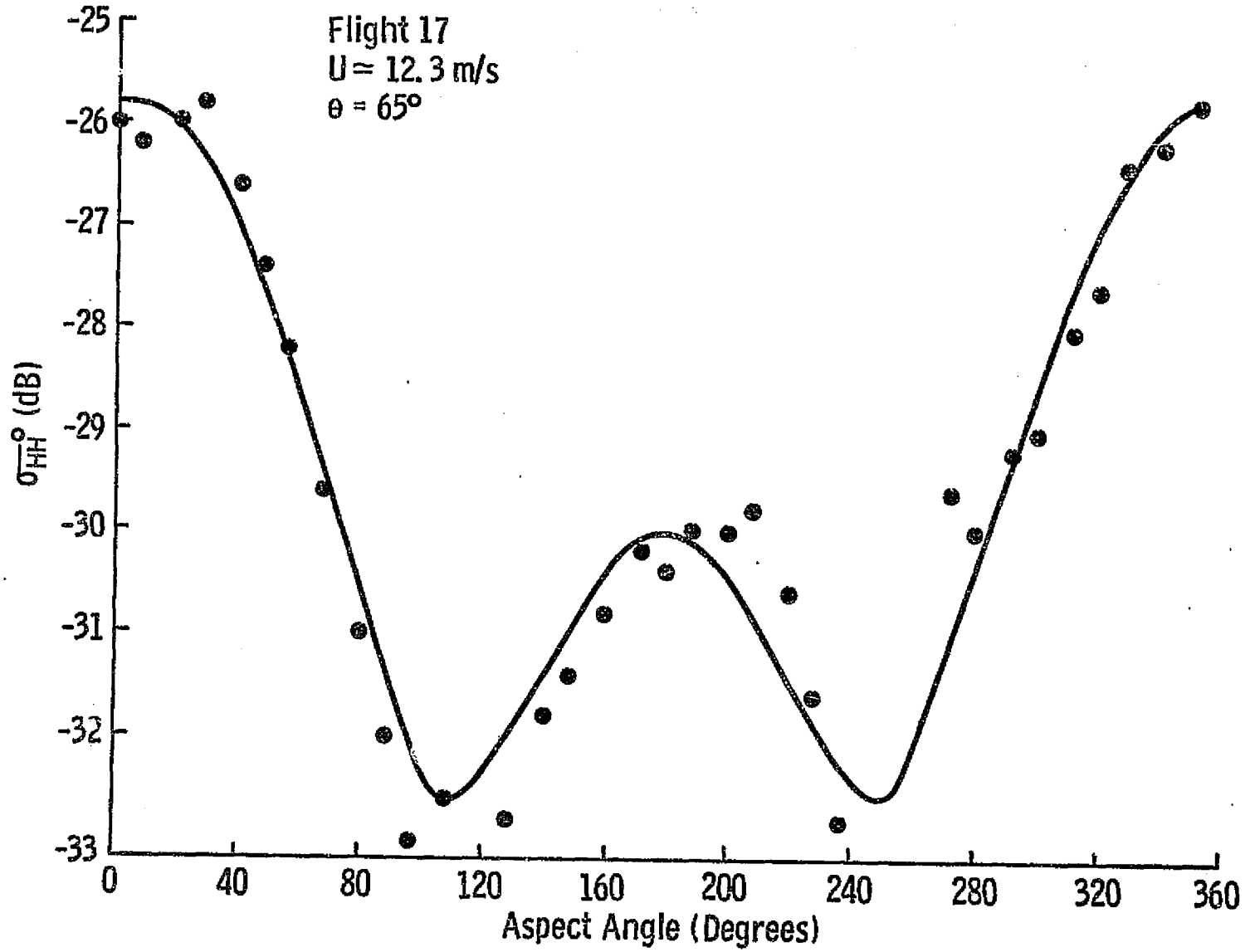
Flight 17
U ≈ 12.3 m/s
θ = 65°
-25
-26
-27
-28
-29
-30
-31
-32
-33
σ°_{HH} (dB)
0
40
80
120
160
200
240
280
320
360
Aspect Angle (Degrees)

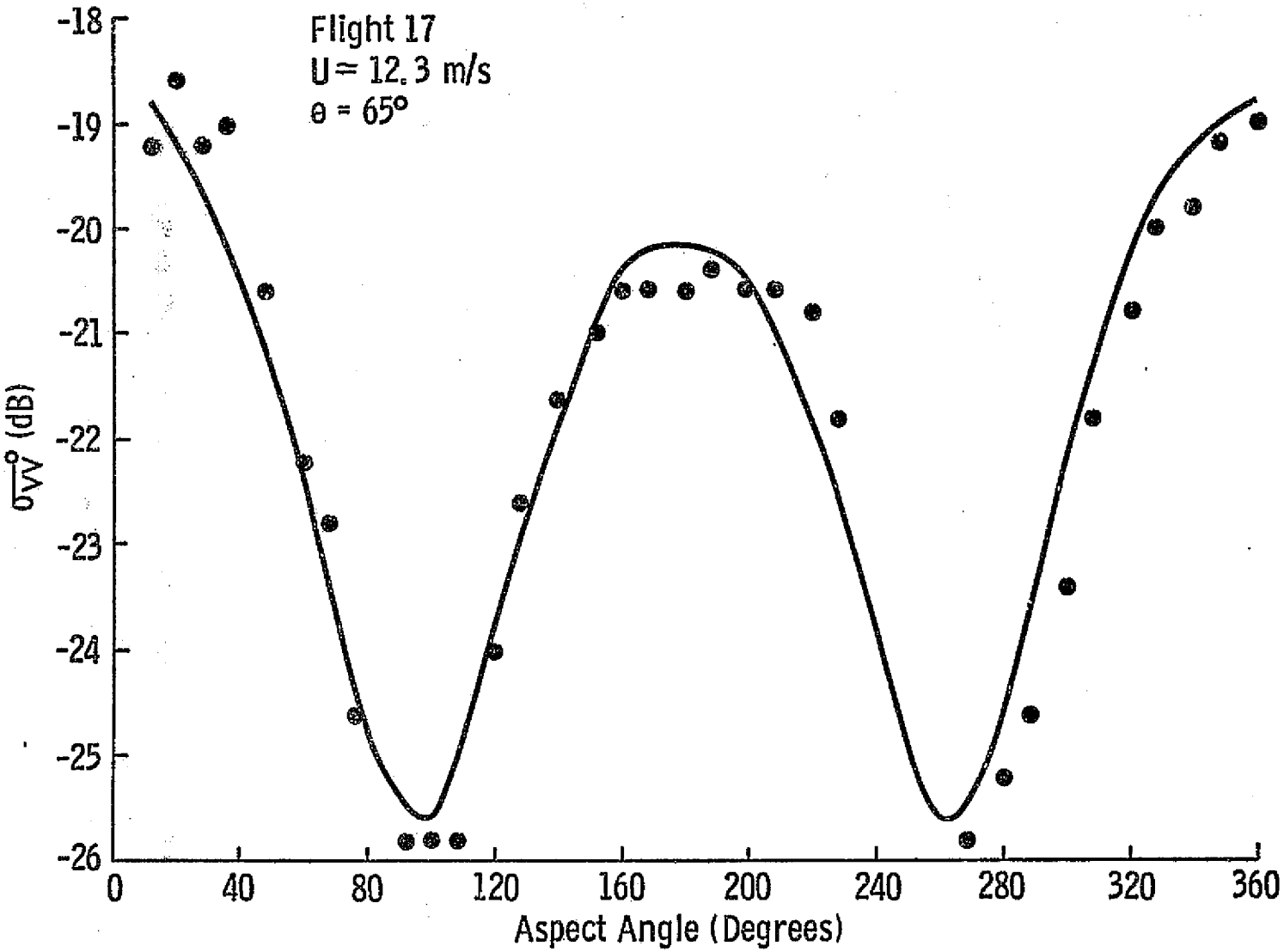
Flight 17
U = 12.3 m/s
θ = 65°
-18
-19
-20
-21
-22
-23
-24
-25
-26
σ°_{VV} (dB)
0
40
80
120
160
200
240
280
320
360
Aspect Angle (Degrees)

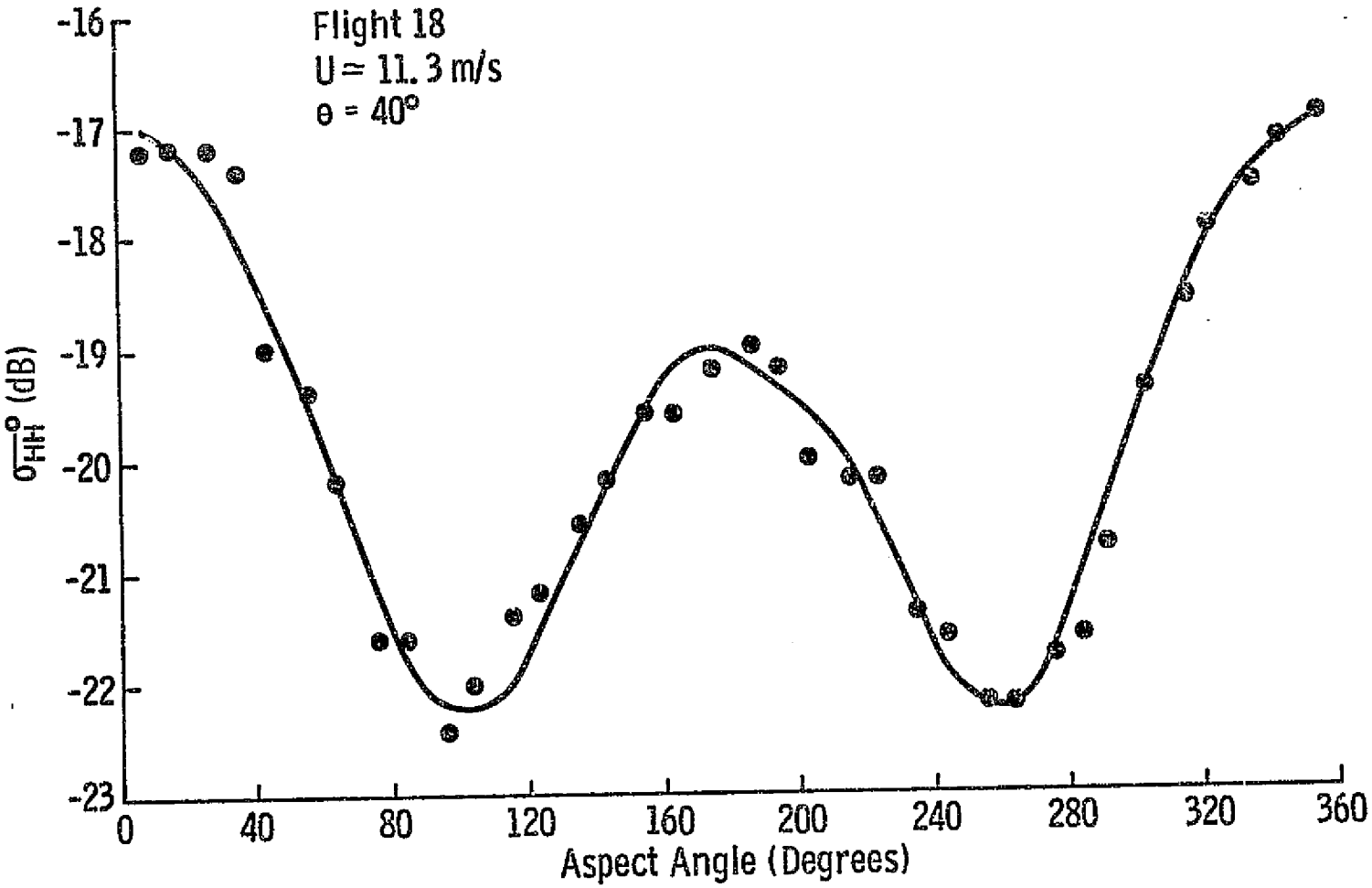
Flight 18
U = 11.3 m/s
θ = 40°
-16
-17
-18
-19
-20
-21
-22
-23
$\overline{\sigma^{\circ}_{HH}}$ (dB)
0
40
80
120
160
200
240
280
320
360
Aspect Angle (Degrees)

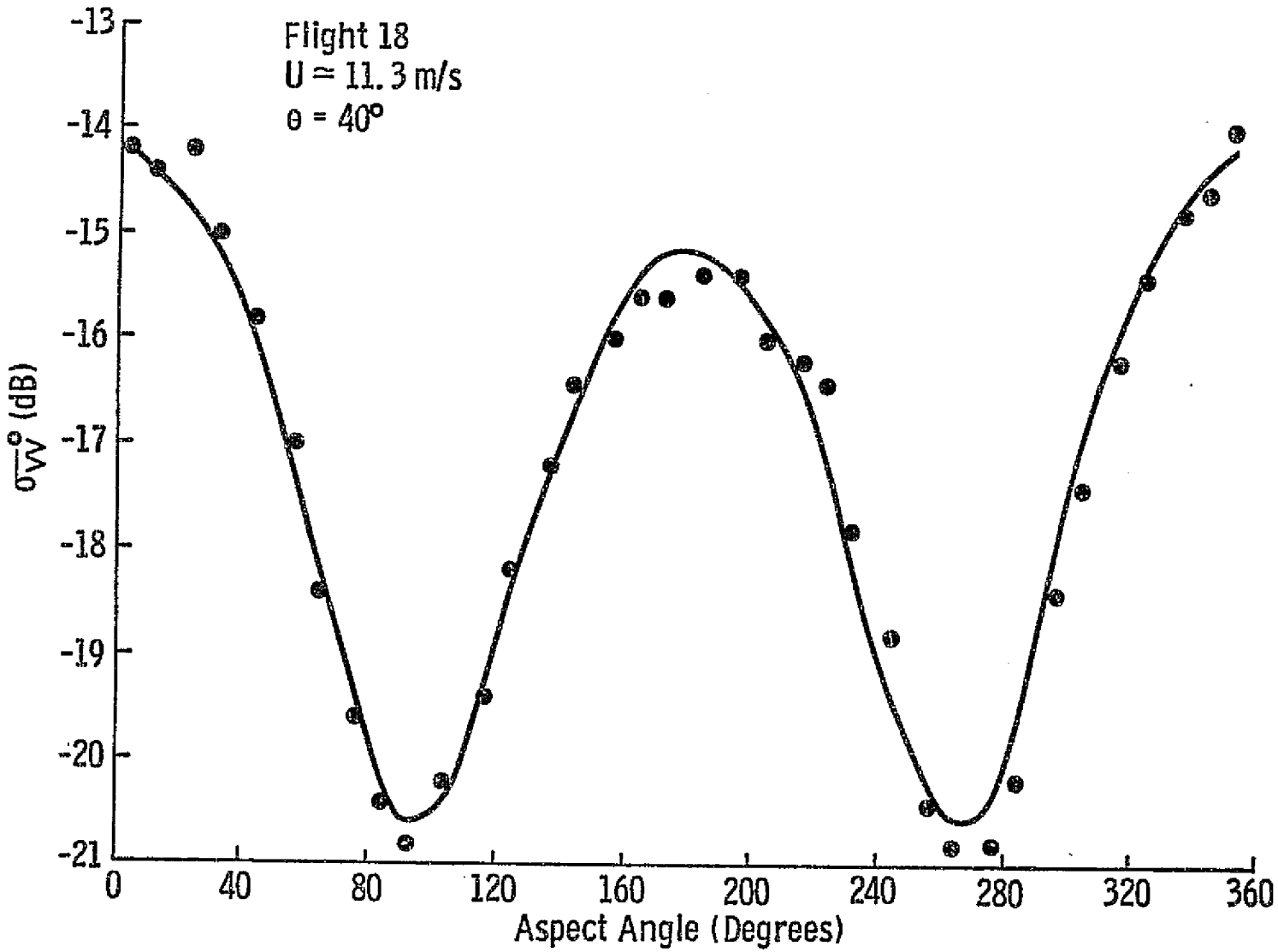
Flight 18
U ≃ 11.3 m/s
θ = 40°
-13
-14
-15
-16
-17
-18
-19
-20
-21
$\overline{\sigma_{VV}^{\circ}}$ (dB)
0
40
80
120
160
200
240
280
320
360
Aspect Angle (Degrees)

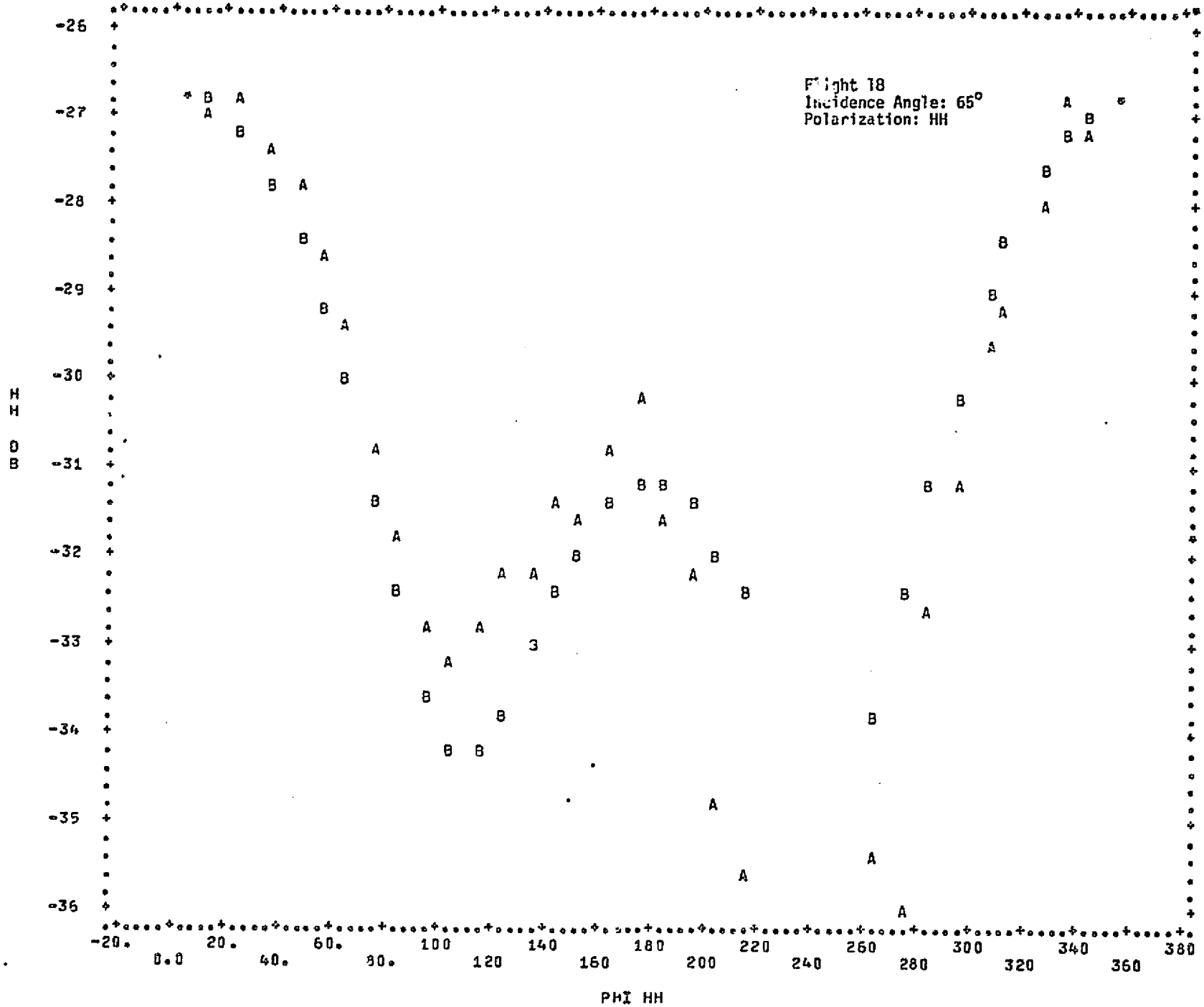
Flight 18
Incidence Angle: 65°
Polarization: HH
-25
-27
-28
-29
-30
-31
-32
-33
-34
-35
-36
H
H
O
B
-20.
0.0
20.
40.
60.
80.
100
120
140
160
180
200
220
240
260
280
300
320
340
360
PHI HH

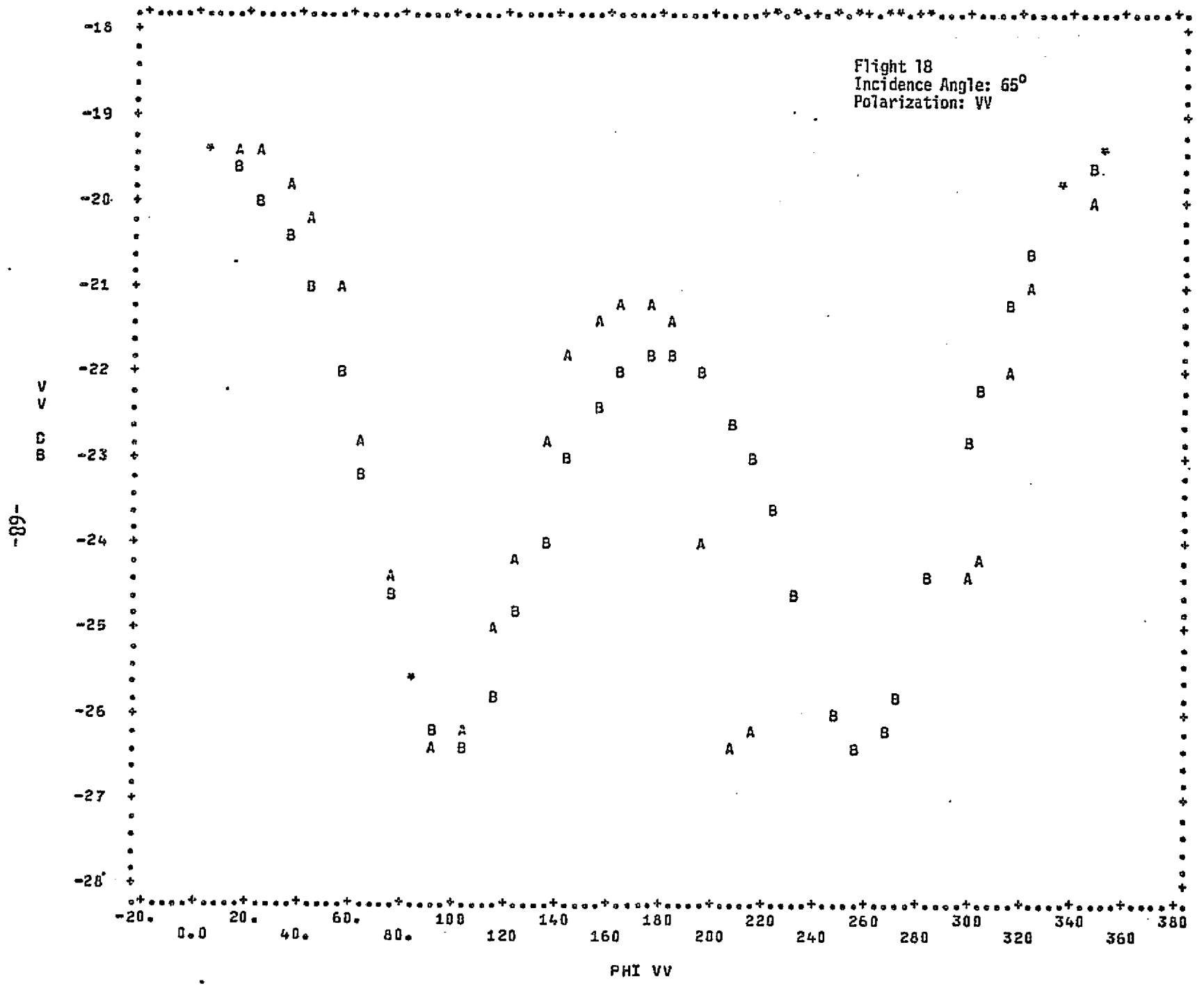
Flight 18
Incidence Angle: 65°
Polarization: VV
VV DB
PHI VV
-18
-19
-20
-21
-22
-23
-24
-25
-26
-27
-28
-20.
0.0
20.
40.
60.
80.
100
120
140
160
180
200
220
240
260
280
300
320
340
360
380

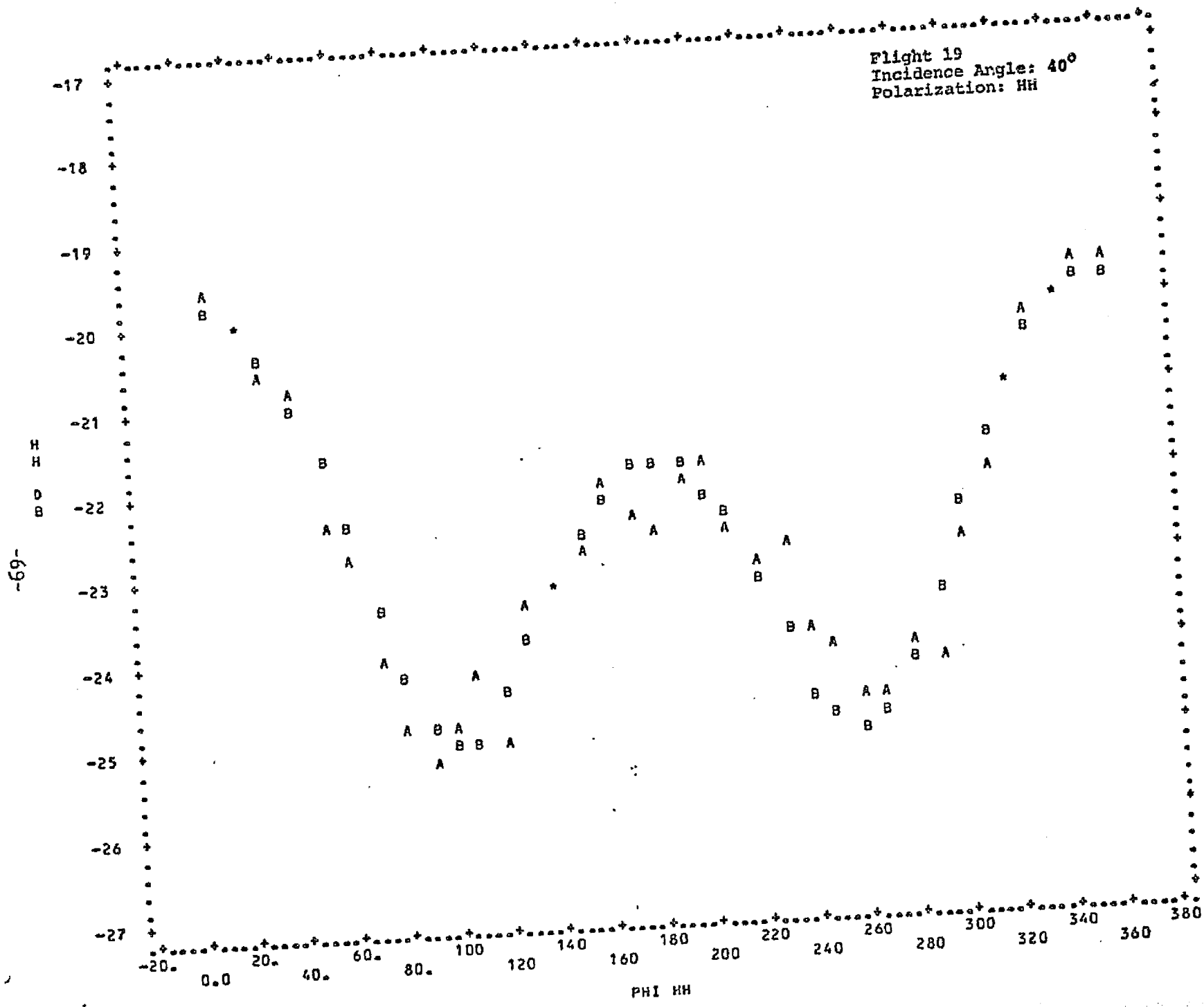
Flight 19
Incidence Angle: 40°
Polarization: HH
HH DB
-17
-18
-19
-20
-21
-22
-23
-24
-25
-26
-27
-20.
0.0
20.
40.
60.
80.
100
120
140
160
180
200
220
240
260
280
300
320
340
360
380
PHI HH

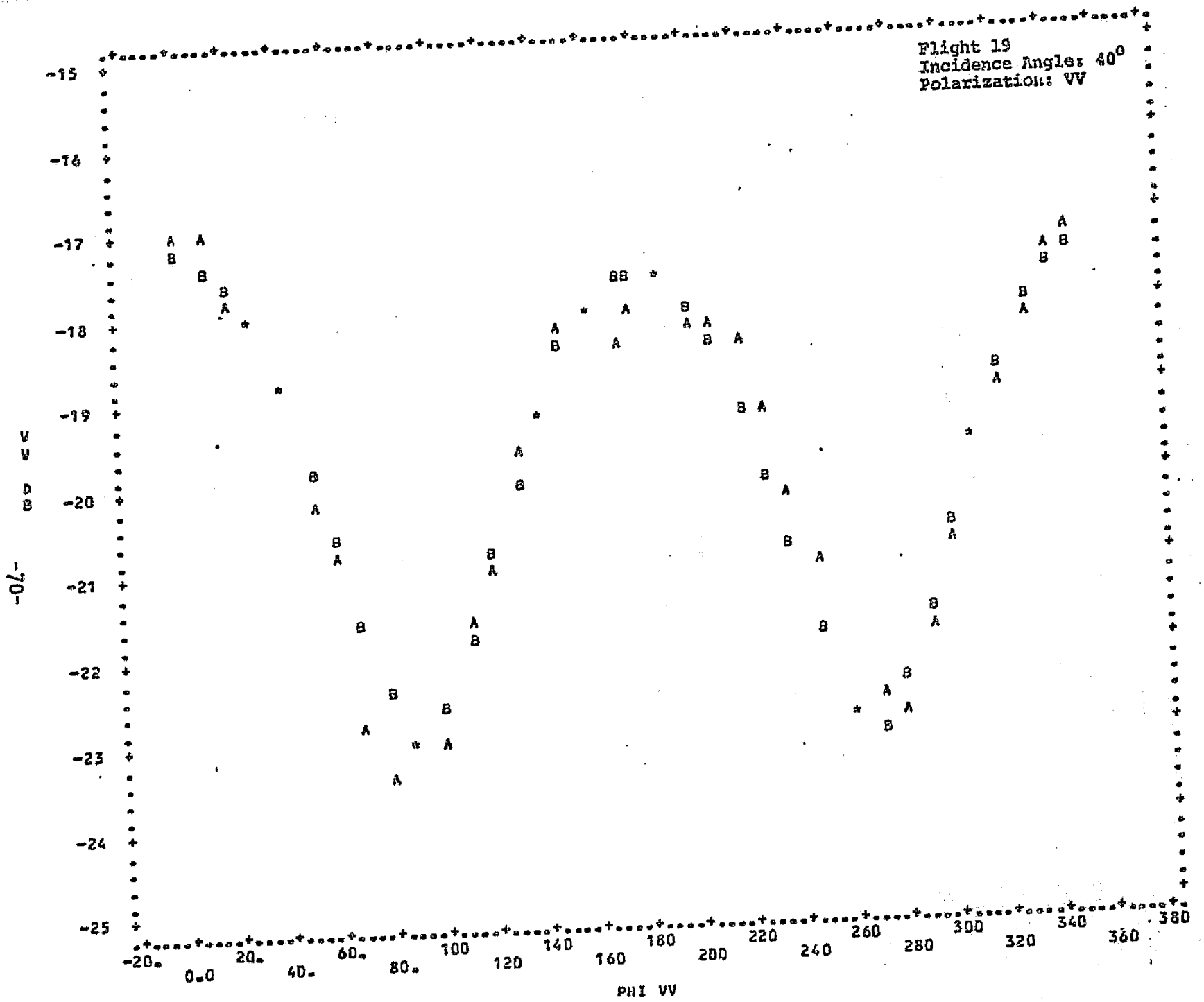
Flight 19
Incidence Angle: 40°
Polarization: VV
-15
-16
-17
-18
-19
-20
-21
-22
-23
-24
-25
VV DB
-20.
0.0
20.
40.
60.
80.
100
120
140
160
180
200
220
240
260
280
300
320
340
360
380
PHI VV

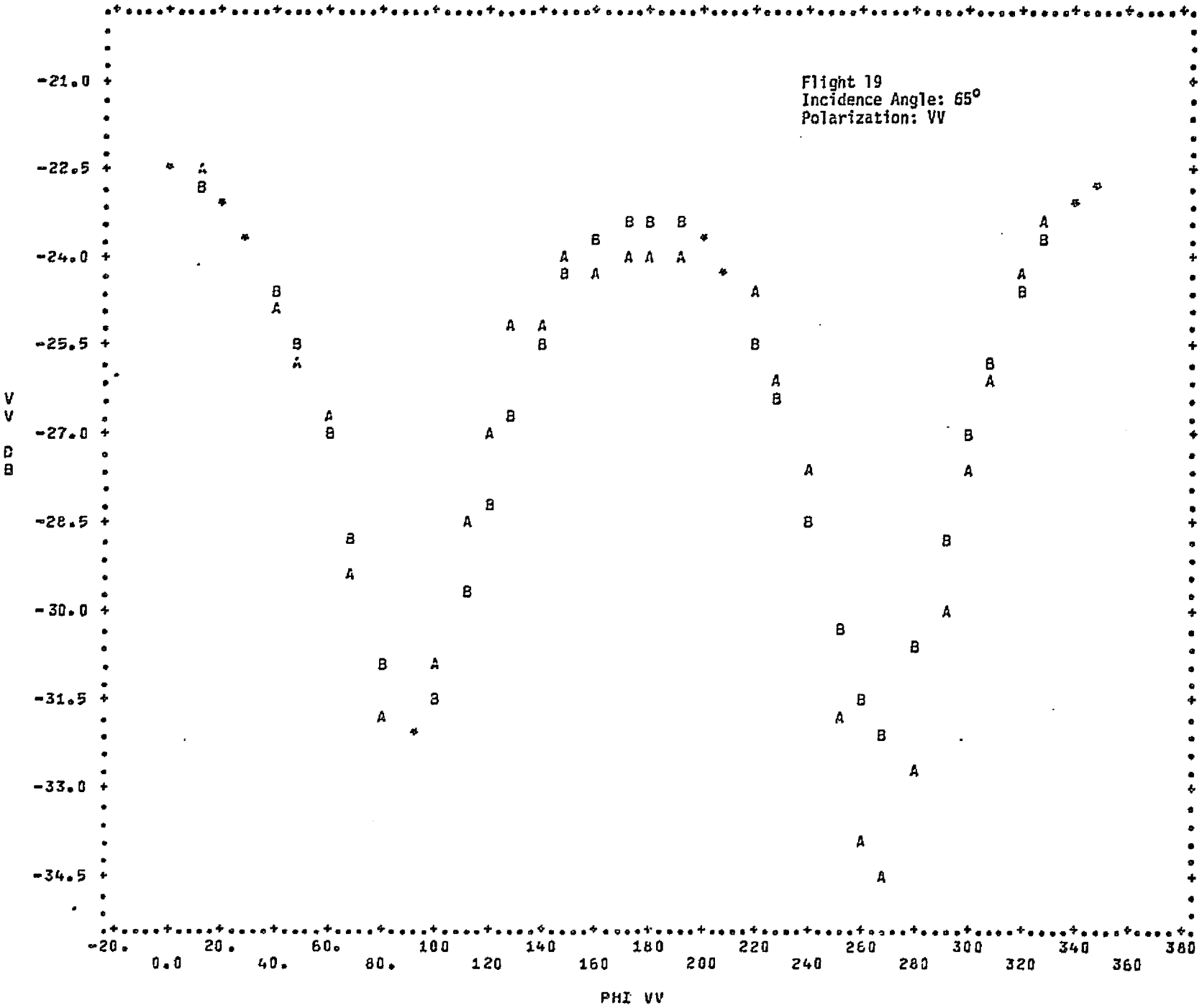
Flight 19
Incidence Angle: 65°
Polarization: VV
-21.0
-22.5
-24.0
-25.5
-27.0
-28.5
-30.0
-31.5
-33.0
-34.5
VV DB
-20.
0.0
20.
40.
60.
80.
100
120
140
160
180
200
220
240
260
280
300
320
340
360
PHI VV

APPENDIX B

Relationship Between 2nd Harmonic Coefficients and Wind Speed Using Both AAFE and JONSWAP Data

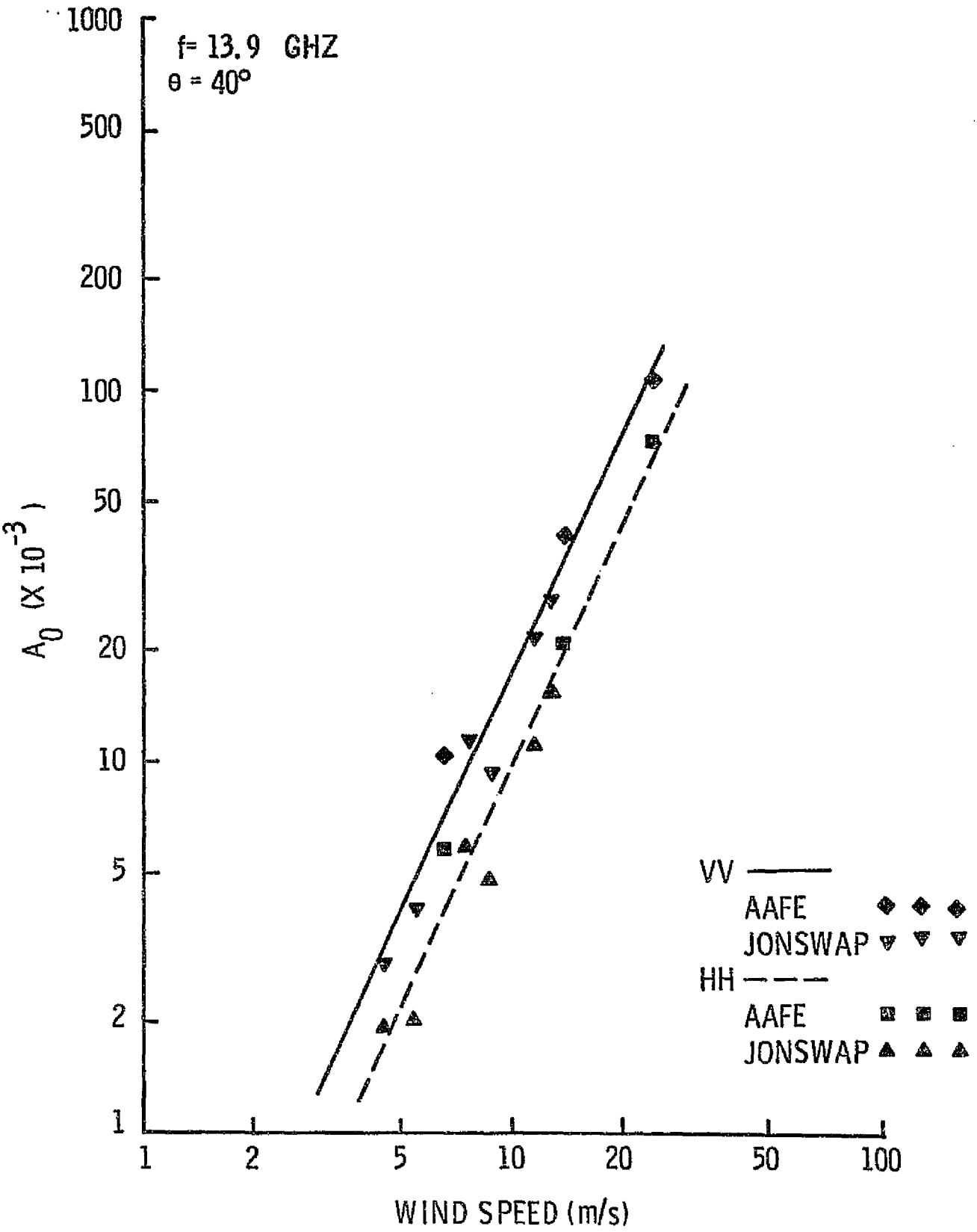
f= 13.9 GHZ
θ = 40°
1000
500
200
100
50
20
10
5
2
1
A_0 (X 10^{-3})
1
2
5
10
20
50
100
WIND SPEED (m/s)
VV
AAFE
JONSWAP
HH
AAFE
JONSWAP

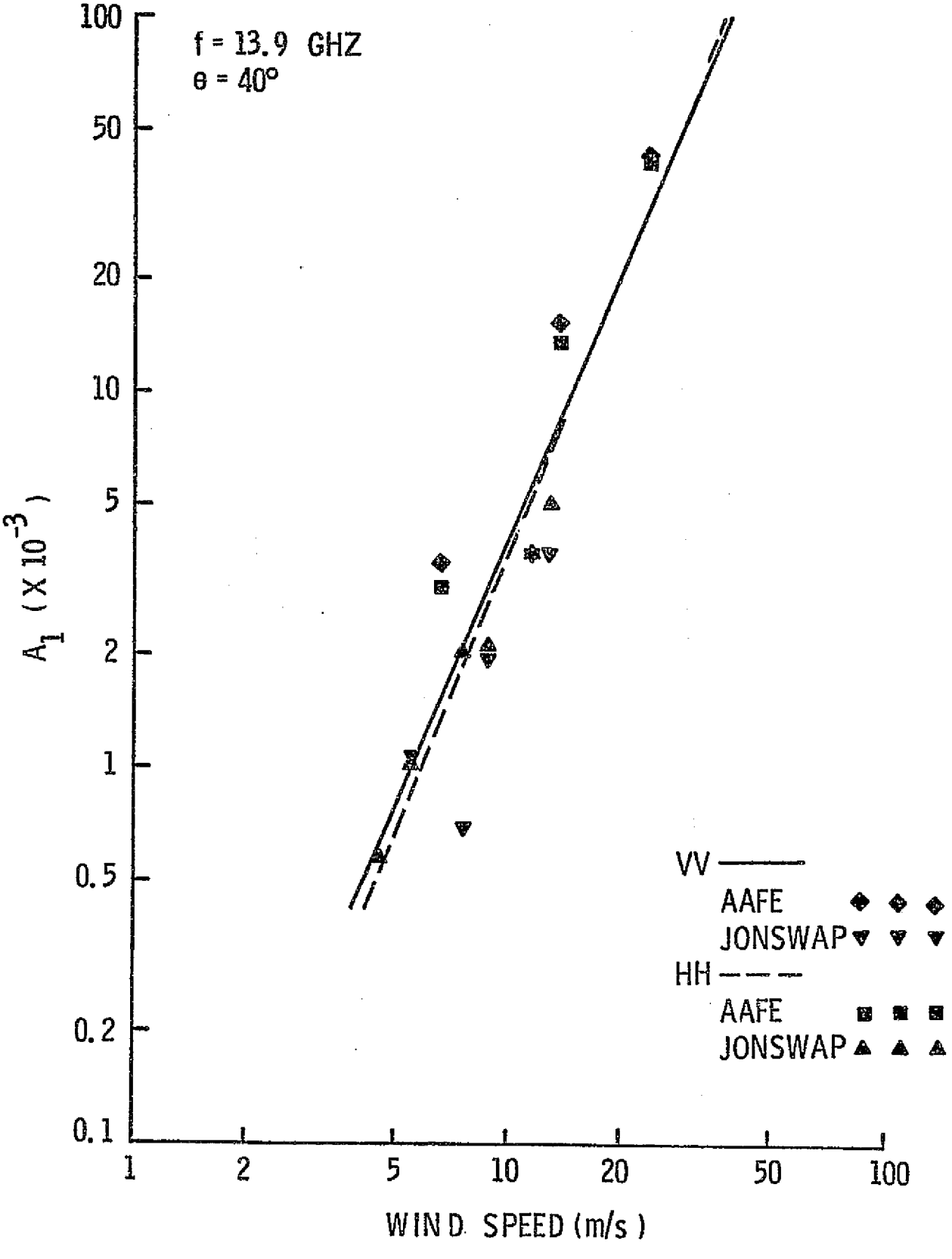
f = 13.9 GHZ
θ = 40°
100
50
20
10
5
2
1
0.5
0.2
0.1
A_1 (X 10^{-3})
1
2
5
10
20
50
100
WIND SPEED (m/s)
VV
AAFE
JONSWAP
HH
AAFE
JONSWAP

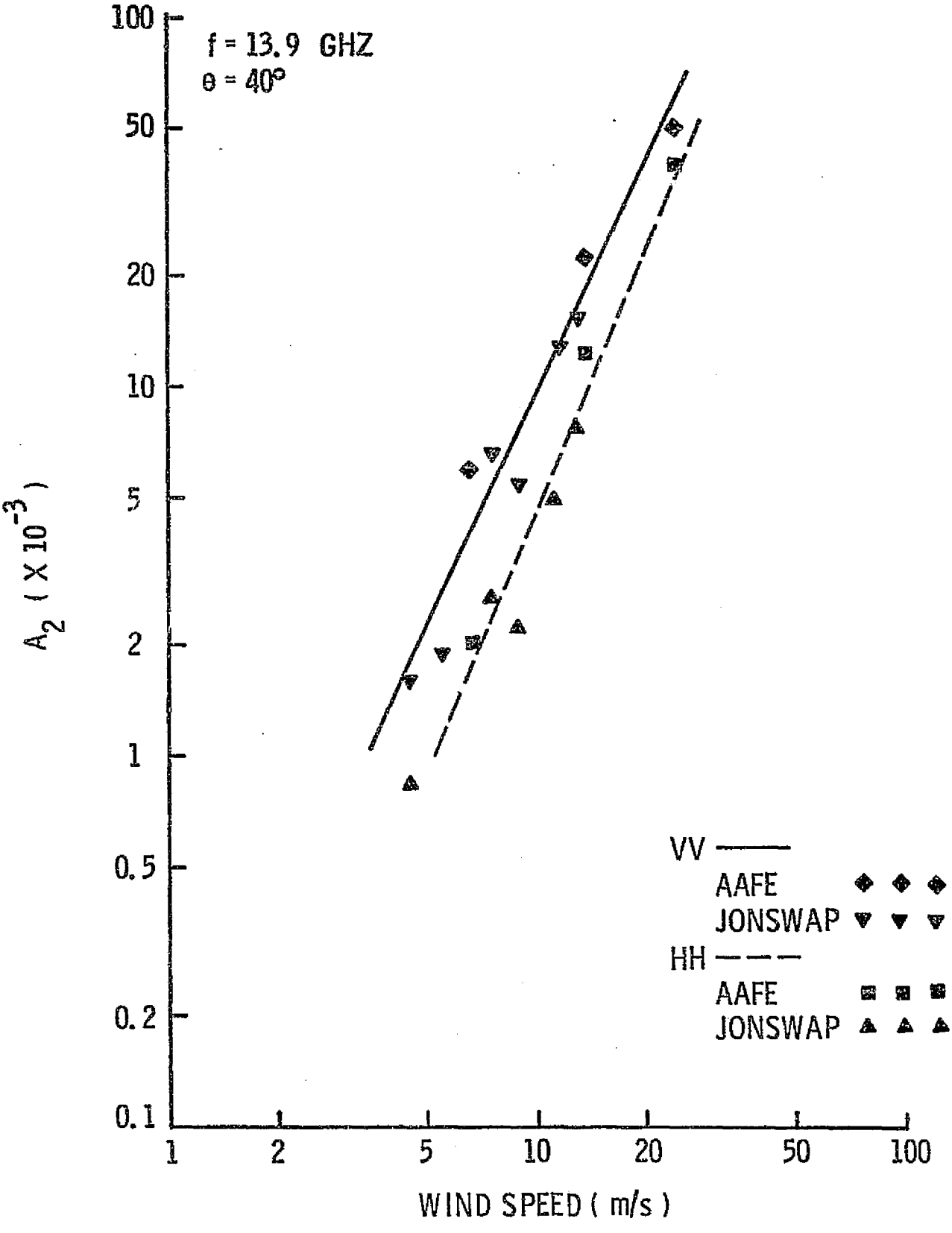
f = 13.9 GHZ
θ = 40°
100
50
20
10
5
2
1
0.5
0.2
0.1
A_2 (X 10^{-3})
1
2
5
10
20
50
100
WIND SPEED (m/s)
VV
AAFE
JONSWAP
HH
AAFE
JONSWAP

APPENDIX C

Wind Speed Errors Obtained Using WINDVEC

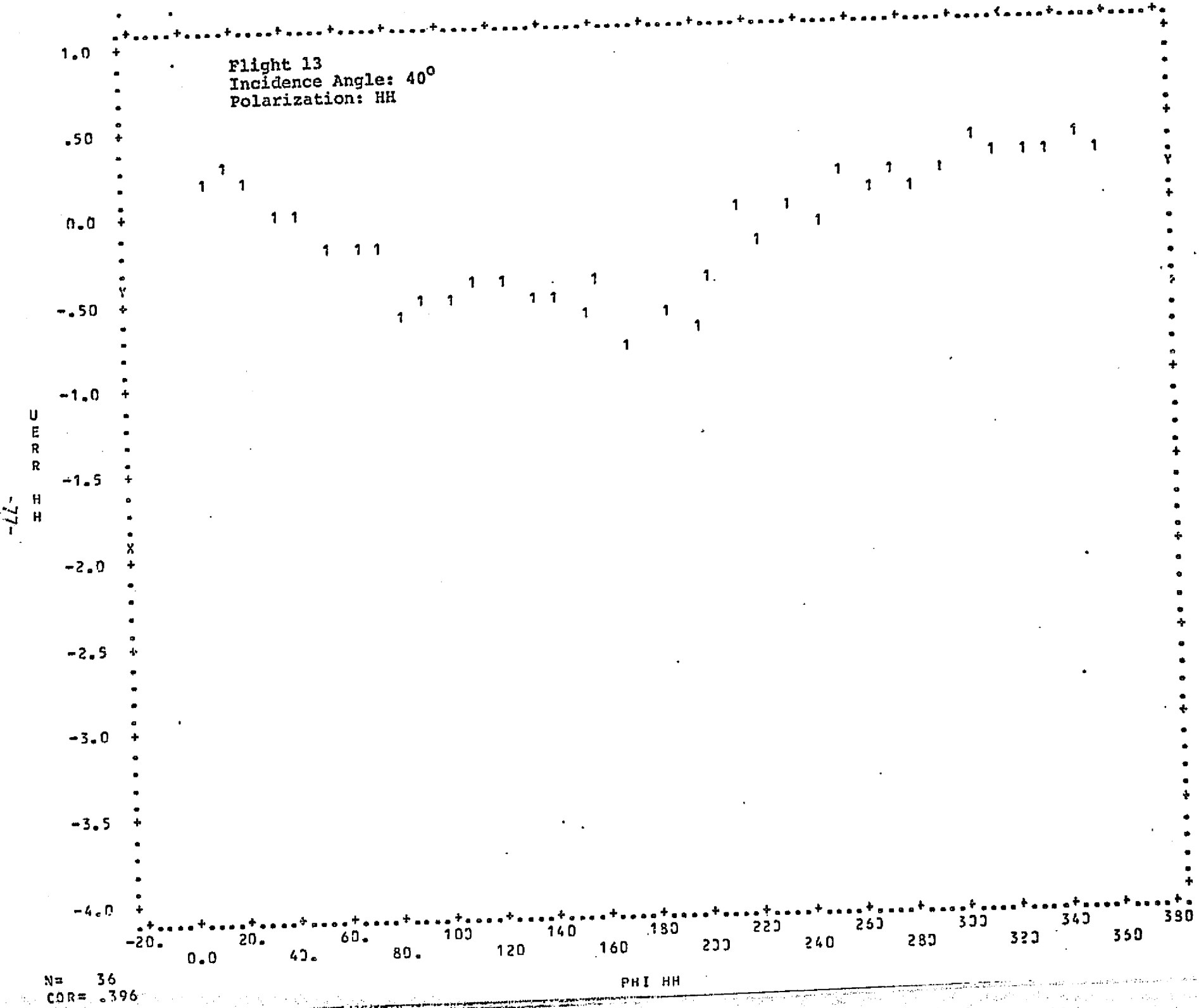
Flight 13
Incidence Angle: 40°
Polarization: HH
1.0
.50
0.0
-.50
-1.0
-1.5
-2.0
-2.5
-3.0
-3.5
-4.0
UERR HH
-20.
0.0
20.
40.
60.
80.
100
120
140
160
180
200
220
240
260
280
300
320
340
360
PHI HH
N= 36
COR= .396

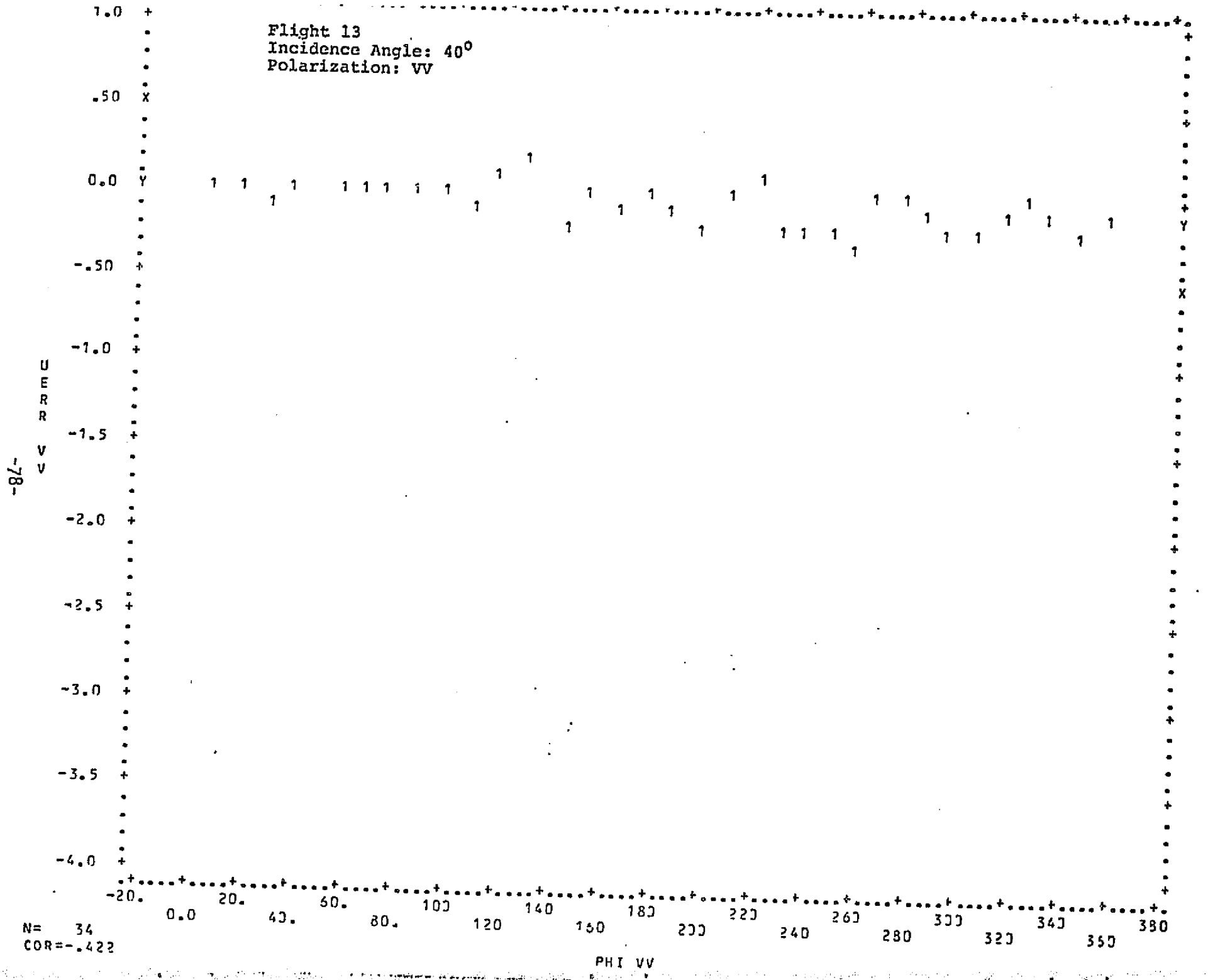
Flight 13
Incidence Angle: 40°
Polarization: VV
1.0
.50
0.0
-.50
-1.0
-1.5
-2.0
-2.5
-3.0
-3.5
-4.0
UERVV
-20.
0.0
20.
40.
60.
80.
100
120
140
160
180
200
220
240
260
280
300
320
340
360
PHI VV
N= 34
COR=-.422

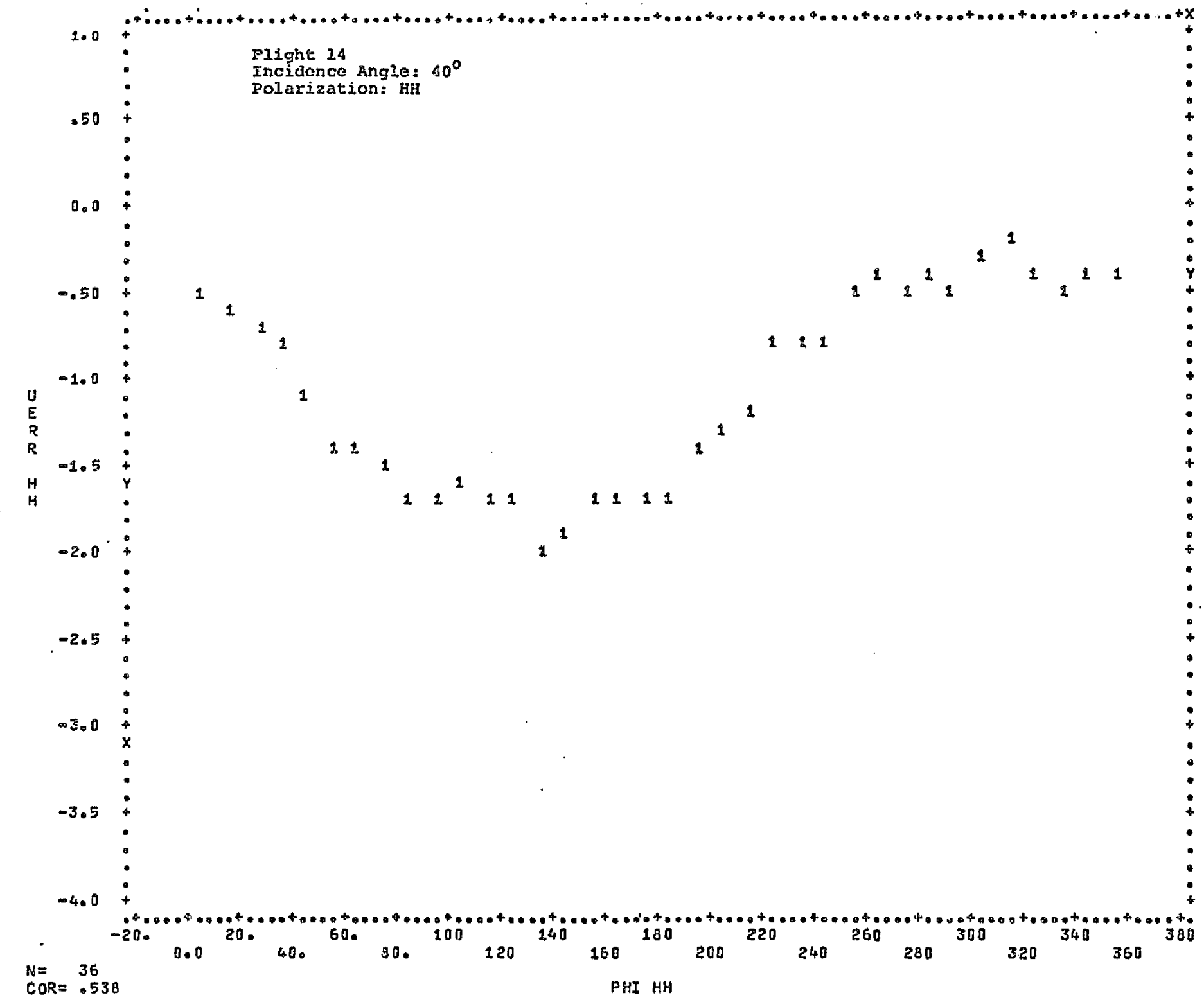
Flight 14
Incidence Angle: 40°
Polarization: HH
1.0
.50
0.0
-.50
-1.0
-1.5
-2.0
-2.5
-3.0
-3.5
-4.0
UERR HH
-20.
0.0
20.
40.
60.
80.
100
120
140
160
180
200
220
240
260
280
300
320
340
360
PHI HH

N= 36
COR= .538

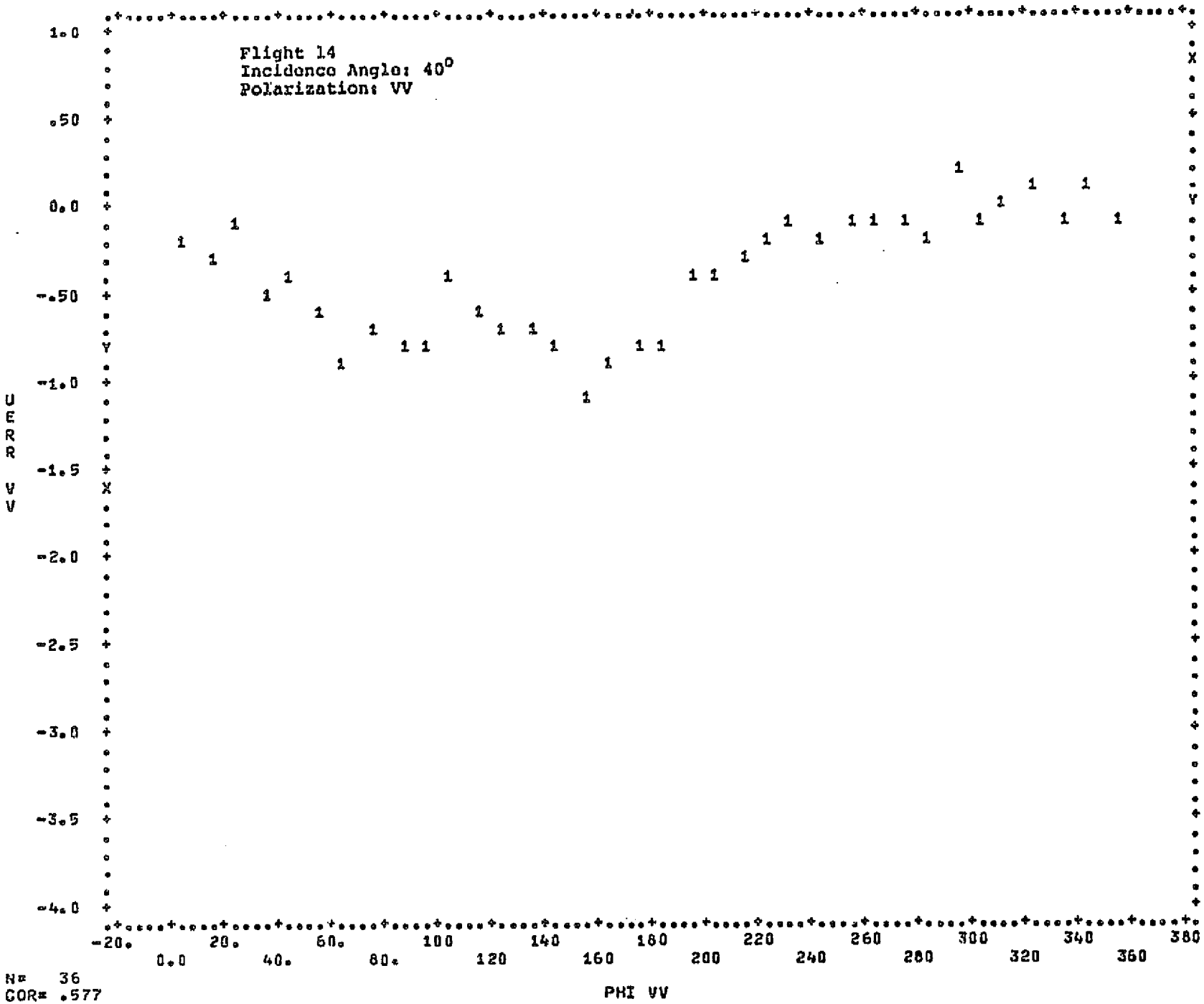

N= 36
COR= .577

MEAN ST.DEV. REGRESSION LINE RES.MS.

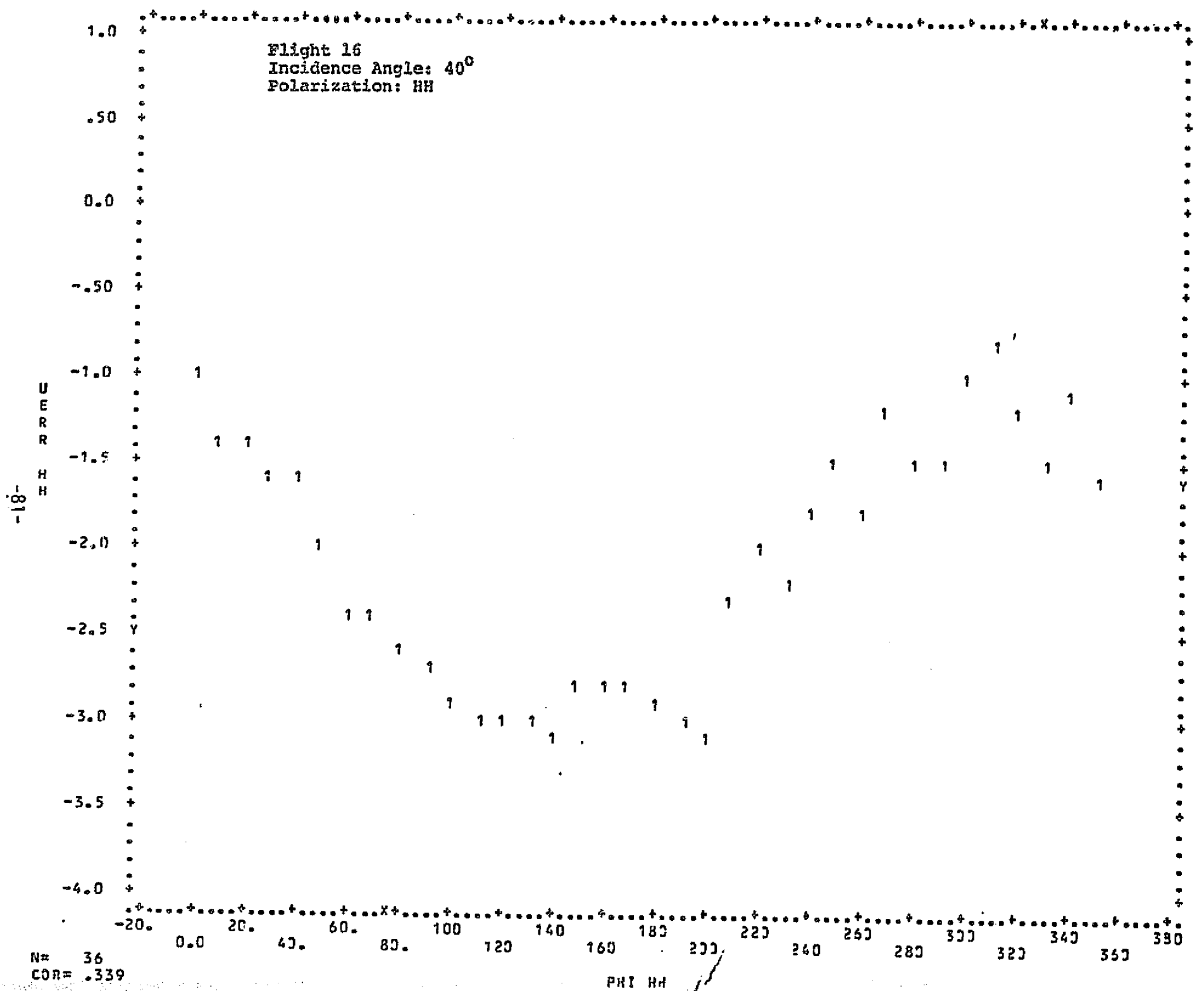
Flight 16
Incidence Angle: 40°
Polarization: HH
1.0
.50
0.0
-.50
-1.0
-1.5
-2.0
-2.5
-3.0
-3.5
-4.0
UERR HH
-20.
0.0
20.
40.
60.
80.
100
120
140
160
180
200
220
240
260
280
300
320
340
360
PHI HH
N= 36
COR= .339

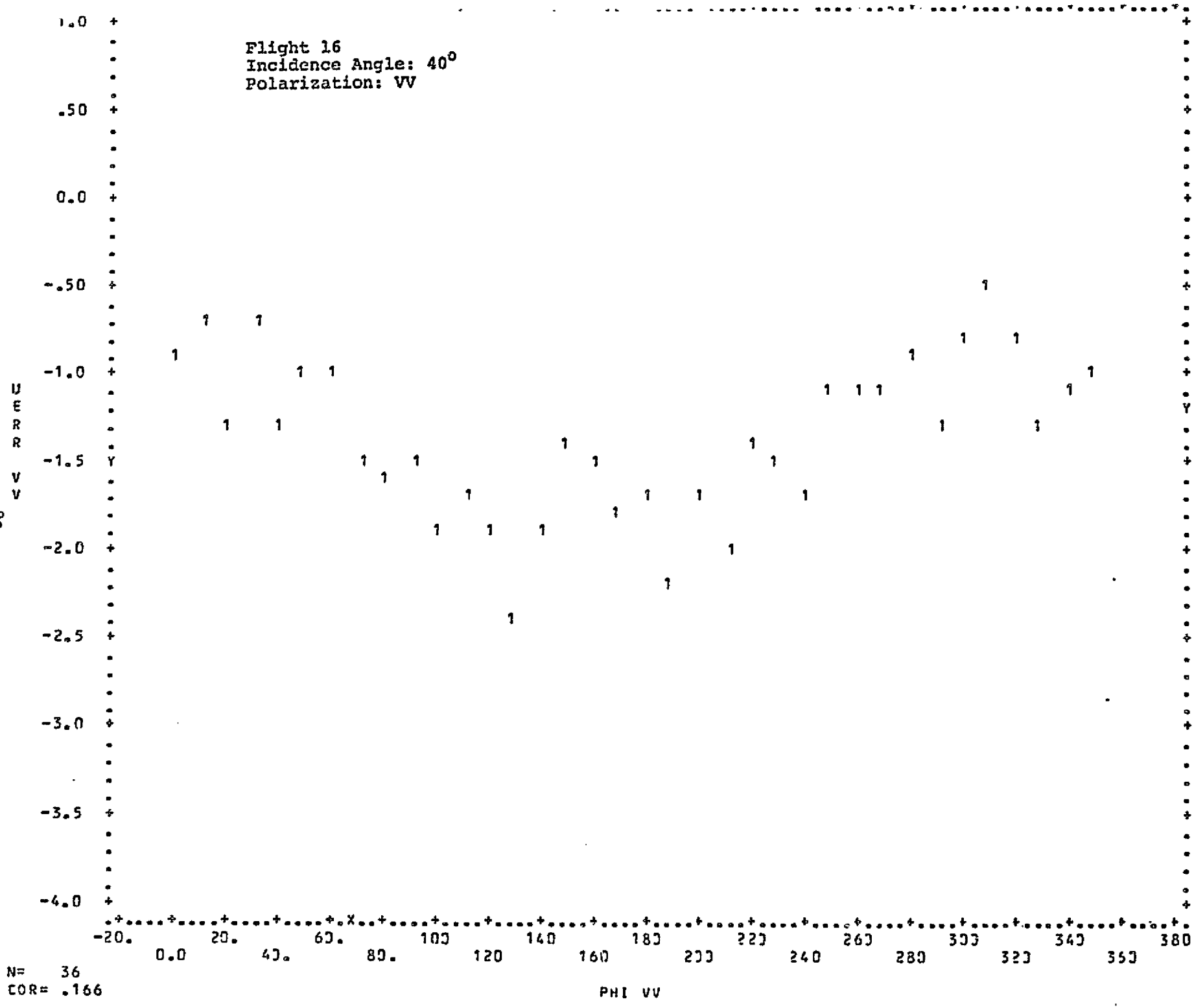
Flight 16
Incidence Angle: 40°
Polarization: VV
1.0
.50
0.0
-.50
-1.0
-1.5
-2.0
-2.5
-3.0
-3.5
-4.0
UERR VV
-20.
0.0
20.
40.
60.
80.
100
120
140
160
180
200
220
240
260
280
300
320
340
360
N= 36
COR= .166
PHI VV

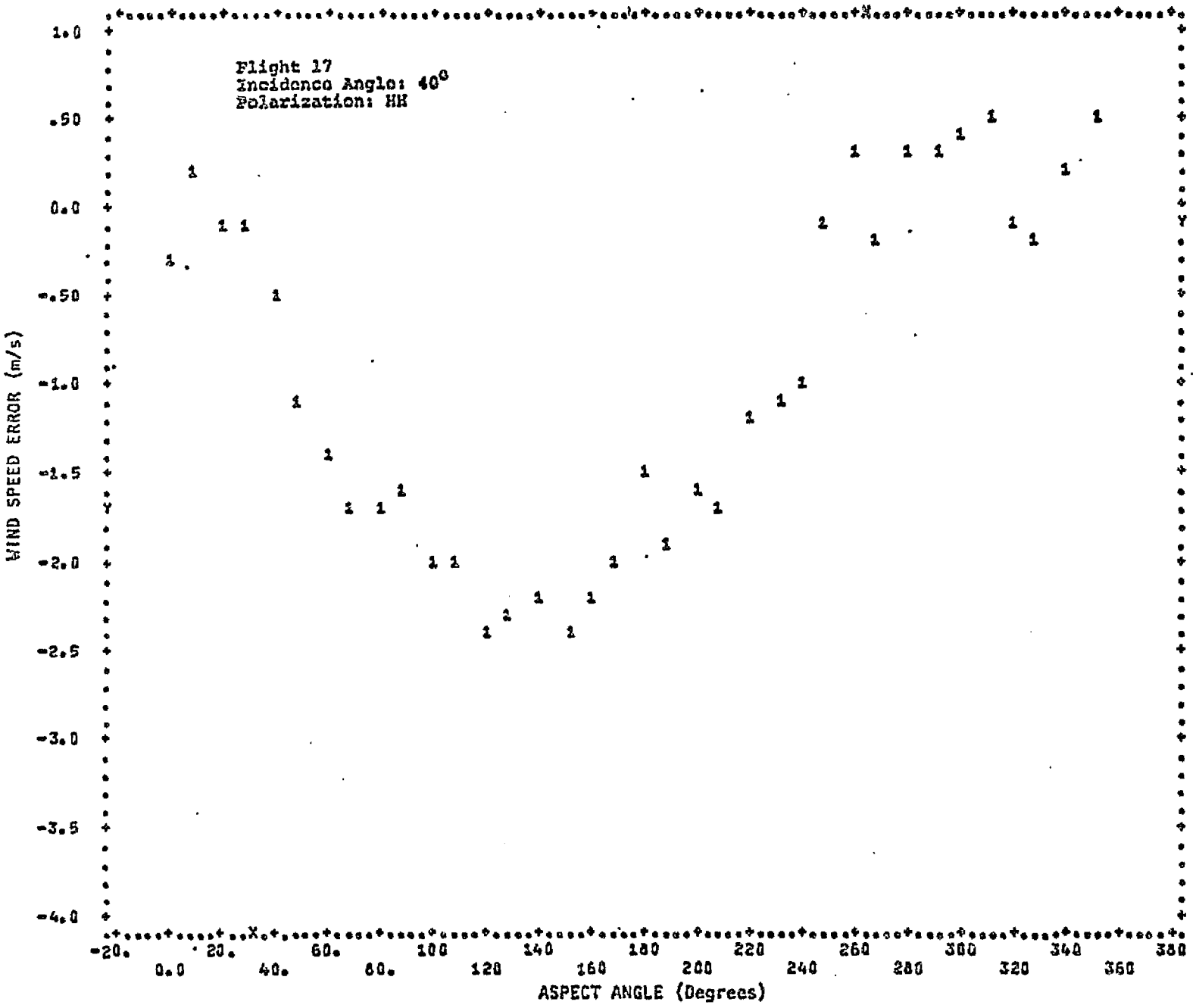
Flight 17
Incidence Angle: 40°
Polarization: HH
WIND SPEED ERROR (m/s)
1.0
.50
0.0
-.50
-1.0
-1.5
-2.0
-2.5
-3.0
-3.5
-4.0
-20.
0.0
20.
40.
60.
80.
100
120
140
160
180
200
220
240
260
280
300
320
340
360
380
ASPECT ANGLE (Degrees)

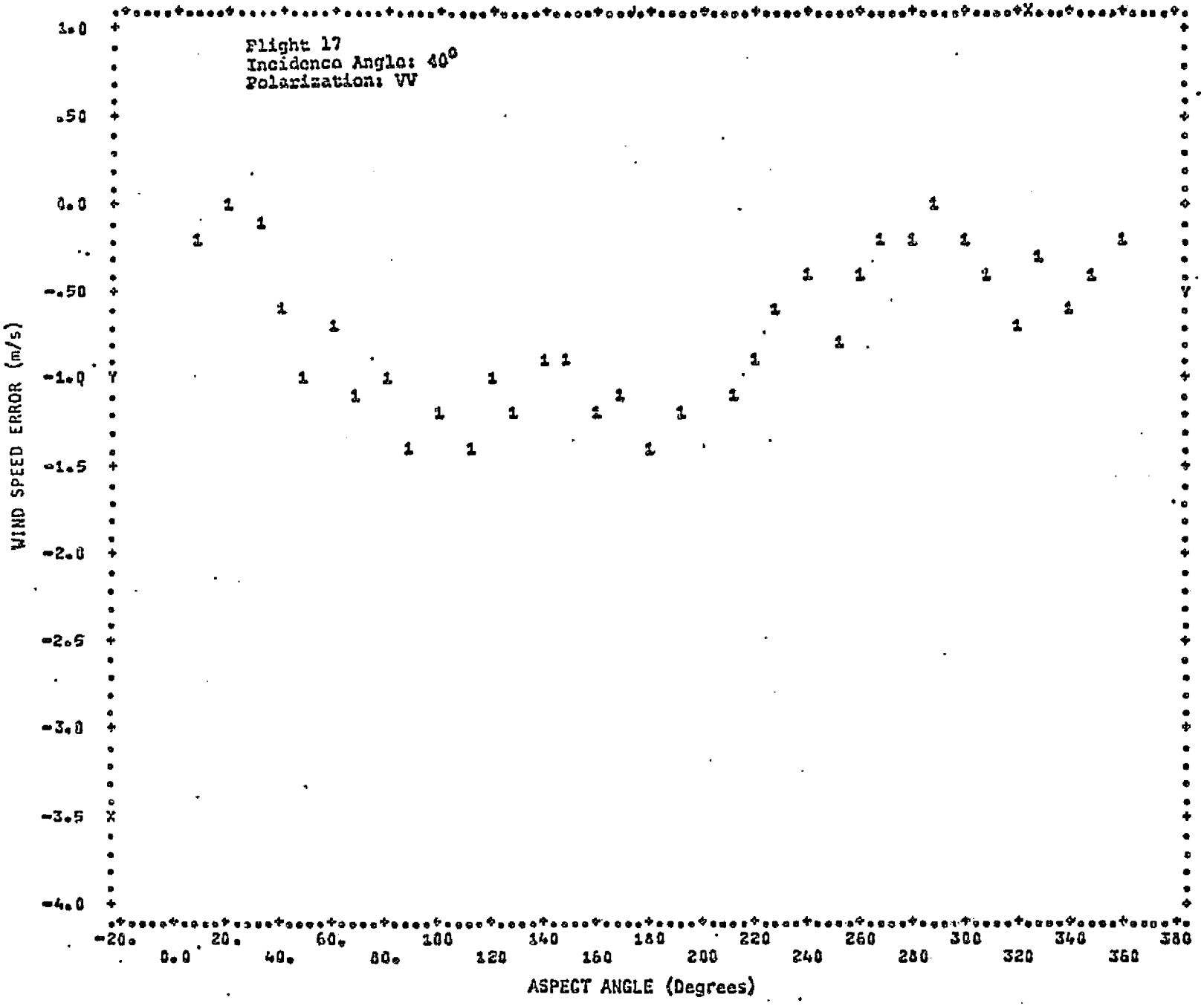
Flight 17
Incidence Angle: 40°
Polarization: VV
WIND SPEED ERROR (m/s)
1.0
.50
0.0
-.50
-1.0
-1.5
-2.0
-2.5
-3.0
-3.5
-4.0
-20.
0.0
20.
40.
60.
80.
100
120
140
160
180
200
220
240
260
280
300
320
340
360
ASPECT ANGLE (Degrees)

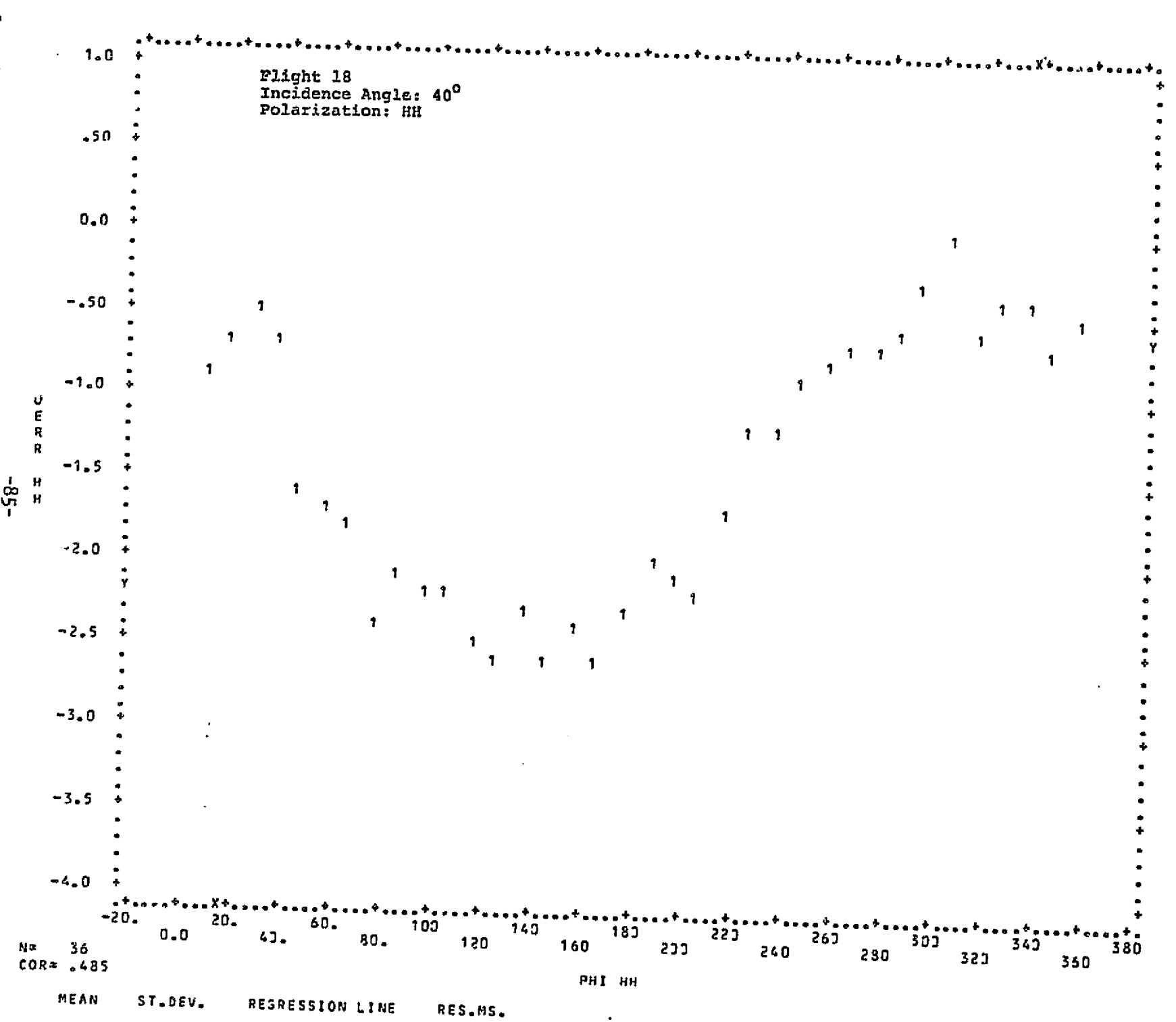
Flight 18
Incidence Angle: 40°
Polarization: HH
1.0
.50
0.0
-.50
-1.0
-1.5
-2.0
-2.5
-3.0
-3.5
-4.0
-20.
0.0
20.
40.
60.
80.
100
120
140
160
180
200
220
240
260
280
300
320
340
360
380
PHI HH
ERR HH
N= 36
COR= .485
MEAN ST.DEV. REGRESSION LINE RES.MS.

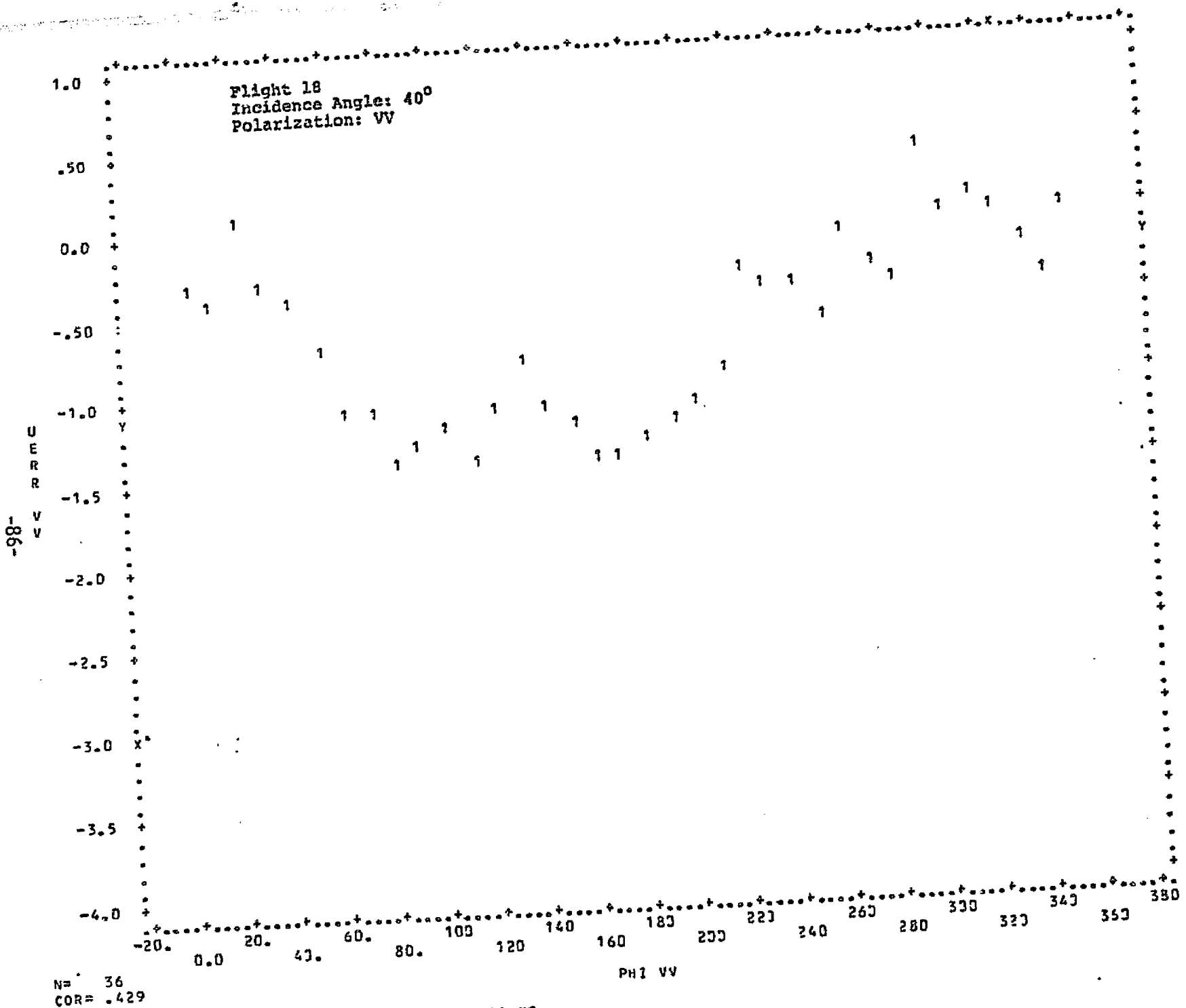

N= 36
COR= .429

MEAN ST.DEV. RESRESSION LINE RES.MS.

APPENDIX D

Wind Direction Errors Obtained Using WINDEX

Wind Direction Error:

(PHIERR) vs ϕ

A. Direction errors using antenna 1.
B. Direction error using antenna 2.

Wind Direction Error:

(ERRAUG) vs ϕ

A Direction errors using averaged estimates.

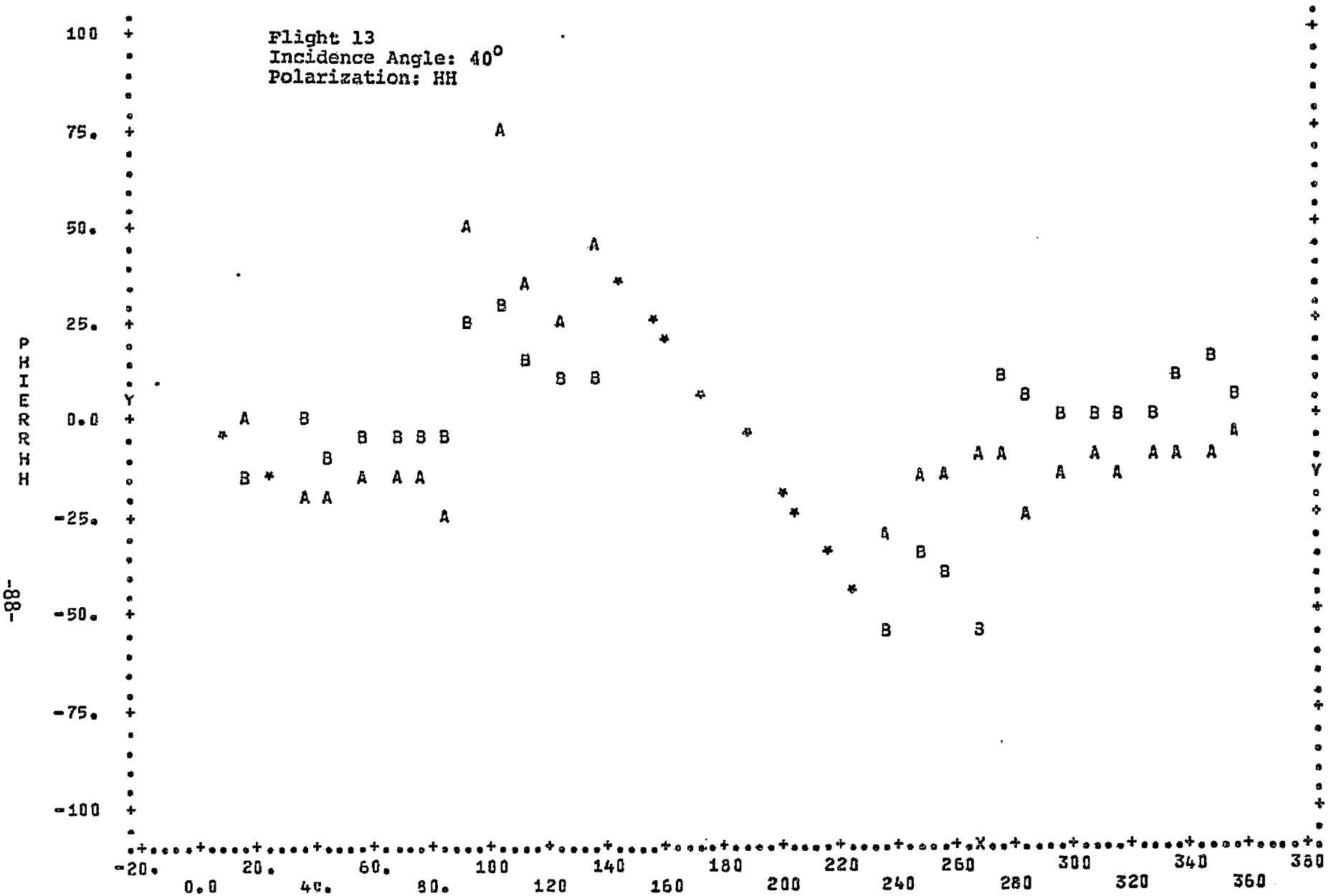

N= 72
COR=-.193

	MEAN	ST.DEV.	REGRESSION LINE	RES.MS.
X	180.72	105.08	X=-.83578*Y+ 177.48	10784.
Y	-3.8760	24.227	Y=-.04443*X+ 4.1531	573.23

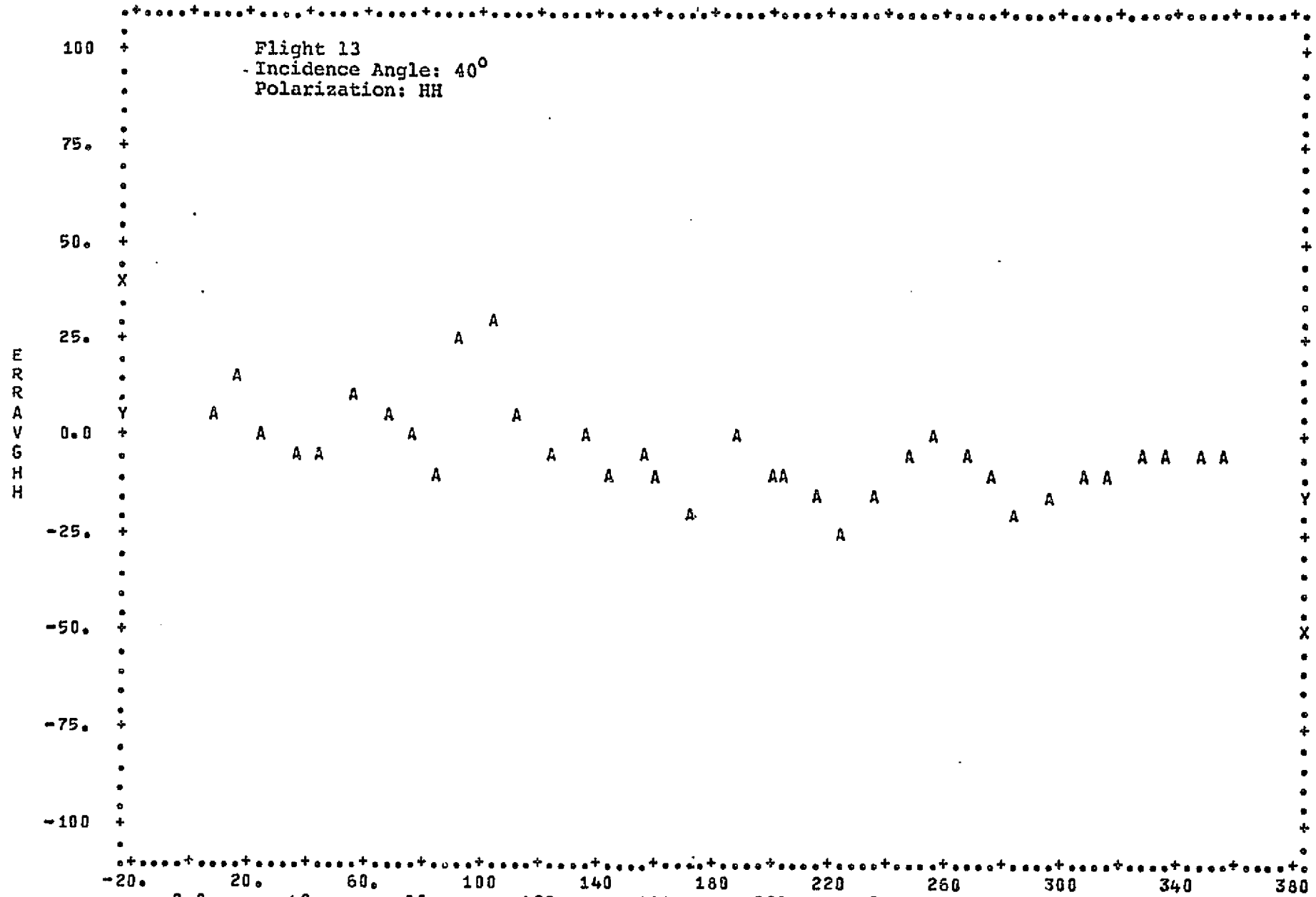

N= 36
COR=-.486

	MEAN	ST.DEV.	REGRESSION LINE	RES.MS.
X	180.72	105.83	X=-4.5890*Y+ 162.93	8803.0
Y	-3.8767	11.214	Y=-.05152*X+ 5.4349	98.838

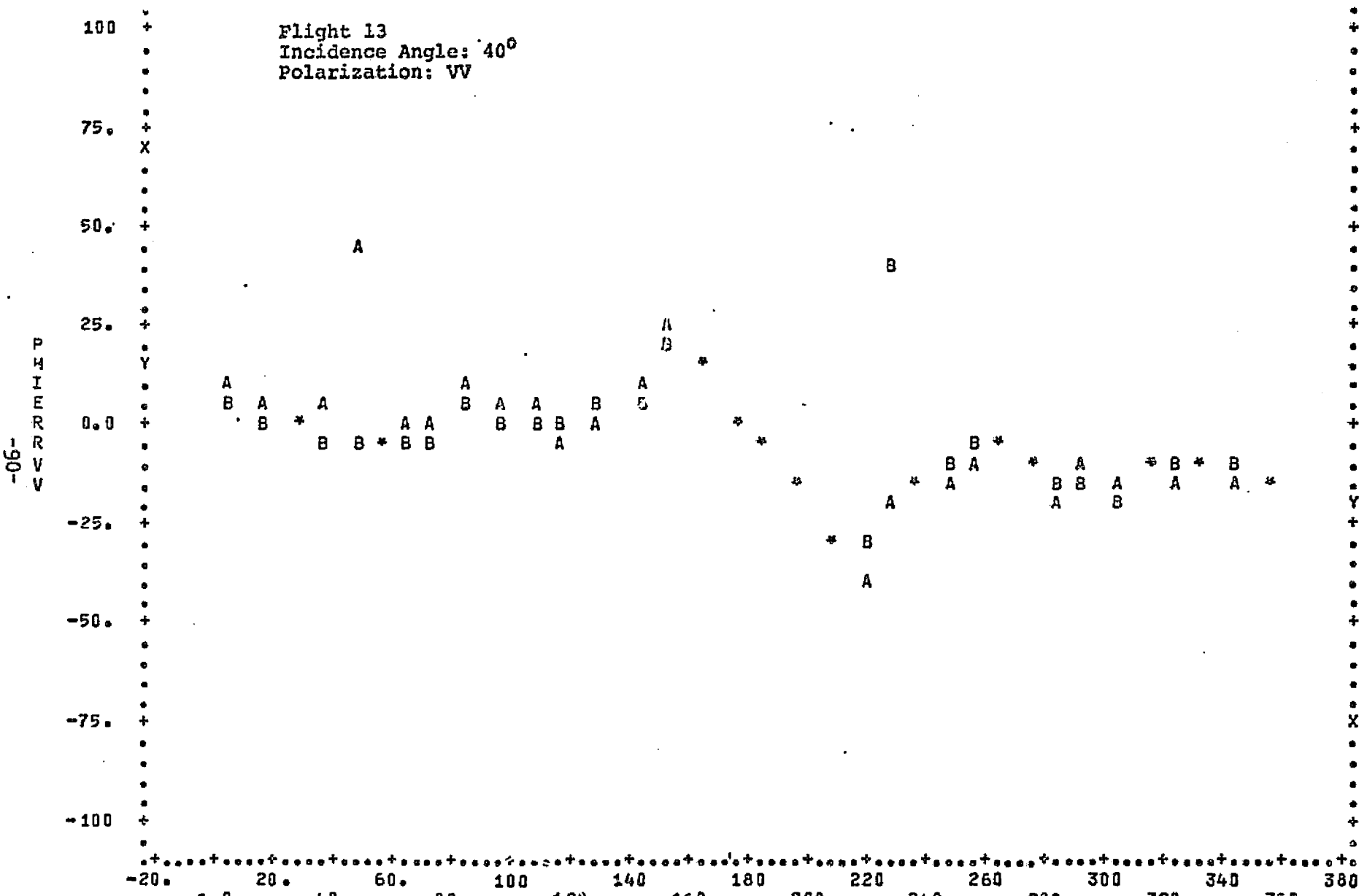

N= 72
COR=-.456

PHI VV

	MEAN	ST.DEV.	REGRESSION LINE	RES.MS.
X	180.27	104.62	X=-2.7410*Y+ 173.61	8795.9
Y	-2.4303	17.395	Y=-.07577*X+ 11.229	243.16

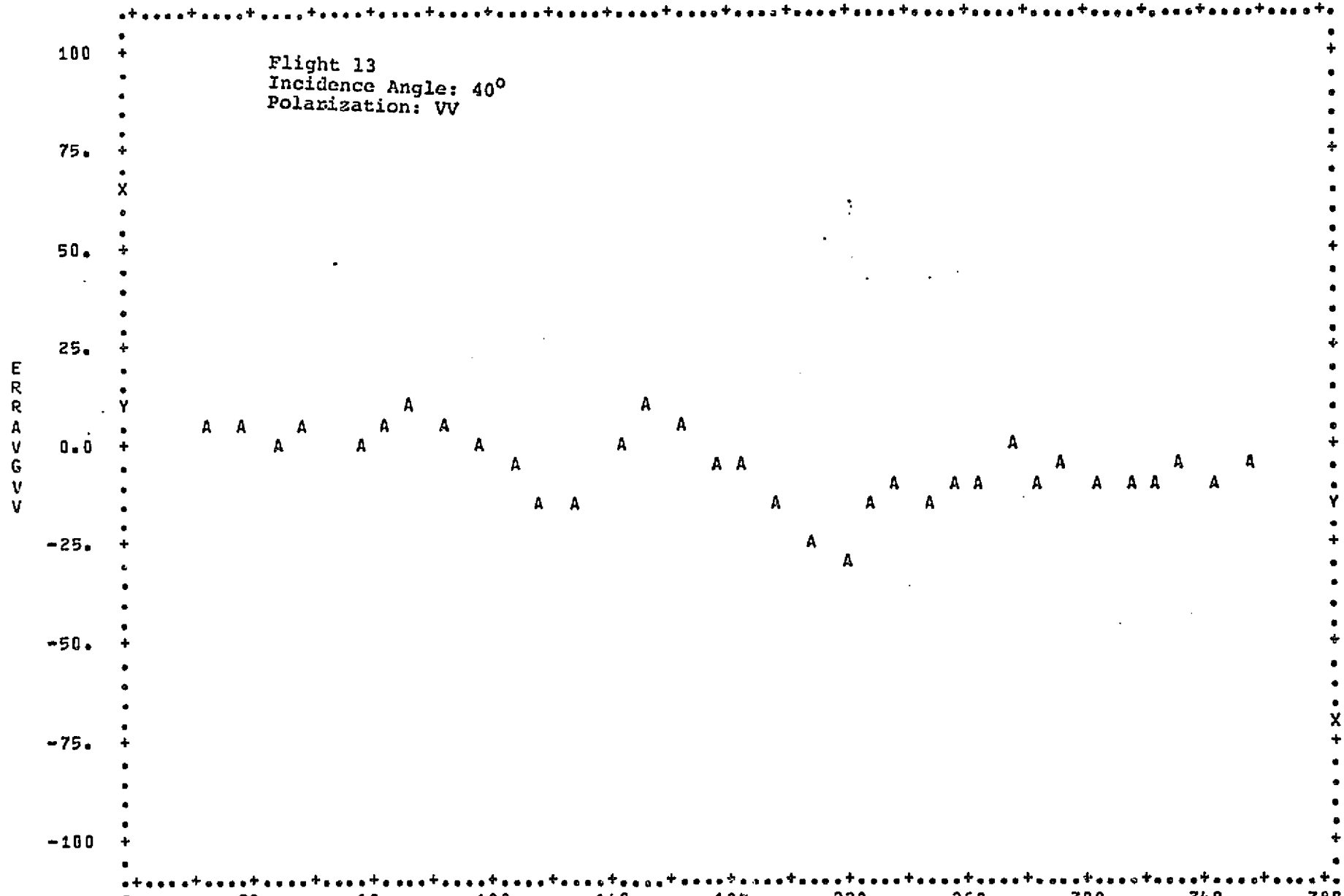

N= 36
COR=-.454

	MEAN	ST.DEV.	REGRESSION LINE	RES.MS.
X	180.27	105.36	X=-2.9625*Y+ 173.07	9072.5
Y	-2.4306	16.147	Y=-.06958*X+ 10.112	213.08

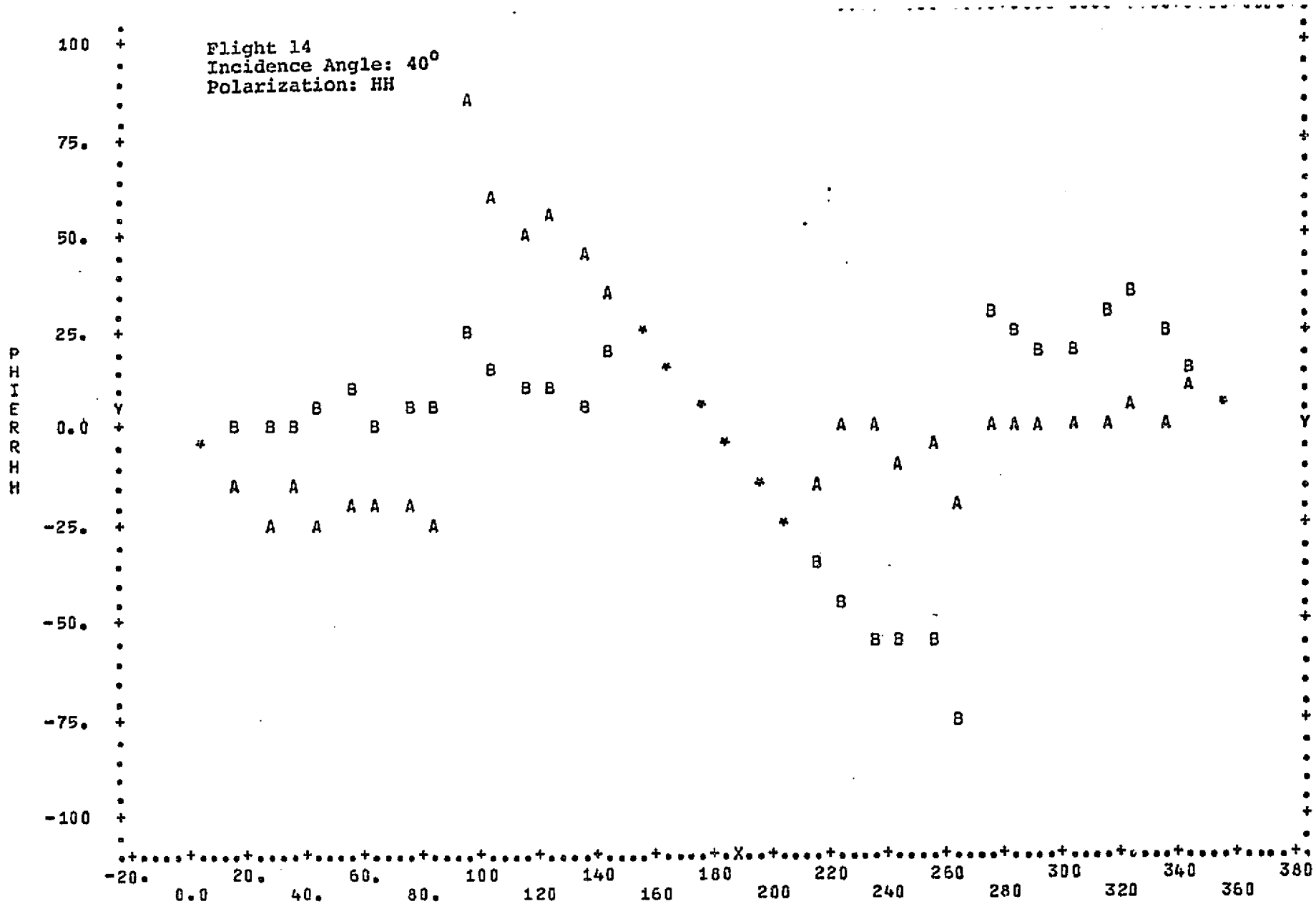

N= 72
COR=-.023

	MEAN	ST.DEV.	REGRESSION LINE	RES.MS.
X	180.12	104.38	X=-.08635*Y+ 180.25	11046.
Y	1.4860	27.334	Y=-.00592*X+ 2.5525	757.45

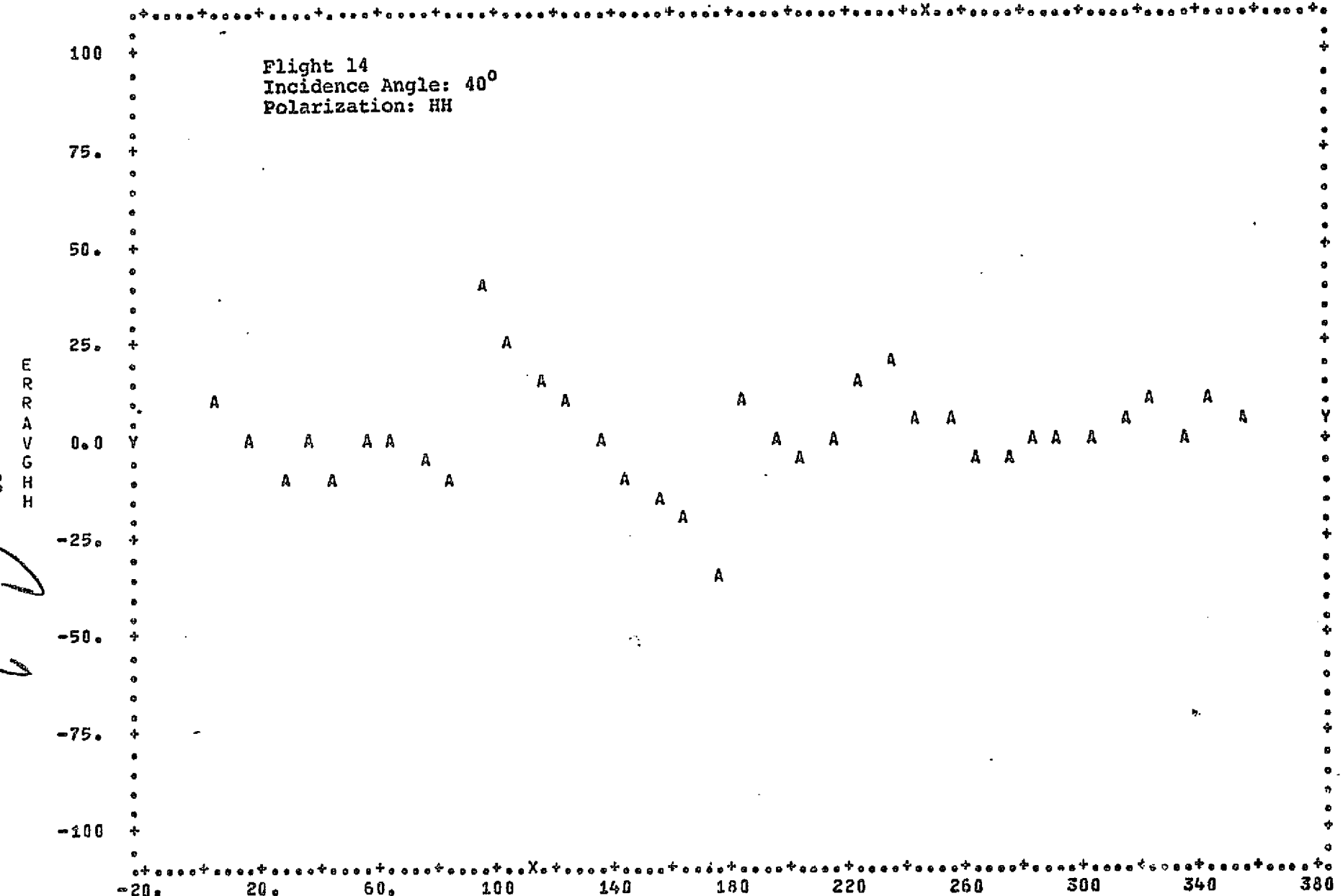

N= 36
COR= .076

	MEAN	ST.DEV.	REGRESSION LINE	RES.MS.
X	180.12	105.13	X= .62856*Y+ 179.19	11310.
Y	1.4869	12.781	Y= .00929*X-.18642	167.17

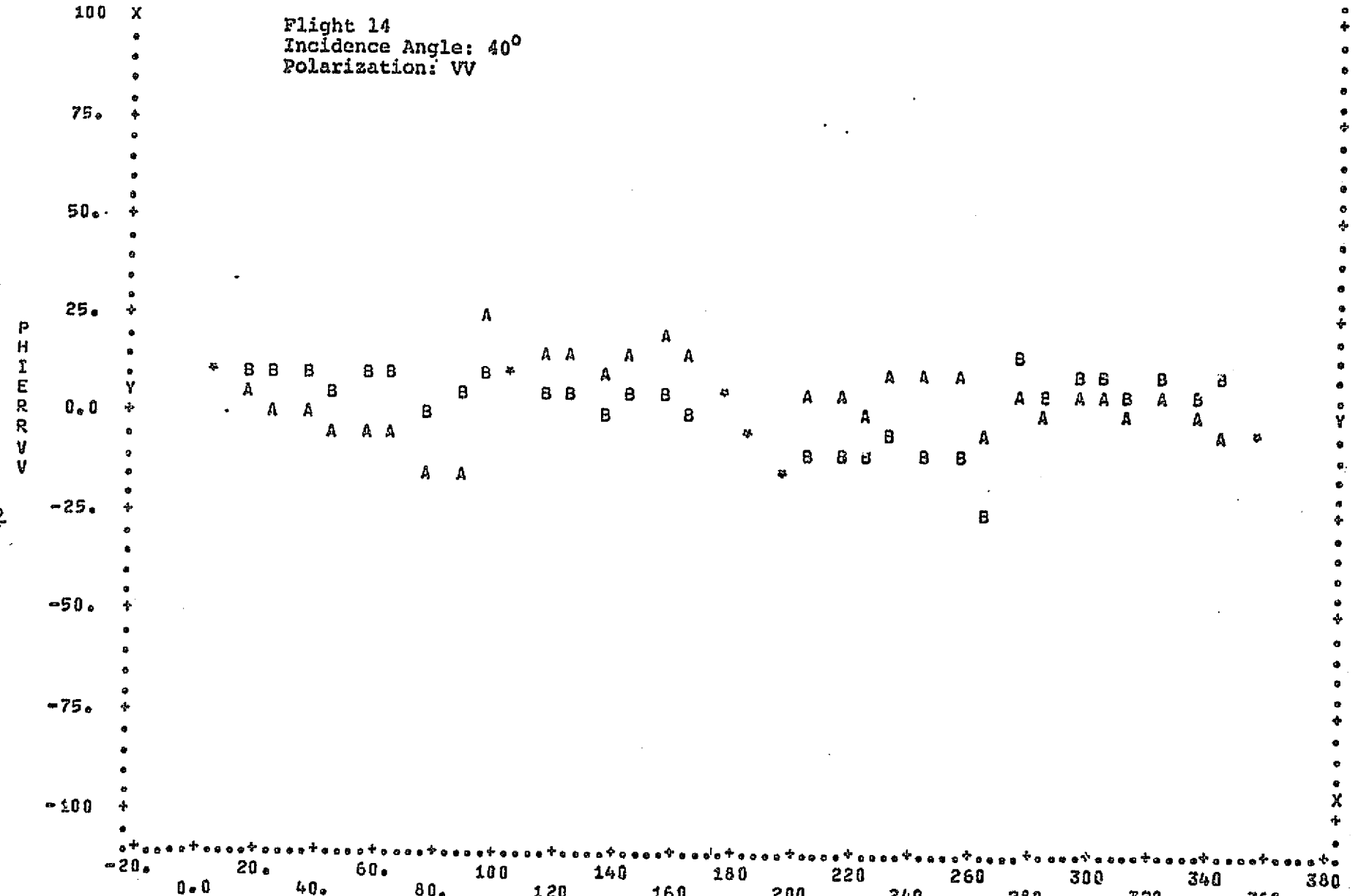

N= 72
COR=-.182

	MEAN	ST.DEV.	REGRESSION LINE	RES.MS.
X	179.97	104.47	X=-2.0737*Y+ 185.93	10702.
Y	2.8717	9.1905	Y=-.01605*X+ 5.7598	82.822

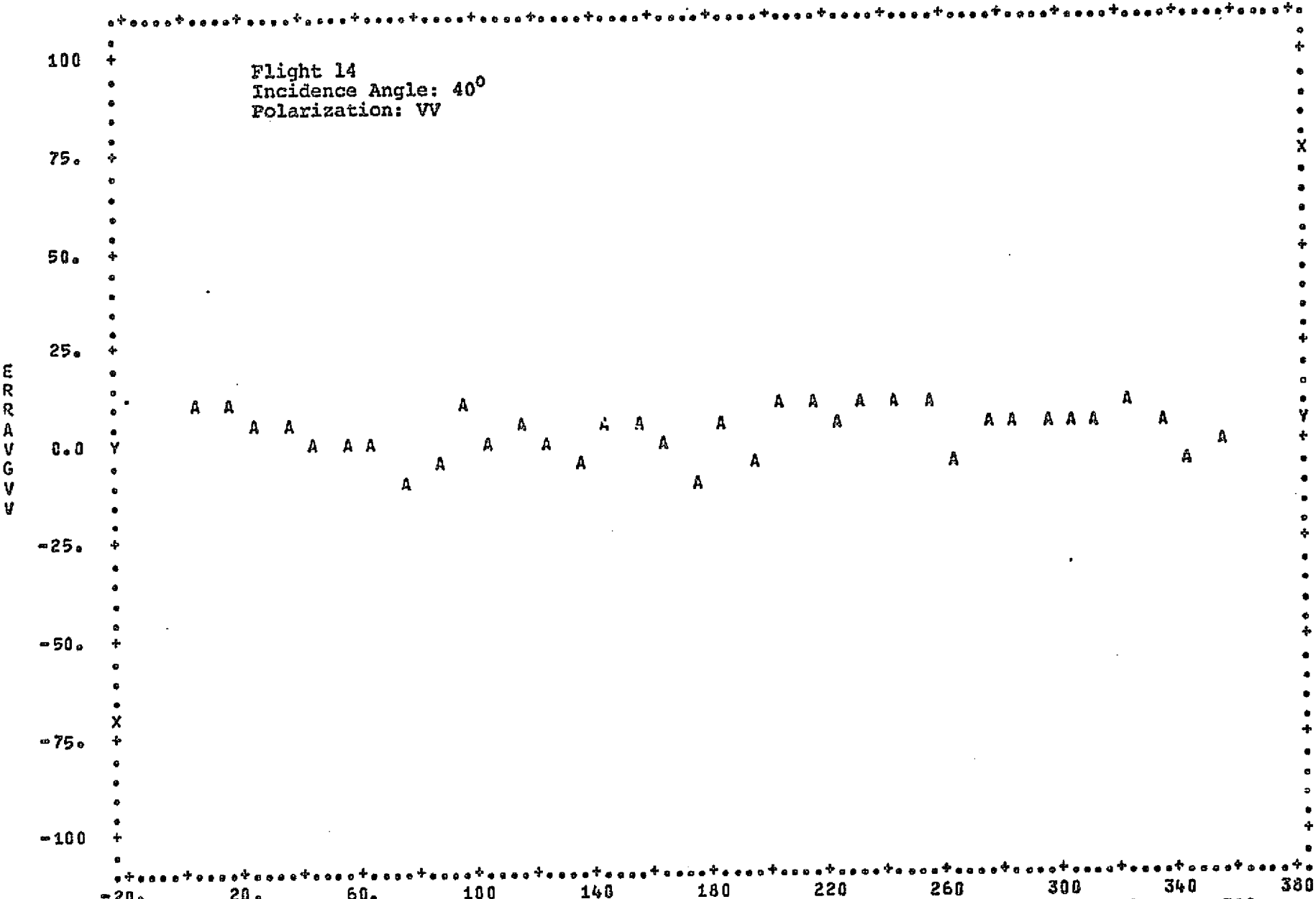

N= 36
COR= .143

	MEAN	ST.DEV.	REGRESSION LINE	RES.MS.
X	179.97	105.22	X= 2.7506*Y+ 172.07	11164.
Y	2.8711	5.4542	Y= .00739*X+ 1.5409	30.001

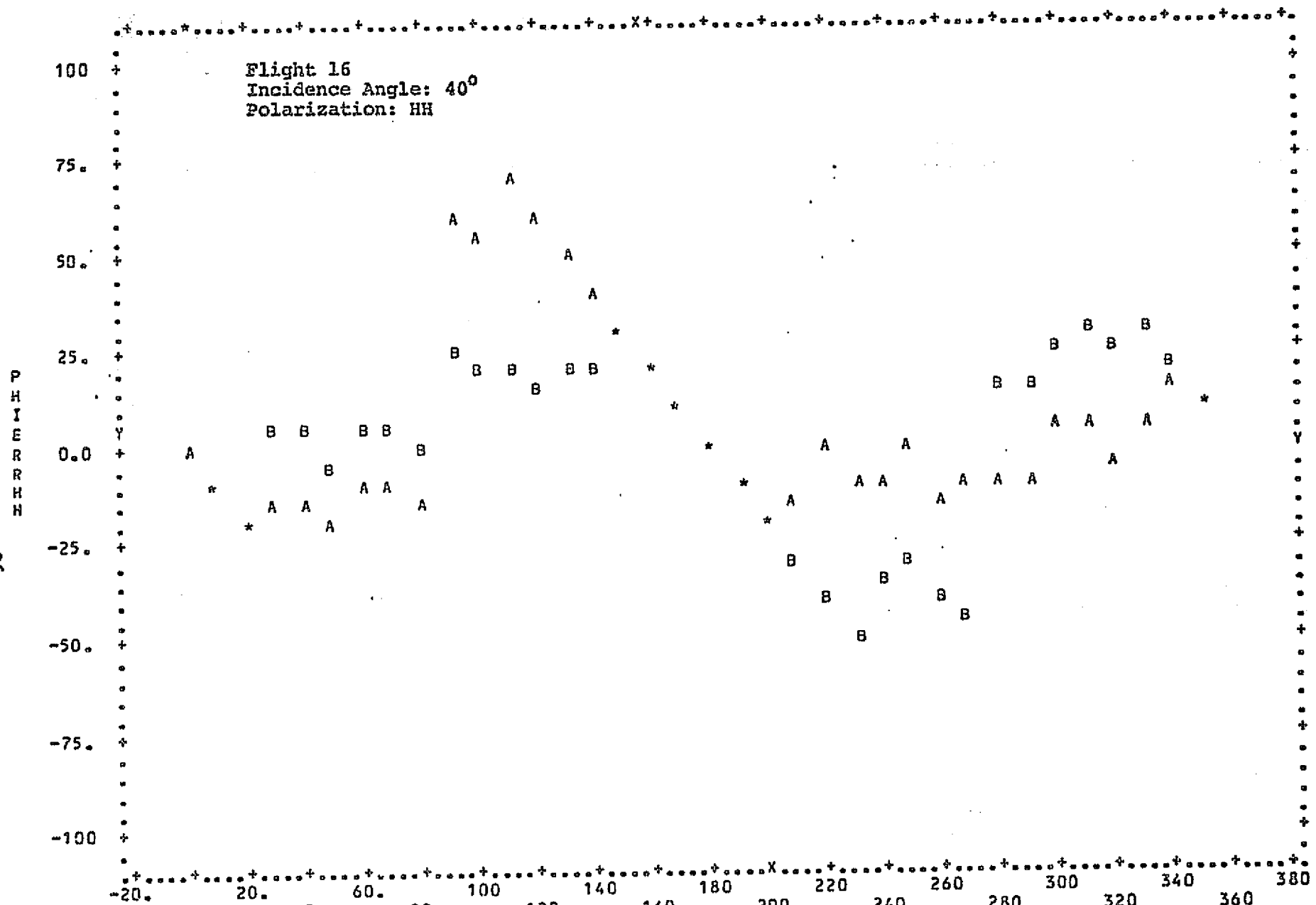

N= 71
COR=-.044

	MEAN	ST.DEV.	REGRESSION LINE	RES.MS.
X	177.38	103.42	X=-.18359*Y+ 177.97	10829.
Y	3.2318	24.959	Y=-.01069*X+ 5.1285	630.73

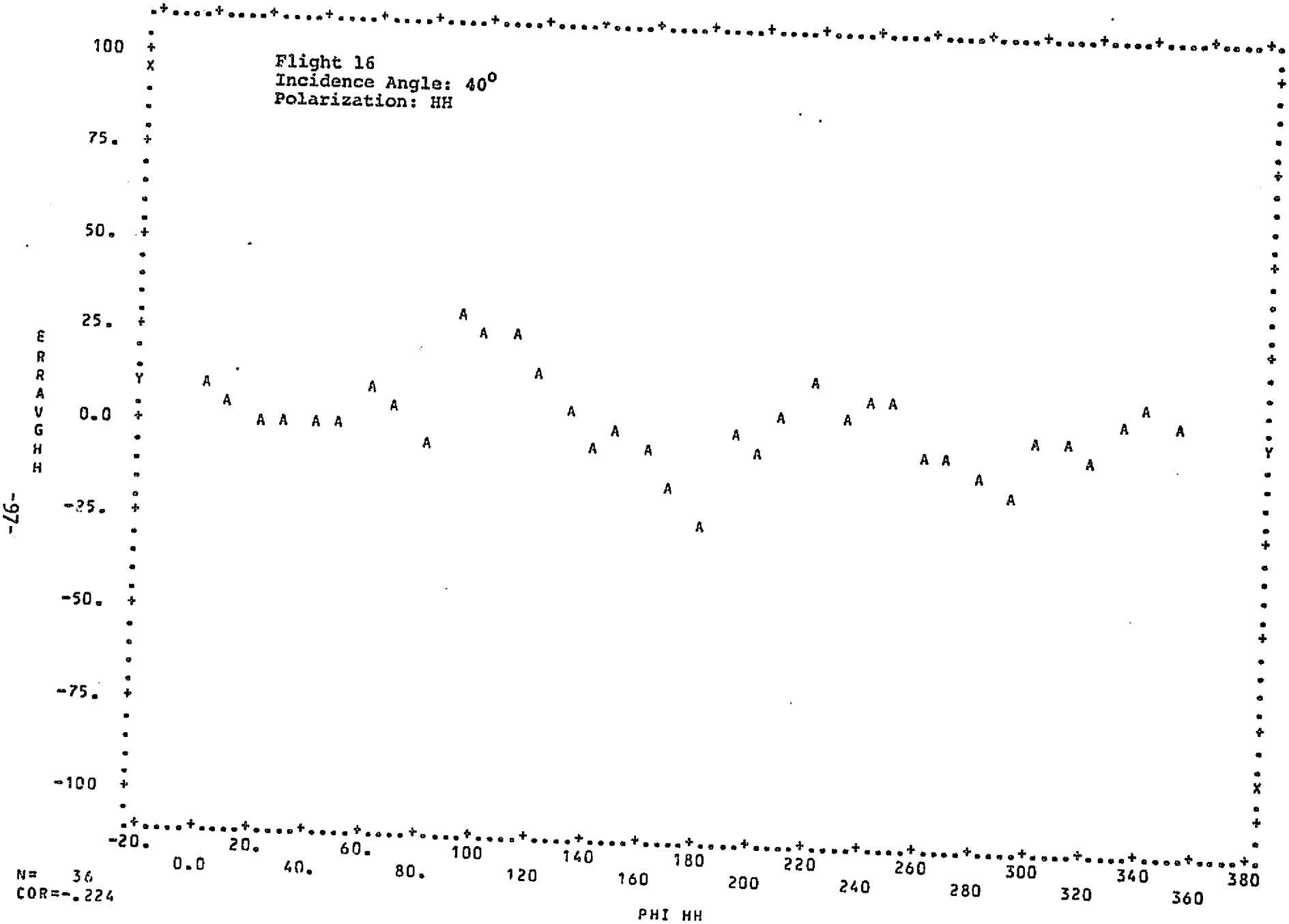

N= 36
COR=-.224

	MEAN	ST.DEV.	REGRESSION LINE	RES.MS.
X	174.91	105.54	X=-2.1969*Y+ 181.91	10890.
Y	3.1872	10.774	Y=-.02289*X+ 7.1915	113.48

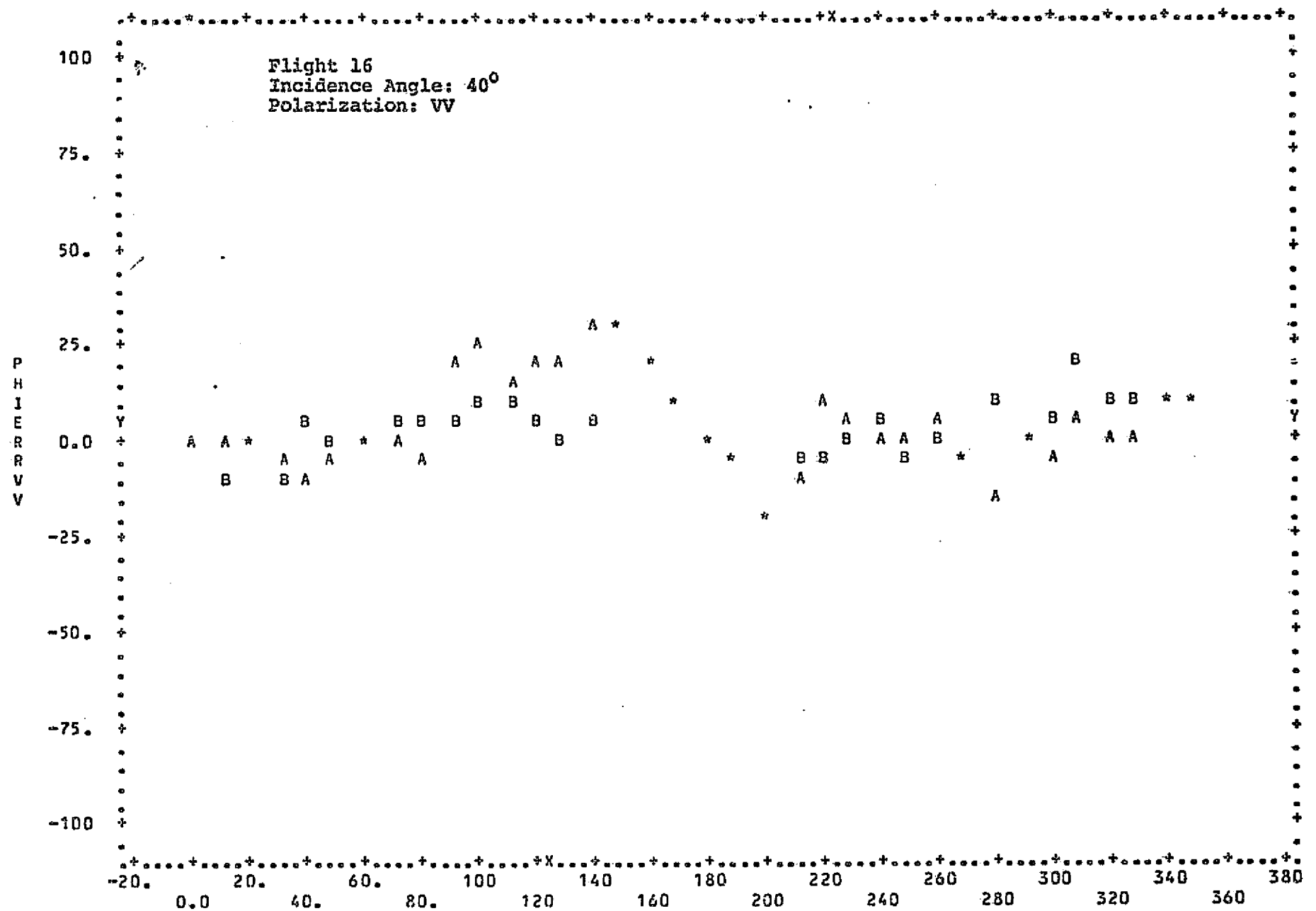

N= 71
COR= .048

	MEAN	ST.DEV.	REGRESSION LINE	RES.MS.
X	177.27	102.89	X= .45915*Y+ 175.49	10714.
Y	3.8835	10.862	Y= .00512*X+ 2.9763	119.41

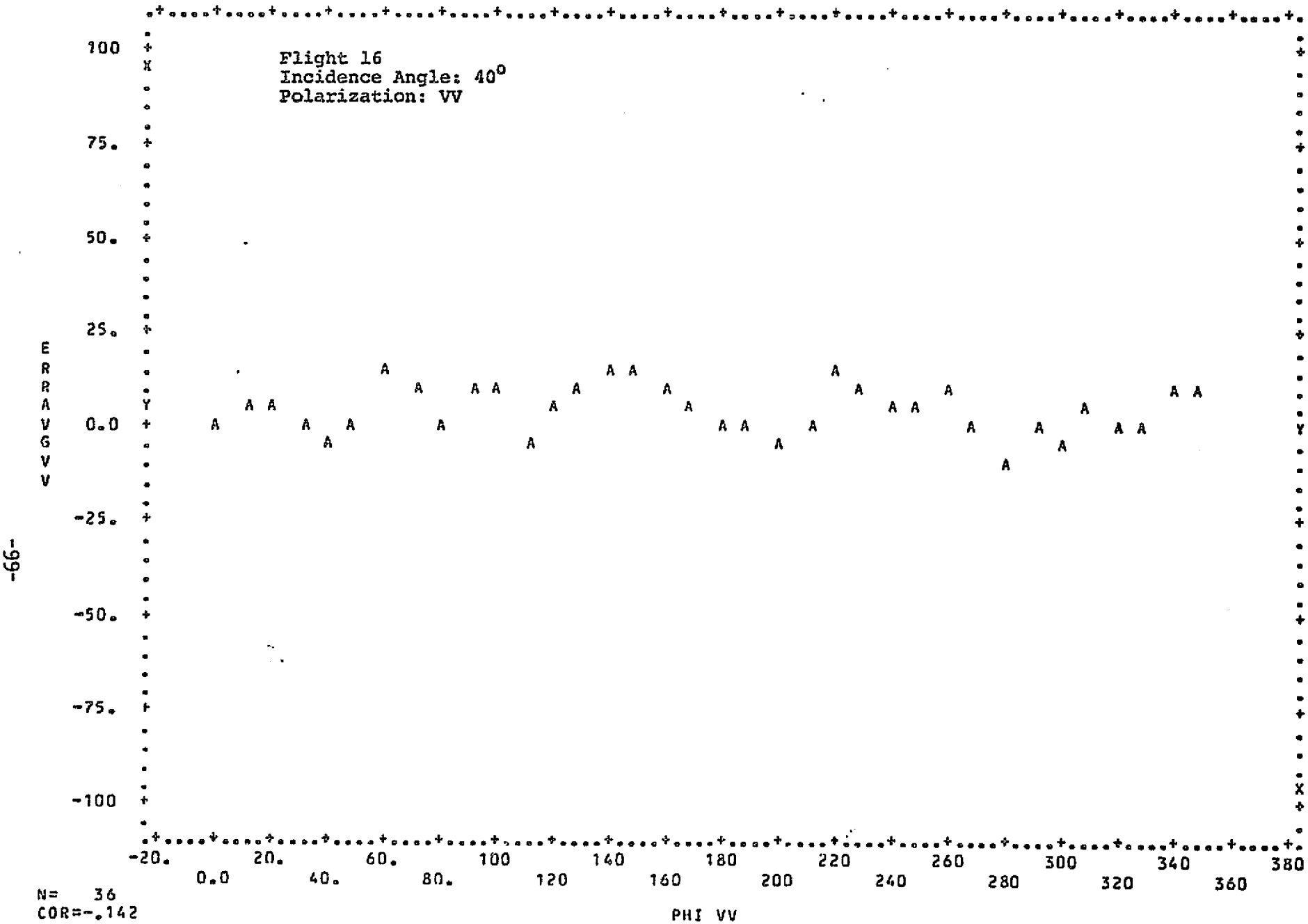

N= 36
COR=-.142

	MEAN	ST.DEV.	REGRESSION LINE	RES.MS.
X	174.83	104.99	X=-2.1693*Y+ 183.10	11119.
Y	3.8122	6.8543	Y=-.00925*X+ 5.4288	47.395

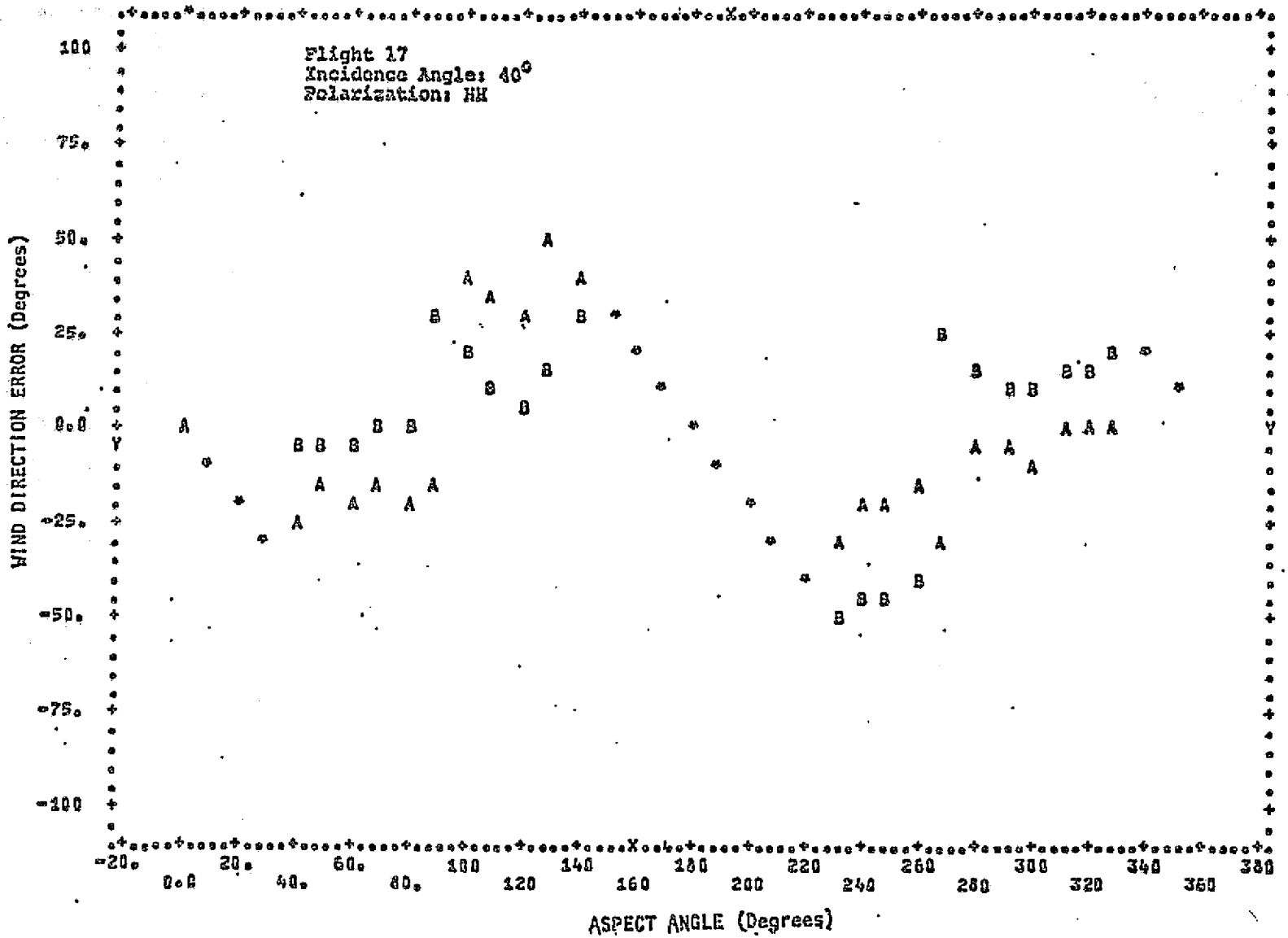
Flight 17
Incidence Angle: 40°
Polarization: HH
WIND DIRECTION ERROR (Degrees)
100
75.
50.
25.
0.0
-25.
-50.
-75.
-100
-20.
0.0
20.
40.
60.
80.
100
120
140
160
180
200
220
240
260
280
300
320
340
360
ASPECT ANGLE (Degrees)

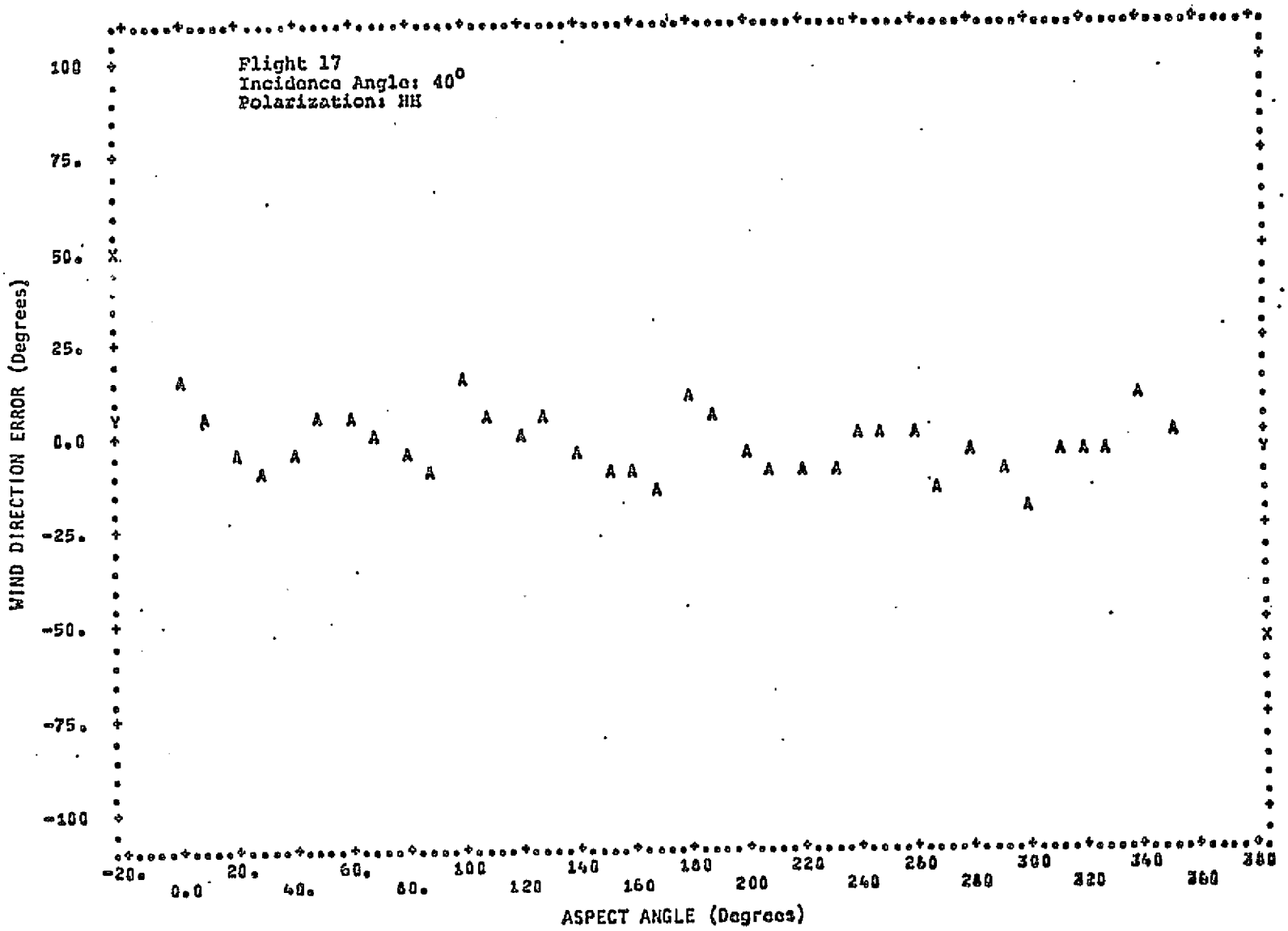
Flight 17
Incidance Angle: 40°
Polarization: HH
WIND DIRECTION ERROR (Degrees)
100
75.
50.
25.
0.0
-25.
-50.
-75.
-100
-20.
0.0
20.
40.
60.
80.
100
120
140
160
180
200
220
240
260
280
300
320
340
360
ASPECT ANGLE (Degrees)

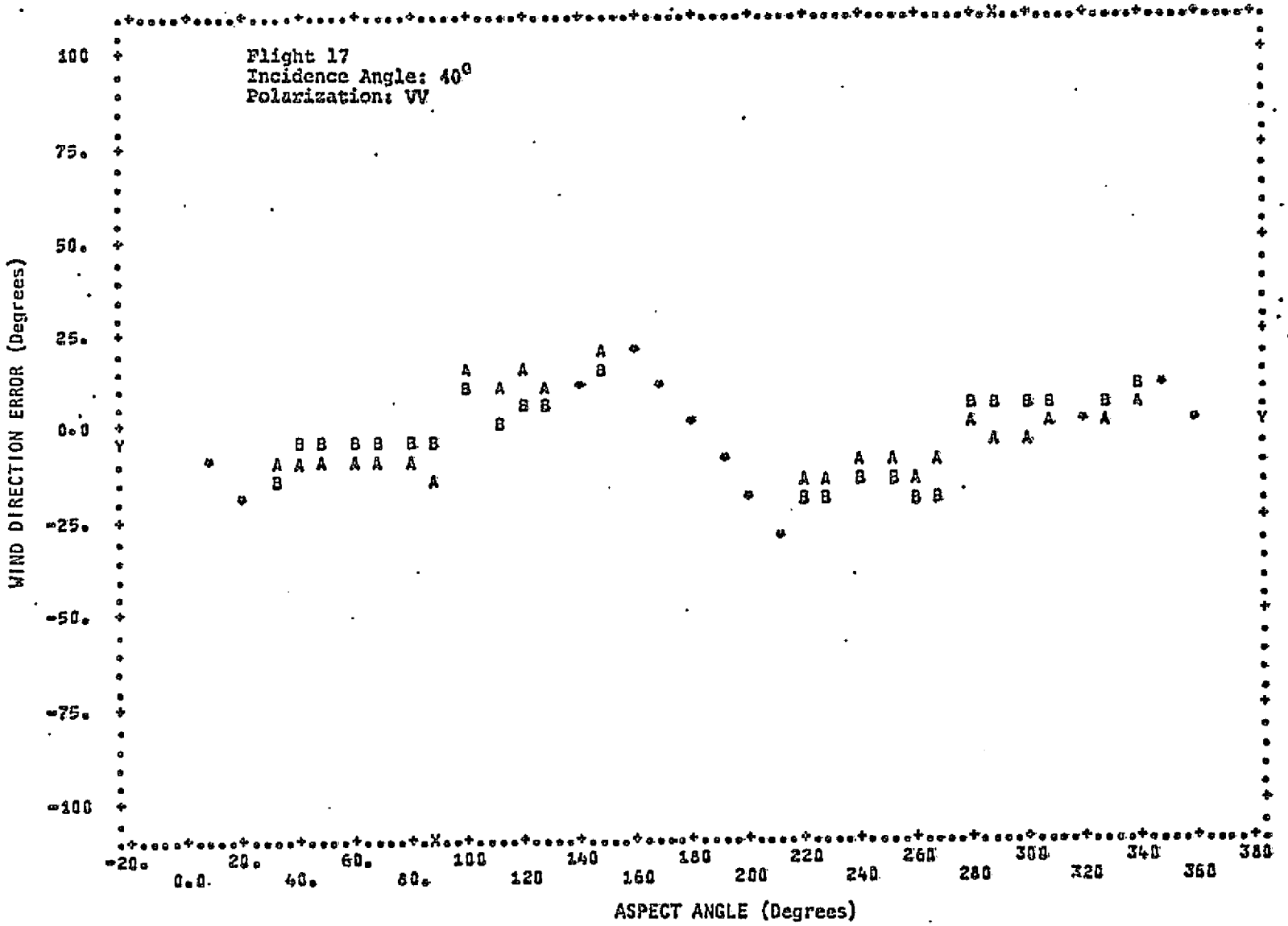
Flight 17
Incidence Angle: 40°
Polarization: VV
WIND DIRECTION ERROR (Degrees)
100
75.
50.
25.
0.0
-25.
-50.
-75.
-100
-20.
0.0
20.
40.
60.
80.
100
120
140
160
180
200
220
240
260
280
300
320
340
360
ASPECT ANGLE (Degrees)

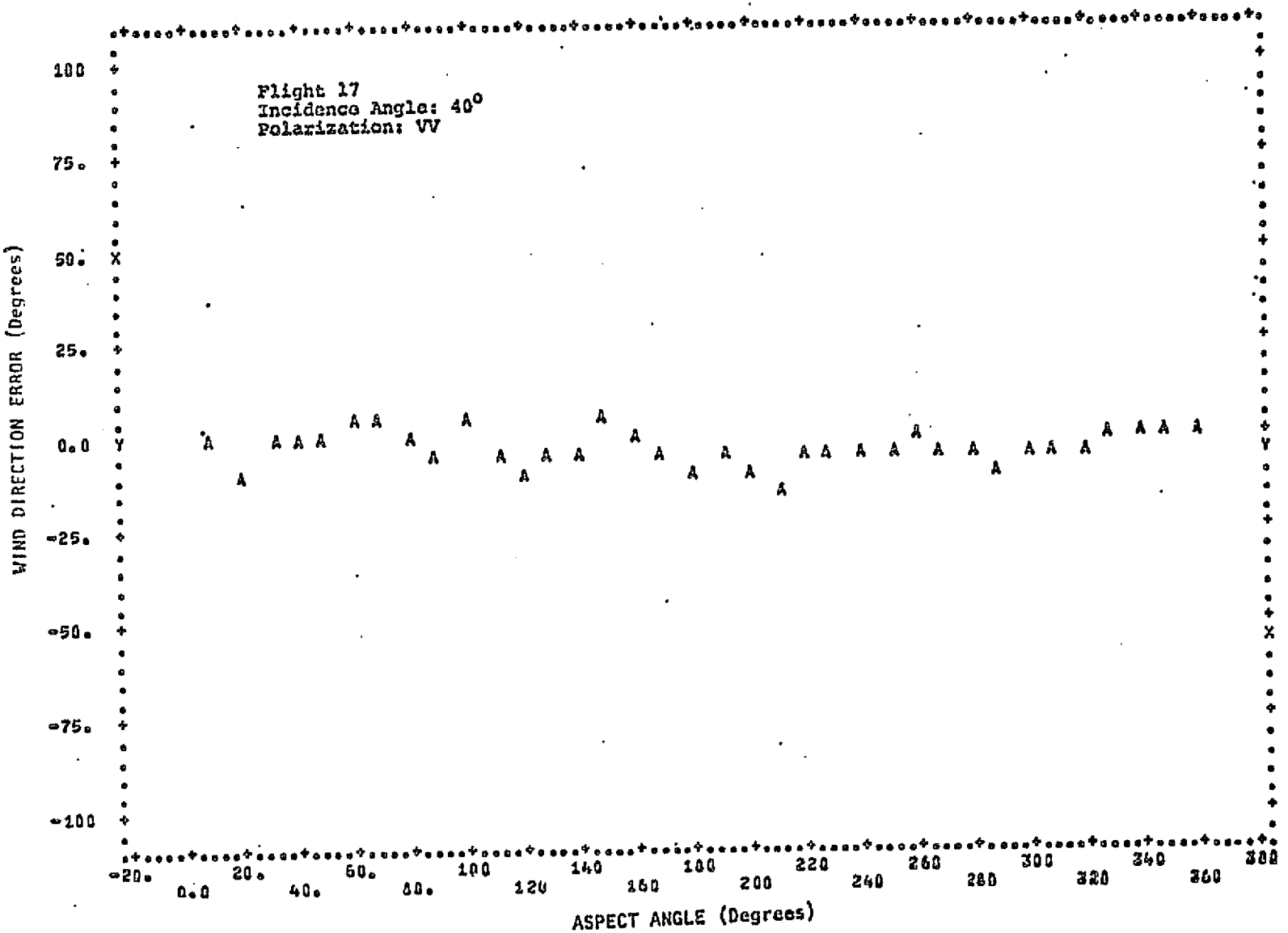
Flight 17
Incidence Angle: 40°
Polarization: VV
WIND DIRECTION ERROR (Degrees)
100
75.
50.
25.
0.0
-25.
-50.
-75.
-100
-20.
0.0
20.
40.
60.
80.
100
120
140
160
180
200
220
240
260
280
300
320
340
360
ASPECT ANGLE (Degrees)

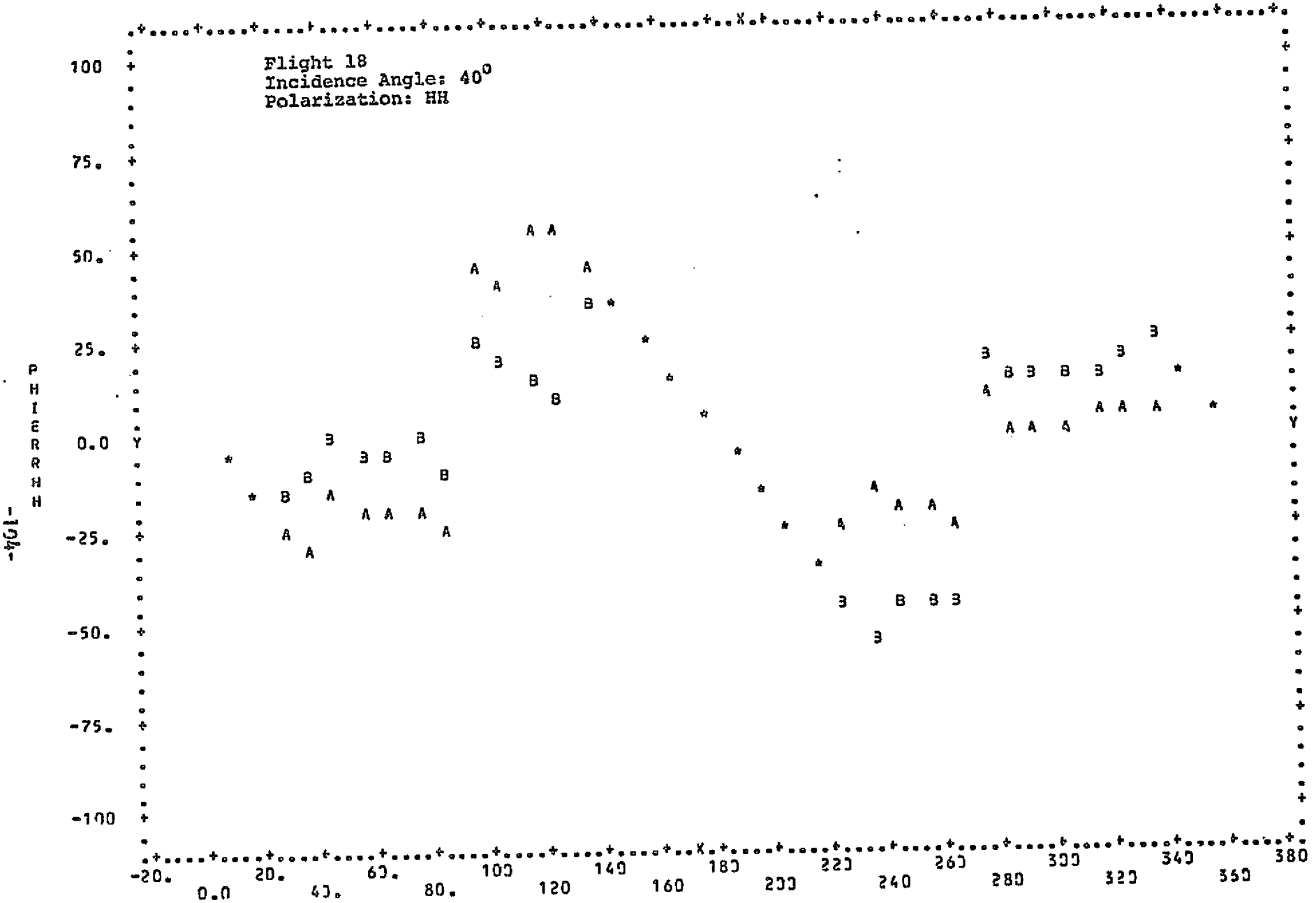

N= 72
COR= .022

	MEAN	ST.DEV.	REGRESSION LINE	RES.MS.
X	180.38	104.25	X= .09393*Y+ 180.45	11018.
Y	-.80875	24.833	Y= .00533*X-1.7701	625.17

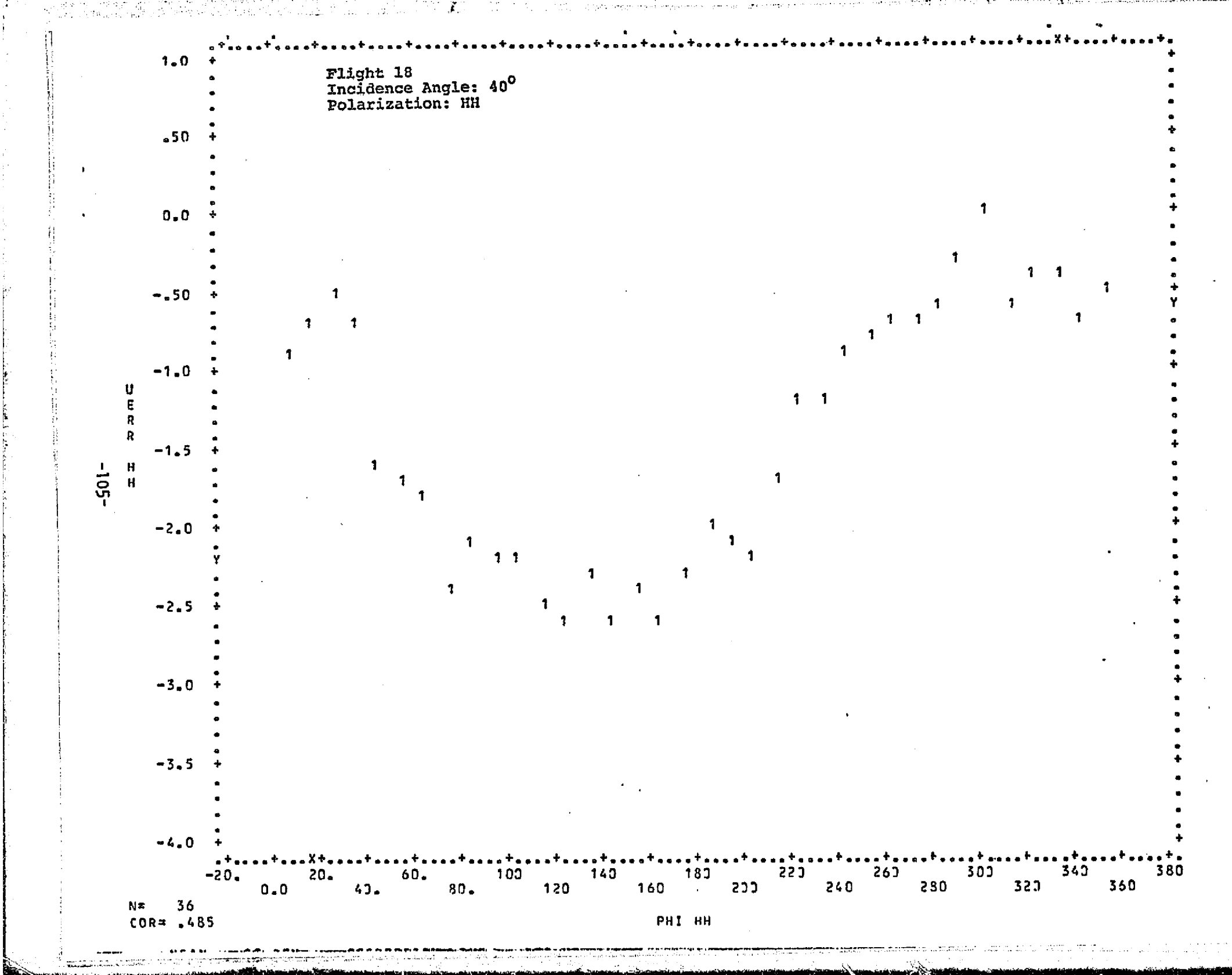
Flight 18
Incidence Angle: 40°
Polarization: HH
1.0
.50
0.0
-.50
-1.0
-1.5
-2.0
-2.5
-3.0
-3.5
-4.0
UERR HH
-105-
-20.
0.0
20.
40.
60.
80.
100
120
140
160
180
200
220
240
260
280
300
320
340
360
380
PHI HH
N= 36
COR= .485

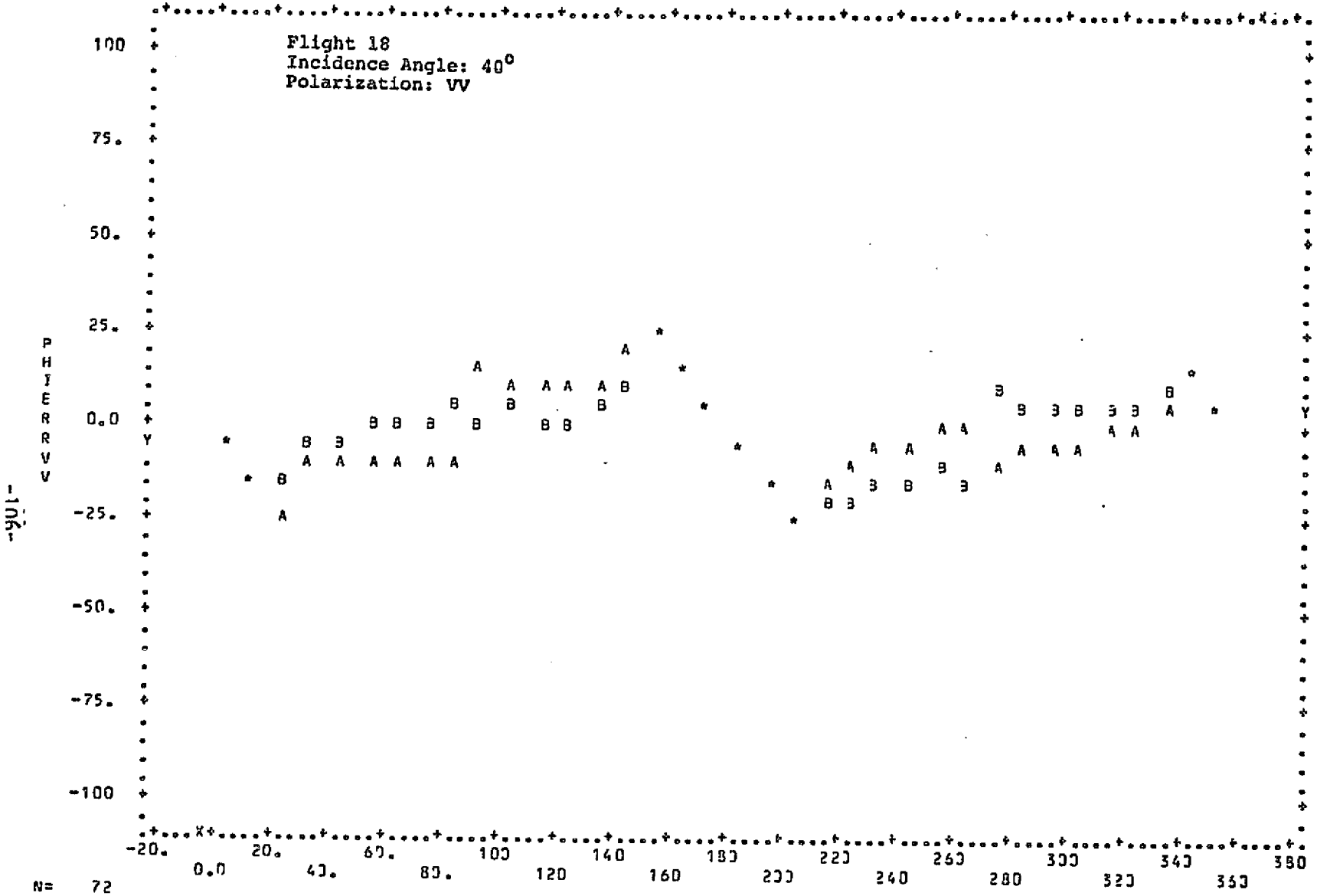

N= 72
COR= .186

	MEAN	ST.DEV.	REGRESSION LINE	RES.MS.
X	179.35	104.76	X= 1.7021*Y+ 181.44	10744.
Y	-1.2290	11.478	Y= .02043*X-4.8934	128.97

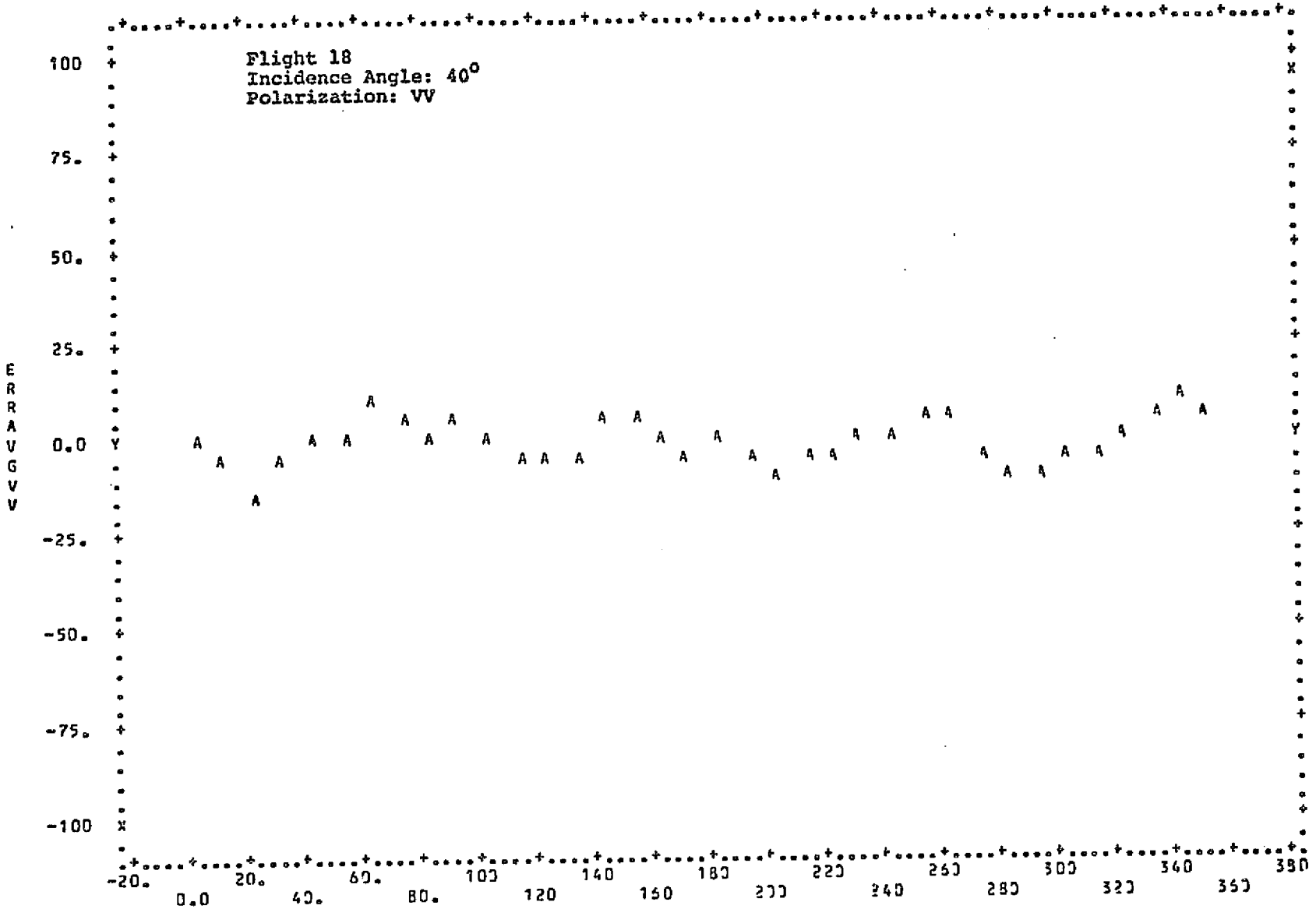

N= 36
COR= .108

	MEAN	ST.DEV.	REGRESSION LINE	RES.MS.
X	179.35	105.50	X= 2.1025*Y+ 181.93	11325.
Y	-1.2292	5.4215	Y= .00555*X-2.2249	29.904

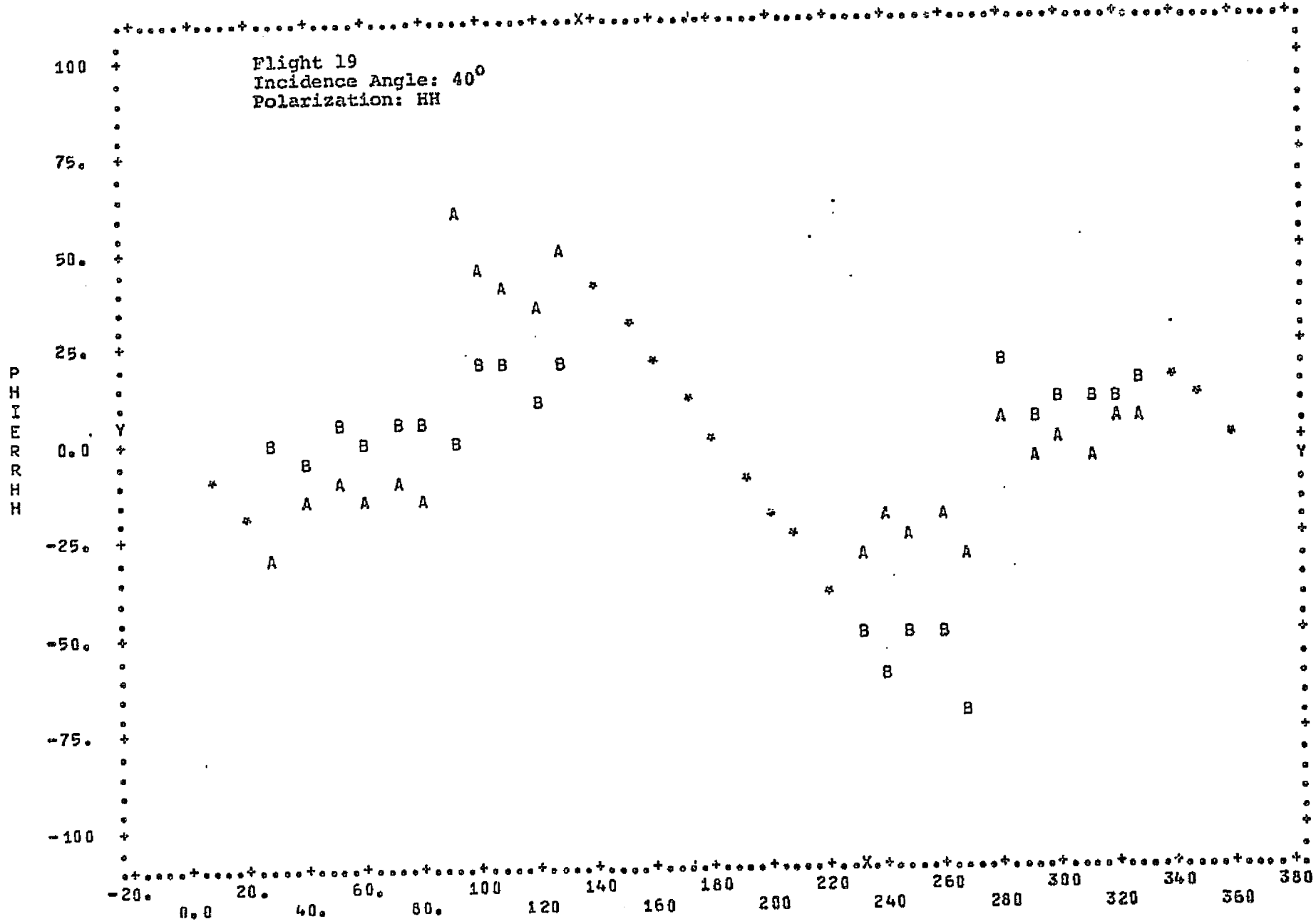

N= 72
COR=-.113

	MEAN	ST.DEV.	REGRESSION LINE	RES.MS.
X	184.70	104.74	X=-.45432*Y+ 183.99	10984.
Y	-1.5519	26.110	Y=-.02823*X+ 3.6627	682.60

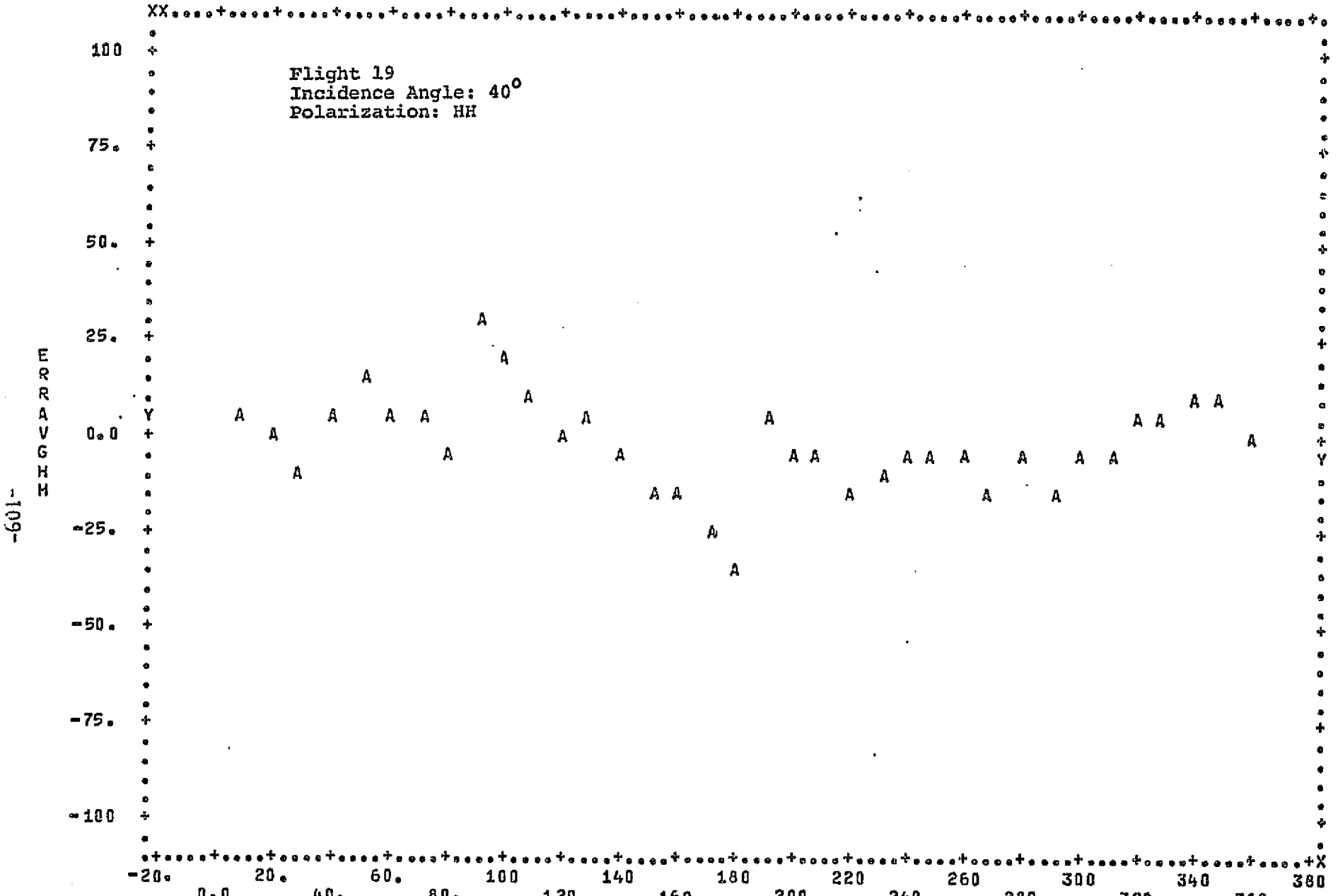

-601-

N= 36
COR=-.208

	MEAN	ST.DEV.	REGRESSION LINE	RES.MS.
X	184.70	105.48	X=-1.8373*Y+ 181.85	10958.
Y	-1.5514	11.951	Y=-.02359*X+ 2.8049	140.66

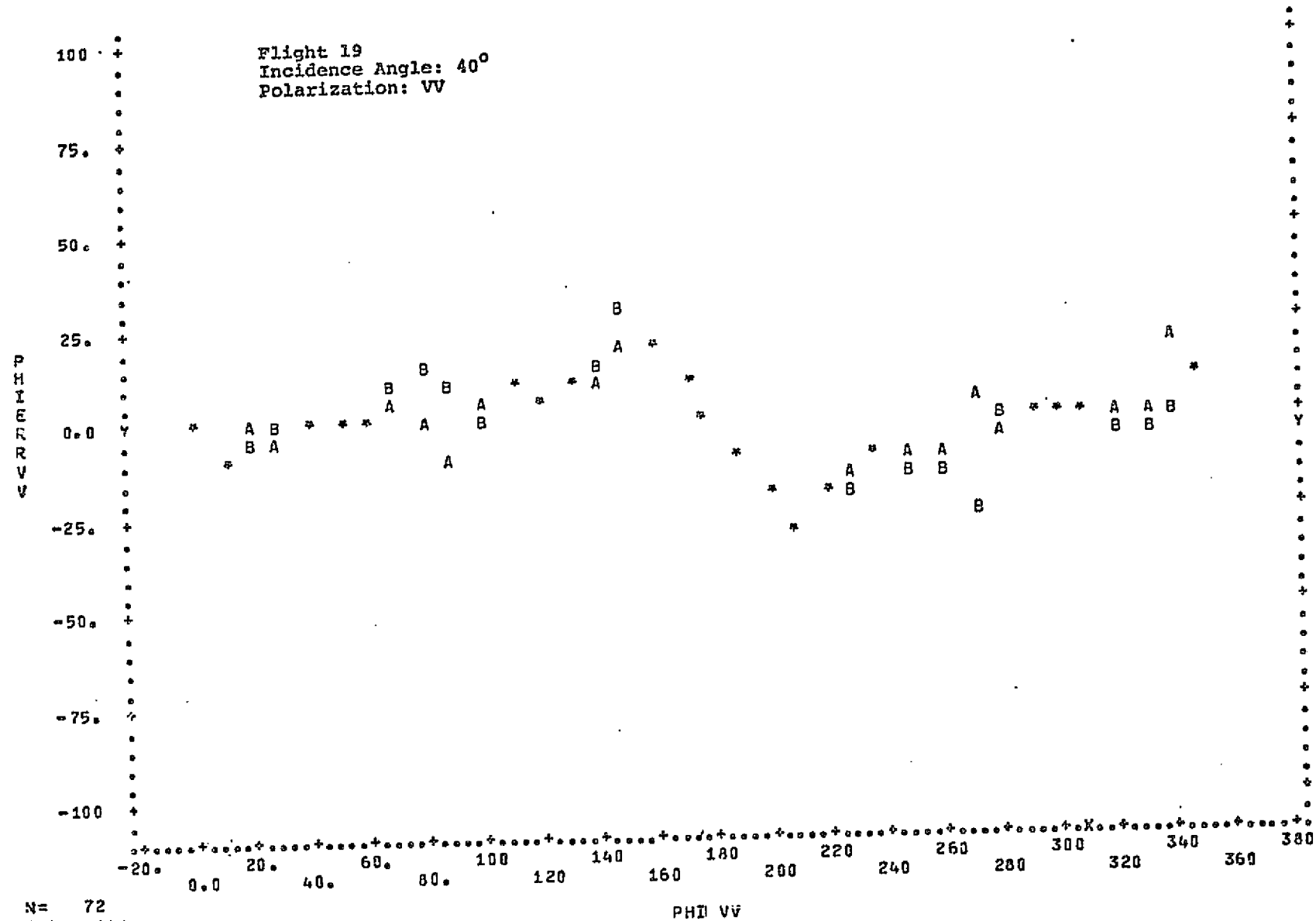

N= 72
COR=-.141

	MEAN	ST.DEV.	REGRESSION LINE	RES.MS.
X	174.97	104.46	X=-1.2300*Y+ 174.05	10849.
Y	-.74931	11.967	Y=-.01614*X+ 2.0751	142.38

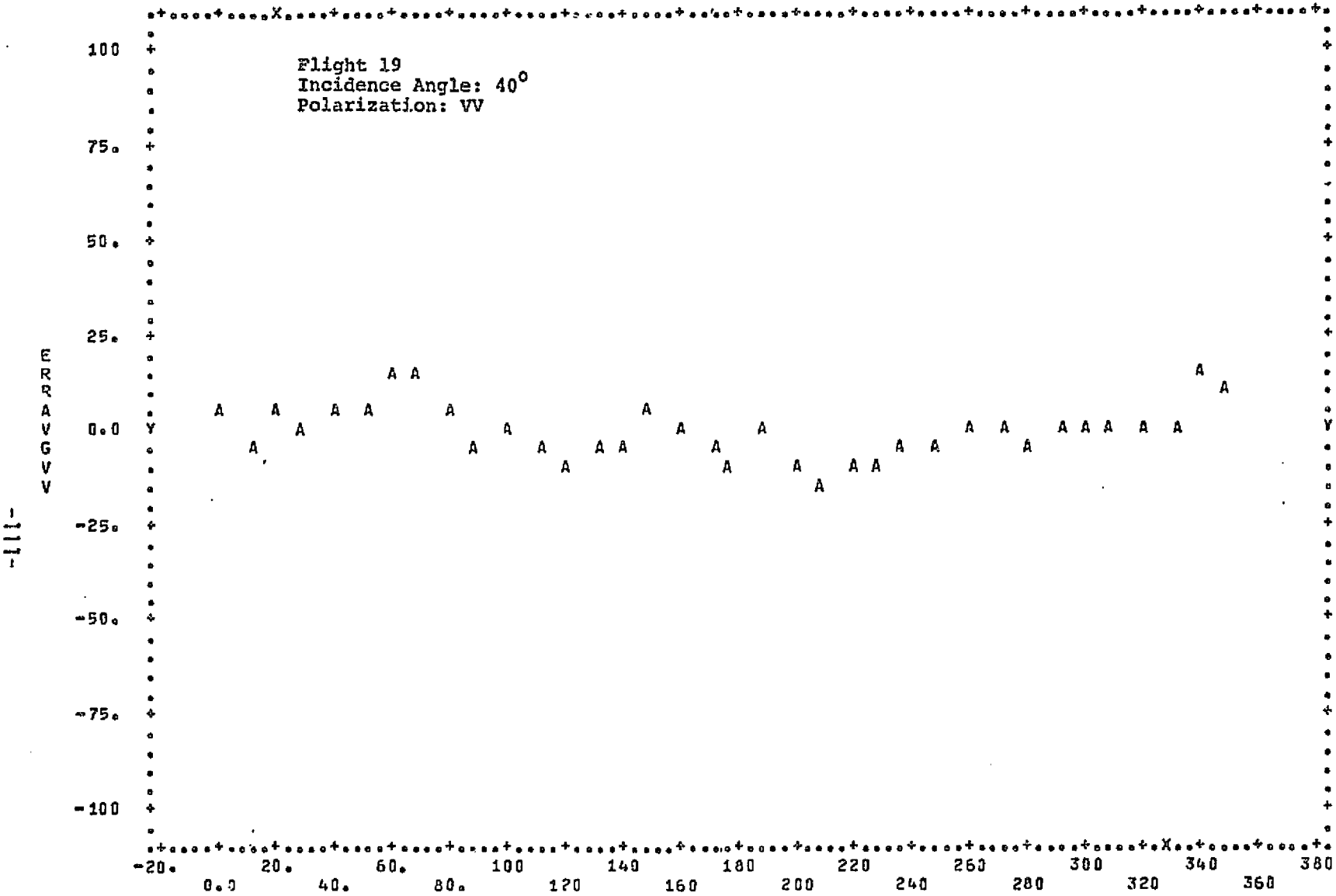

N= 36
COR=-.100

	MEAN	ST.DEV.	REGRESSION LINE	RES.MS.
X	174.97	105.21	X=-1.4152*Y+ 173.91	11280.
Y	-.74944	7.4325	Y=-.00706*X+ .48644	56.298